DESIGN, PREPARATION, AND CHARACTERIZATION OF NANOPARTICLES AS DELIVERY SYSTEMS FOR BIOACTIVE PHENOLIC PHYTOCHEMICALS

By

ZHENG LI

A DISSERTATION PRESENTED TO THE GRADUATE SCHOOL
OF THE UNIVERSITY OF FLORIDA IN PARTIAL FULFILLMENT
OF THE REQUIREMENTS FOR THE DEGREE OF
DOCTOR OF PHILOSOPHY

UNIVERSITY OF FLORIDA

2013

© 2013 Zheng Li

To my family and friends

ACKNOWLEDGMENTS

I want to express my sincere appreciation to my major advisor, Dr. Liwei Gu, for his patience, advice and mentorship. Without his guidance and support, this research could not be accomplished. I am grateful for my committee members, Dr. Susan S. Percival, Dr. Jesse F. Gregory III, Dr. Brij M. Moudgil, and Dr. Kevin W. Powers, for their valuable time and suggestions.

I cherished the friendship with my lab members: Amandeep K. Sandhu, Bo Zhao, Haiyan Liu, Kaijie Song, Keqin Ou, Timothy Buran, Sara M. Marshall, Dr. Tao Zou, and Wei Wang. They were always willing to offer me helping hands and emotional support.

Last and most important, I express my deepest gratitude to my parents for their constant love and commitment to my education. They were my first teachers and gave me many good lessons. They always encouraged me to pursue my dream. I would also like to extend my gratitude to my beloved girl friend, Qiong Cheng, who is always proud of every single achievement I obtain. Because of her love, patience, and unconditional support, I gained the strength to complete this program.

TABLE OF CONTENTS

page

LIST OF TABLES

LIST OF FIGURES

LIST OF ABBREVIATIONS

ANOVA	Analysis of variance
ATP	Adenosine triphosphate
BEN	BSA-EGCG nanoparticles
BSA	Bovine serum albumin
CBEN	Chitosan coated BSA-EGCG nanoparticles
CO_2	Carbon dioxide
DAD	Diode array detector
DLS	Dynamic light scattering
EGCG	(-)-Epigallocatechin gallate
ESI	Electrospray ionization
FITC	Fluorescein isothiocyanate
FTIR	Fourier transform infrared
g	gram
HBSS	Hank’s balanced salt solution
HCl	Hydrochloric acid
HPLC	High performance liquid chromatogram
IMDM	Iscove’s modified dulbecco’s media
KBr	Potassium bromide
L	Liter
LDL	Low density lipoprotein
mg	Milligram
min	Minute(s)
MS	Mass spectrometer
mV	Millivolts

µg	Microgram
µL	Microliter
mL	Milliliter
NaOH	Sodium hydroxide
nm	Nanometer
m/z	Mass to charge ratio
P_{app}	Apparent permeability coefficient
PBEN	Poly-ε-lysine coated BSA-EGCG nanoparticles
PBS	Phosphate buffered saline
PLA	Poly(D,L-lactic acid)
PLGA	Poly(lactic-co-glycolic acid)
PPE	Partially purified ellagitannins
rpm	Revolutions per minute
SDS-PAGE	Sodium dodecyl sulfate-polyacrylamide gel electrophoresis
SEM	Scanning electron microscopy
SGF	Simulated gastric fluid
SIF	Simulated intestinal fluid
TEER	Transepithelial electric resistance
TEM	Transmission electron microscopy
UV	Ultraviolet

Abstract of Dissertation Presented to the Graduate School
of the University of Florida in Partial Fulfillment of the
Requirements for the Degree of Doctor of Philosophy

DESIGN, PREPARATION, AND CHARACTERIZATION OF NANOPARTICLES AS DELIVERY SYSTEMS FOR BIOACTIVE PHENOLIC PHYTOCHEMICALS

By

Zheng Li

August 2013

Chair: Liwei Gu
Major: Food Science and Human Nutrition

Three types of nanoparticles were designed as delivery systems for ellagitannins or EGCG. In the first design, the PPE were obtained from pomegranate pericarp to contain punicalagin A (16.6%) and B (32.5%, w/w). Punicalagin and gelatin self-assembled into nanoparticles via hydrogen bonding and hydrophobic interactions. Nanoparticles formed at a mass ratio 5:5 had a size of 149 nm, zeta-potential of 17.8 mV, and loading capacity of punicalagin A and B of 14.8% and 25.7%. PPE-gelatin nanoparticles were less effective at inducing early stage apoptosis, but as effective as PPE solution at inducing late stage apoptosis and necrosis on HL-60 cells. PPE-to-gelatin mass ratios from 1:5-6:5 resulted in nanoparticles with sizes of 122-129 nm. Nanoparticles fabricated at pH 4.0-5.3 (gelatin solution) had particle sizes of 21-194 nm and zeta-potentials of 14.7-23.8 mV. Acidic or basic pH hindered particle formation, whereas pH 6-7 caused particle aggregation. Nanoparticles formed at 25-50^{o}C had sizes below 500 nm. Nanoparticles remained stable for 4 days.

In the second design, BSA-EGCG nanoparticles were coated with poly-ε-lysine or chitosan with sizes of 100-200 nm. Loading efficiency and capacity of EGCG were 35.4% and 32.7%, and 17.0% and 16.0%, respectively. Coatings prevented particle

aggregation at pH 4.5-5.0 and changed particle zeta-potentials. Coatings delayed EGCG release from the nanoparticles in simulated fluids with or without digestive enzymes. EGCG in CBEN showed higher P_{app} on Caco-2 monolayers.

In the third design, EGCG ovalbumin-dextran conjugate nanoparticles were self-assembled and further crosslinked by glutaraldehyde. These nanoparticles had sizes of 285 nm and 339 nm. Loading efficiency and capacity of EGCG was 23.4% and 30.0%, and 19.6% and 20.9%, respectively. They showed nano-scale sizes and similar zeta-potentials in the pH range 2.5-7.5. Good nanoparticle stabilities were observed in simulated fluids at 37^{o}C. Digestive enzymes caused quicker release of EGCG from the nanoparticles. The conjugate nanoparticles significantly enhanced P_{app} of EGCG on Caco-2 monolayers.

CHAPTER 1
A REVIEW: USING NANOPARTICLES TO ENHANCE BIOAVAILBILITY AND BIOACTIVITY OF PHENOLIC PHYTOCHEMICALS

Introduction

Phenolic phytochemicals are widely present in the plant kingdom (*1*). They are synthesized in plants as secondary metabolites to modulate plant growth, development, and defense (*2-5*). Both epidemiologic and experimental studies have associated the consumption of phenolic phytochemical rich foods with better health in humans (*6-9*). However, the low absorption rate of phenolic phytochemicals limits their health promoting properties (*10-12*).

Nanoparticles are used to encapsulate and deliver drugs to the gastroinstestinal tract and result in enhanced absorption (*13-14*). In this chapter, classification, health benefits, and absorption of phenolic phytochemicals will be outlined. Fabrication methods, analytical methods, and absorption of nanoparticles will be reviewed.

Phenolic Phytochemicals

Phenolic phytochemicals represent a variety of plant secondary metabolites consisting of at least one aromatic ring with attached polyhydroxyl groups. More than 8,000 phenolic phytochemicals have been reported to exist in different fruits, vegetables, and cereals (*15*). Phenolic phytochemicals can be divided into flavonoids and non-flavonoids according to chemical structure. Flavonoids consist of fifteen carbons, with two aromatic rings conjugated by a three-carbon bridge (C_6-C_3-C_6). The major flavonoids include flavonols, anthocyanidins, flavan-3-ols, and isoflavones (*3-4, 16-21*). Non-flavonoids include phenolic acid (C_6-C_1), hydroxycinammates and its derivates (C_6-C_3), and stilbenes (C_6-C_2-C_6) (*22-26*).

Health Benefits

Consumption of phenolic phytochemicals and phenolic-rich foods showed anti-cancer properties and offered benefits for human health. The “French paradox” phenomenon suggests high wine consumption lowers the incidence of coronary heart disease in France despite a high intake of saturated fat (*27*). Resveratrol in red wine contributed to cardioprotection, decreased platelet aggregation, suppression of prostaglandin biosynthesis, improvement of mitochondrial function, inhibition of LDL oxidation, cancer cell apoptosis, and extended life span (*28-38*). Similarly, flavonols also showed anti-cancer, anti-inflammatory, and anti-diabetic functions (*39-42*). Anthocyanidin and its glycosides induced apoptosis of cancer cells and inhibited cancer cell proliferation by regulation of gene expression (*43-44*). Anthocyanins also protected against UV-induced oxidative damages, and inhibited diethylnitrosamine-induced hepatocellular carcinogenesis (*45-46*). Soy isoflavones inhibited activity of transcription factors and genes essential for tumor cell proliferation, invasion, and neovascularization (*47-49*). EGCG prevented oxidative damage in healthy cells, as well as provided antiangiogenic and antitumor properties (*50*). EGCG also induced apoptosis and caused cell growth arrest in cancer cells (*51-53*).

Factors Affecting Oral Bioavailability of Phenolic Phytochemicals

Poor stability, lack of absorptive transporters, metabolism and active efflux in epithelial cells contributed to the low absorption of phenolic phytochemicals.

Poor Stability

The gastrointestinal tract has different pH segments and contains reactive oxygen species. Reactive oxygen species can oxidize phenolic phytochemicals. Phenolic phytochemicals are unstable in both low and neutral pH conditions. For

example, anthocyanins experienced a rapid degradation at neutral pH (*54*). EGCG was degraded in a first-order reaction in both acidic (pH below 2.0) and neutral pH conditions because of the gallate moiety (*55-56*). In addition, anaerobic bacteria in the colon can degrade phenolic phytochemicals to yield small molecular-weight metabolites (*57-58*).

Lack of Absorptive Transporters

No absorptive transporters have been identified for phenolic phytochemicals. Passive diffusion was thought to be the major absorption route. Permeability of phenolic phytochemicals decreases when molecular weight increases. For example, proanthocyanidin dimers and trimers were absorbed, whereas polymers were not transported because of higher molecular weights (*59*). Flavonoid aglycones had much higher apparent permeability coefficients (P_{app}) compared to their glycosides on Caco-2 monolayers (*60-63*). For example, isoflavone and resveratrol showed higher P_{app} compared to their glycosides (*64-66*). This is because glycoside conjugates are less lipophilic than aglycones.

Metabolism and Active Efflux in Epithelial Cells

Once absorbed, phenolic phytochemicals are metabolized by uridine 5'-diphospho-glucuronosyltransferases (UGTs) and sulfotransferases (SULFs) to form conjugates in ephithelial cells. Both absorbed phenolic phytochemicals and their conjugates are substrates of efflux transporters. These efflux transporters include p-glycoprotein, multidrug resistance-associated protein 2, and breast cancer resistance protein on the apical cell membrance and multidrug resistance-associated protein 3 on the basolateral membrance (*67*). The majority of conjugates are pumped by efflux transporters to the lumen of intestine where they are excreted or degraded (*66, 68-69*).

A smaller portion of conjugates may be absorbed via multidrug resistance-associated protein 3 (*67*).

Nanoparticles for Phytochemical Delivery

In pharmaceutical science, particles with sizes below 1000 nm are classified as nanoparticles because of their unique physicochemical properties compared to bulk materials. Nanoparticles have the capacity to enhance the absorption of loaded drugs or other bioactive compounds.

Nanoparticle Fabrication

Nanoparticles are fabricated using two basic approaches, i.e. the ‘top-down’ (mechanical process) and ‘bottom-up’ (chemical process) approaches (*70-71*). Bulk materials are shrunk to nano-scale particles by a size-reduction mechanical process, whereas small molecules are aggregated to yield nanoparticles using a chemical process.

In a chemical process, the desolvation method is a well-established fabrication approach. This method uses three important components, including a polymer, an internal solvent, and an external solvent. Polymer molecules are dissolved in the internal solvent. Subsequently, the external solvent is gradually added to the internal solvent. When the concentration of the external solvent reaches a certain threshold, polymer molecules start to aggregate into nanoparticles (*72*). Self-assembly of polymers is often used in the chemical process. It takes advantage of direct and/or indirect interactions among polymers and ions. Particle formation is affected by reaction conditions, such as temperature and pH (*73-76*).

Methods of Nanoparticle Analysis

A number of technologies have been applied to characterize nanoparticles for their size, surface charge, and morphology. These methods are summarized in **Table 1-1**.

Dynamic light scattering

Dynamic light scattering (DLS) is a common analytical technique to evaluate the particle size distribution. The mechanism behind DLS measurement is particle motility due to Brownian motion. DLS measures the fluctuation intensity of scattered light and applies an algorithm to determine the size distribution (*77-79*). DLS can measure the particle size distribution quickly and gives a good statistics. Also, the conversion from intensity distribution to volume- and/or number-weighted distribution can be achieved by Mie theory.

Electron microscopy

Electron microscopy measures the size and morphology of dry particles. Methods include transmission electron microscopy (TEM) and scanning electron microscopy (SEM) (*77*). A beam of electrons is transmitted through particles, interacting with them; as a result an image is formed from the interaction of the electrons transmitted through the particle. The image is magnified and focused onto an imaging device (*80*). The advantages of electron microscpy include the ability to measure particle sizes below 1 nm and visual particle shape and morphology. However, samples need to be dried before the electron microscopy measurements, the size distribution is difficult to analyze, and electron beam may affect particle characterization (*81*).

Nanoparticles for Phytochemical Delivery

Nanoparticles enhance the absorption of loaded drugs or phytochemicals by several mechanisms.

Nanoparticles enhance solubility of loaded phytochemicals

Nanoparticles often have hydrophobic groups inside and polar groups on their surface. Such structural features help to increase solubility of encapsulated compounds. For example, proanthocyanidins have extremely low solubility in aqueous solution. After encapsulating them in zein nanoparticles, the solubility of proanthocyanidins increased significantly (*82*). Curcumin is insoluble in water. Nanoparticles made of PLGA, chitosan, and proteins were reported to improve the solubility of encapsulated curcumin in aqueous solution (*83-90*).

Nanoparticles enhance stability of phytochemicals

Phenolic phytochemicals are unstable in the gastrointestinal tract. For example, EGCG was rapidly degraded in both acidic (pH below 2) and neutral conditions (*55*). Encapsulating EGCG into particles, such as chitosan nanoparticles and Eudragit microparticles, significantly delayed its degradation in simulated digestive fluids (*55-56, 91-92*).

Nanoparticle transport on epithelium

Nanoparticles can penetrate small intestinal epithelium by either the paracellular or transcellular pathway. Tight junctional proteins connect epithelial cells to protect the integrity of epithelium. Paracellular transport refers to diffusion through intercellular spaces among epithelial cells (*93-94*). Nanoparticles with sizes below 20 nm can reversibly disrupt tight junctions and release bioactive compounds to facilitate the paracellular diffusion (*95-97*). Additionally, tight junction mediators, such as chitosan,

thiolated chitosan, chitosan derivatives, and polyacrylate derivatives were reported to improve the paracellular transport in the form of either nanoparticles or coatings on nanoparticles (*13, 98-105*).

Small intenstine epithelium consists of goblet cells, enterocytes, M-cells, and hormone-secreting cells. Goblet cells secrete mucus for protection of the epithelium surfaces, whereas enterocytes and M-cells internalize nanoparticles by cellular uptake. PLA nanoparticles, silica coated rhoadime 6G isothiocyanate nanoparticles, PLGA nanoparticles, and protein-based nanoparticles showed much higher cellular uptake at 37^{o}C compared to 4^{o}C (*106-114*). This is because cellular uptake of nanoparticles requires energy in the form of ATP.

Nanoparticles are taken up by cells via macropinocytosis or endocytosis. Macropinocytosis is an actin-driven process without receptor mediation. Macropinosomes are formed on the surface of cells. Particles with sizes below 2000 nm are enclosed by macropinosomes and internalized to cells. The internalized particles can be further translocated to endolysosome (*115-117*).

Epithelial cells also take up nanoparticles via endocytosis. Endocytosis includes clathrin-mediated endocytosis, caveolae-medated endocytosis, and clathrin- and caveolae-independent endocytosis (*118*). Clathrin-mediated endocysotis requires clathrin-coated pits formed by assembly of clathrin. Coated pits develop to form vesicles of 120 nm, a process mediated by GTPase. These vesicles engulf nanoparticles into cells via low-density lipoprotein receptors or iron-loaded transferrin receptors that interact with clathrin adaptor proteins (*119*). Nanoparticles with an average size below 200 nm had the ability to stabilize the clathrin-coated pits, and the internalization route

was primarily clathrin-mediated endocytosis (*120*). Nanoparticles internalized by clathrin-mediated endocytosis are translocated to lysosomes (*119, 121-122*). In caveolae-mediated endocytosis, caveolae is formed by assembling caveolin protein, choloestrol, and sphingolipids on the cell membrane (*121, 123-125*). Nanoparticles with sizes below 60 nm tend to be internalized by caveolae-mediated endocytosis (*126*). However, 500 nm nanoparticles were also observed to be taken up in caveolae-mediated pathway (*127*).

After being internalized in epithelial cells, nanoparticles are translocated to endo/lysosome for degradation. Nanoparticles also may remain intact in endo/lysosome and enter blood circulation by excytosis (*128-130*). Additionally, nanoparticles may be translocated to endoplasmic reticulum and Golgi complex and further undergo excytosis across the membrane (*131*).

Research Objectives

The overall objective of this research is to design, prepare, and characterize nanoparticles as delivery systems for phenolic phytochemicals. The goal is to improve the absorption and the bioactivity of loaded phytochemicals. This research has four specific aims:

1. To fabricate ellagitannin-gelatin nanoparticles using self-assembly method and to evaluate its bioactivity on HL-60 cells.
2. To investigate the effects of ellagitannin-to-gelatin mass ratio, pH, temperature, and reaction time on characterization of ellagitannin-gelatin nanoparticles.
3. To fabricate coated BSA-EGCG nanoparticles using a desolvation method and to evaluate EGCG permeability on Caco-2 monolayer.
4. To fabricate EGCG ovalbumin-dextran conjugate nanoparticles using self-assembly and to investigate EGCG permeability on Caco-2 monolayer.

Table 1-1. Analytical methods and technologies for nanoparticle characterization

Technology	Size range	Sensitivity and reliability	Suspension in vitro fluids
Dynamic light scattering	1-1000 nm	Accurate for monodisperse Inaccurate for polydisperse samples Large influence on size accuracy and distribution Measurement fast (about 2-5 min per measurement) No sample visualization Approximate size distribution, intensity distribution	Yes
Scanning mobility analyzing	2.5-1000 nm	High resolution data Fast measurements Discreet particle measurement Automatically flow control	No
Nanoparticle tracking analysis	30-1000 nm	Accurate for both mono- and poly-disperse samples Peak resolution high Little influence on size accuracy and size distribution Measurement slow (5 min to 1 hour) per measurement Individual particle size, number distribution Sample visualization More reliable size distribution	Yes
Electron microscopy	0.3 nm - micron	High resolution No calibration necessary Particle sample shape (two-dimension) Samples preparation before measurement Poor statistics on size distribution High vacuum needed	Maybe Particles need to be dried
Atomic force microscopy	5 nm - micron	A three-dimensional surface profile No vacuum, wrok well in ambient air or a liquid environment Limitation on scanning speed Only see surface of sample	Maybe in ambient or Liquid condition

CHAPTER 2
FABRICATION OF NANOPARTICLES USING PARTIALLY PURIFIED POMEGRANATE ELLAGITANNINS AND GELATIN AND THEIR APOPTOTIC EFFECTS

Background

Nanoparticles are defined in biological sciences as particles with at least one dimension less than 1000 nm (*132*). They possess many unique chemical, biological, and physical properties compared to bulk materials. Drugs or other bioactive ingredients encapsulated in nanoparticles or other nanocarriers had drastically increased bioavailability and bioactivity. For instance, epigallocathecin gallate (EGCG) encapsulated in nanoparticles was 10-fold as effective as EGCG that was not encapsulated (*133*). Carboplatin-loaded chitosan-alginate nanoparticles showed greater antiproliferative activities and apoptotic effects compared to the drug in solution (*134*). Cisplatin incorporated in gelatin nanoparticles provided stronger antitumor activities and was less toxic compared to free cisplatin *in vivo* (*135*).

Pomegranate contains several types of ellagitannins, including punicalagin, punicalin, gallagic acid, ellagic acid, and ellagic acid-glycosides (*136-137*). These ellagitannins have been reported to prevent cancer and cardiovascular diseases, scavenge oxidative free radicals, and reduce the risk for atherosclerosis and other chronic diseases (*138-141*). The affinity between tannins and proteins is a well known phenomenon (*142-143*). The present study takes advantage of such affinity to fabricate the self-assembled nanoparticles using partially purified pomegranate ellagitannins (PPE) and gelatin. The PPE-gelatin nanoparticles, to our knowledge, have not been reported before. Three different mass ratios of PPE and gelatin were applied and characteristics of nanoparticles including particle size, zeta-potential, morphology, and

interaction binding modes were measured by Microtrac Nanotrac, ZetaPlus, Scanning Electron Microscopy, and Fourier Transform Infrared Spectroscopy, respectively. Loading capacity of ellagitannins in the resultant nanoparticles were investigated using HPLC-ESI-MS^n. The Annexin V Staining Assay on a leukemic cell line HL-60 was selected to evaluate the apoptotic effect of PPE-gelatin nanoparticles and compare that to the PPE solution.

Materials and Methods

Samples and Chemicals

Pomegranates (*Punica granatum* L.) were obtained from Publix Supermarket (Gainesville, FL). The pericarp of the fruits was manually separated. Pure punicalagin and ellagic acid was purchased from Quality Phytochemicals LLC (Edison, NJ) and Sigma-Aldrich (St. Louis, MO), respectively. Ethanol, formic acid, methanol, gelatin type A, and other chemicals were products of Fisher Scientific (Pittsburgh, PA). Amberlite XAD-16N resin was purchased from Dow Company (Piscataway, NJ).

Extraction and Purification of Pomegranate Ellagitannins

Extraction and purification of pomegranate ellagitannins followed a published method with minor modifications (*137*). Frozen pomegranate pericarp (50 g) was blended in a kitchen blender and mixed with water (250 mL). The water suspension was sonicated for 5 min and kept at 25^{o}C for 30 min. The sonication step was repeated for two more times. Water extract was obtained after filtration and then dried on an ISS110 SpeedVac evaporator (Fisher Scientific, Pittsburgh, PA) at 25^{o}C. The resultant solid was re-dissolved in 20 mL of water and loaded onto a column (30 × 400 mm, ID × Length) packed with Amberlite XAD-16N resin. The column was eluted with 2 liters of

water. Ellagitannins were recovered from the column using 400 mL of ethanol. Ethanol elute was evaporated at 25^{o}C to yield PPE as dry power (approximately 2.5 g).

HPLC-ESI-MS^{n} Analyses

An Agilent 1200 HPLC system consisting of an autosampler, a binary pump, a column compartment, a diode array detector (Agilent Technologies, Palo Alto, CA) was interfaced to a HCT ion trap mass spectrometer (Bruker Daltonics, Billerica, MA). PPE solution was filtered through 0.45 µm filter units and 30 µL was injected on an Agilent Zorbax ODS column (4.6 mm × 25 cm, 5 µm particle size) for separation of ellagitannins. The binary mobile phase consisted of (A) formic acid: water (2:98 v/v) and (B) formic acid: methanol (2:98 v/v). Gradient elution reported by Seeram et *al* was used with minor modifications (*137*). The gradient is described as follows: 0−30 min, 1−20% B linear; 30-45 min, 20- 40% B; 45-60 min, 40-95% B; 60-65 min, 95-1% B; followed by 5 min of re-equilibration of the column before the next run. The detection wavelength on a diode array detector was 378 nm. Electrospray ionization in negative mode was performed using nebulizer 65 psi, dry gas 11 L/min, drying temperature 350^{o}C, and capillary 4000 V. The full scan mass spectra were measured at *m/z* 100-2000. Auto MS^{2} was conducted with 50% compound stability and 60% trap drive level. Punicalagin A, B, and ellagic acid were used as external standard for quantification. Data was collected and calculated using Chemstation software (Version B. 01.03, Agilent Technologies, Palo Alto, CA).

Self-assembly of PPE-gelatin Nanoparticles

Gelatin type A (0.5 g) and PPE powder (0.5 g) were dissolved in DI water (1000 mL) to a concentration of 0.5 mg/mL, respectively. PPE solution with 1 mL, 5 mL, or 7 mL was mixed with 5 mL of gelatin solution, which gave the PPE-to-gelatin mass ratio of

1:5, 5:5, and 7:5, respectively. The mixture was incubated at 25^{o}C for 48 h. The nanoparticle suspensions were then centrifuged at 12,000 rpm for 5 min. The supernatant was removed from the suspension for calculations of loading capacity. The sediments were lyophilized for 48 h to form dry particles and stored at -20^{o}C for further analyses.

Particle Size and Zeta-potential Measurement

Mean particle size and size distribution was measured using Dynamic Light Scattering (DLS) on a Nanotrac ULTRA with an external probe (Microtrac Inc., Largo, FL). Each sample was analyzed in triplicate tests and each replicate was measured six times to yield the average particle size. Zeta-potentials were determined using Brookhaven ZetaPlus (Brookhaven Instrument Corp., Holtsville, NY). Triplicate tests were conducted at a constant temperature of 22^{o}C and each replicate was measured ten times to obtain the average zeta-potential.

Scanning Electron Microscopy (SEM)

Dry particle powders were used for morphology characterization using Field Emission Scanning Electron Microscope (Model JSM-633OF, JEOL Ltd, Tokyo, Japan).

Fourier Transform Infrared (FTIR) Spectroscopy

PPE-gelatin nanoparticles were fabricated at PPE-to-gelatin mass ratio 5:5. Supernatant and nanoparticles were separated by centrifuge and freeze-dried. Dry PPE, gelatin, PPE-gelatin nanoparticles, and dried supernatant were mixed with pure KBr powders using a ratio of 1: 100 sample: KBr (w/w). These mixtures were ground into fine powders and then analyzed using a Thermo Nicolet Magna 760 FTIR (Thermo Nicolet Corp., Madison, WI) with a MCT-A detector. Pure KBr powders were used as

background. The FTIR spectra were obtained over the wave number range from 700 to 4000 cm^{-1} at a resolution of 2 cm^{-1}.

Cell Apoptosis

Annexin V staining was used for cell apoptosis measurements in the HL-60 cell line. Four PPE-gelatin nanoparticle suspension samples were prepared, and each PPE-gelatin nanoparticle suspension with the concentration of 0.0156, 0.0313, 0.0625, and 0.125 mg/mL was added to the appropriate wells in triplicate. PPE solution with the concentration of 0.0156, 0.0313, 0.0625, and 0.125 mg/mL was added to wells in triplicate. HL-60 cells in IMDM media (100 µL containing 120,000 cells) were seeded into each well of a 48-well tissue culture plate (Costar, Corning, NY). Four hundred microliters of IMDM (Lonza, Basel, Switzerland) complete media (100,000 U/L penicillin; 100mg/L streptomycin; 0.25mg/L fungizone; 50mg/L gentamicin) was added. The plate was incubated for 22 hours at 37^{o}C in a 7.5% CO_2 humidified atmosphere. Cell apoptosis was measured by following the Annexin V staining protocol (eBioscience, San Diego, CA). At 22 hours, the HL-60 cells were harvested and washed once in PBS and diluted binding buffer, respectively. Then, cells were re-suspended in diluted binding buffer (100 µL) and fluorochrome-conjugated Annexin V was added and incubated for 15 min at room temperature. Cells were washed again in diluted binding buffer and resuspended in 200 µL of diluted binding buffer. Propidium Iodide in PBS (5 µL) was added to cells and the cells were then analyzed on a 3 color fluorescence FACsort Flow Cytometer (Becton Dickinson, San Jose, CA) at the UF ICBR Flow Cytometry core facility within 2 hours. Data was analyzed with FlowJo software (TreeStar, Inc. version 7.6).

Statistical Analyses

Data was expressed as mean ± standard deviation. One-way analyses of variance (ANOVA) with Tukey-HSD comparison of the means were performed using JMP software (Version 8.0, SAS Institute Inc., Cary, NC). Student's t-test was use to compare data from two independent groups. A difference with $P \leq 0.05$ was considered significant.

Results

Ellagitannin Identification and Quantification

The PPE were extracted and partially purified using porous adsorption resin. Chromatogram of PPE showed four peaks that corresponded to four ellagitannins (**Figure 2-1**). Peak identification (**Figure 2-2**) was based on mass and product ion spectra (*137*). Peak A and B were identified as punicalagin A and B according to $[M-H]^-$ *m/z* 1083 and a product ion at *m/z* 781 which suggested the existence of punicalin and ellagic acid moiety. Peak C had a deprontonated ion at *m/z* 463 and a product ion at *m/z* 301 formed by ellagic acid. This peak was identified as ellagic acid-hexoside. Peak D had a deprontonated ion at *m/z* 301, which was identified as ellagic acid. Punicalagtins were the major ellagitannins in PPE, and the content of punicalagin A and B was 166.2 and 324.6 mg/g. The content of ellagic acid-hexoside and ellagic acid was 3.4 and 7.5 mg/g, respectively.

Characteristics of Ellagitannin-gelatin Nanoparticles

PPE-gelatin nanoparticles were fabricated using three different PPE-to-gelatin mass ratios (**Table 2-1**). The mean sizes of particles from the PPE-to-gelatin mass ratios at 1:5, 5:5, and 7:5, measured using dynamic light scattering (DLS), were 102, 149, and 229 nm, respectively. The particle sizes increased significantly with the

increase of the PPE-to-gelatin mass ratio. Scanning Electron Microscopy (SEM) image showed that PPE-gelatin nanoparticles fabricated under these mass ratios had a spherical or approximately spherical morphology (**Figure 2-3**). Mean zeta-potentials of these formed nanoparticles were around +18 mV, indicating that PPE-gelatin nanoparticles had a positive charge on the surface.

Interaction bindings between PPE and gelatin were assessed with Fourier Transform Infrared (FTIR) spectra (**Figure 2-4**). The FTIR spectra of gelatin (**Figure 2-4A**) showed the typical amides I and II peaks at 1699 and 1558 cm^{-1}, respectively. The amide I absorption was mainly due to carbonyl C=O stretching vibration whereas the amide II band consisted both C-N stretching and C-N-H in plane bending (*144-145*). Peaks at 1728 and 1599 cm^{-1} in the FTIR spectra of PPE (**Figure 2-4B**) resulted from carbonyl stretching vibration (*146-147*). FTIR profile (**Figure 2-4C**) of supernatant from PPE-gelatin nanoparticle suspension system was similar to that of PPE (**Figure 2-4B**). However, FTIR spectra (**Figure 2-4D**) of PPE-gelatin nanoparticles showed peaks at 1664 and 1535 cm^{-1}, both of which resulted from peak shifts of PPE and gelatin toward lower wavenumbers. It suggested that both amide I and II and carbonyl C=O in PPE were involved in PPE-gelatin binding and α-helical configuration was formed in PPE-gelatin nanoparticles (*144-145, 148*). The primary interaction binding forces were hydrogen bonding and hydrophobic interactions (*149*).

Production Efficiency and Loading Capacity

Among four ellagitannins identified from the PPE, only punicalagins had the capacity to bind gelatin to form PPE-gelatin nanoparticles (**Table 2-2**). Production efficiency (%) was the weight of dry nanoparticles divided by total weight of PPE and gelatin that were used. The production efficiency of nanoparticles at mass ratio 1:5, 5:5,

and 7:5 was 18.5%, 53.0%, and 62.0%, respectively. Loading capacity (% w/w) is the content of ellagitannins in dry nanoparticles. The loading capacity of punicalagin A under PPE-to-gelatin mass ratio at 1:5, 5:5, and 7:5 was 9.0%, 14.8%, and 10.8%, respectively. The loading capacity of punicalagin B was 9.0%, 25.7%, and 20.5%, respectively.

Apoptosis

Apoptotic properties of pomegranate PPE-gelatin nanoparticles and PPE solution were evaluated using HL-60 cancer cell line at four concentrations. Cells that are in the early stage of apoptosis stain positive for Annexin V but negative for propidium iodide. Necrotic cells and cells at the late stage of apoptosis stain positive for both Annexin V and propidium iodide. PPE solution was more effective than PPE-gelatin nanoparticle suspension in inducing the early stage of apoptosis (**Figure 2-5A**). The differences were not significant at the lowest concentration but became significant as the concentrations increased. At concentrations from 0.0156 to 0.0625 mg/mL, no significant differences were observed between PPE-gelatin nanoparticle suspension and PPE solution in inducing late stage of apoptosis and necrosis (**Figure 2-5B**). However, at the higher concentration (0.125 mg/mL), PPE-gelatin nanoparticles suspension was more effective than PPE solution ($p=0.0144$).

Discussion

PPE-gelatin nanoparticles formed spontaneously due to the affinity between ellagitannins and gelatin. Gelatin has an extended random coil conformation in aqueous solution because it contains higher amounts of proline residues than other proteins or polypeptides (*150*). Gelatin and tannin molecules bind to each other when they are mixed in solution (*150-151*). Magnitudes and selectivity of such binding are determined

by molecular weight and tertiary structures of tannins. It has been proposed that tannins of higher molecular weight have more hydroxyl groups and hydrophobic sites, and thus enhance the interaction with gelatin (*151-152*). In the present study, only punicalagins were able to bind gelatin to form nanoparticles. Tannins of smaller molecular weight, such as ellagic acid and ellagic acid-hexoside, lack tertiary structures and binding capacity (*153*). On the contrary, punicalagin, with higher molecular weight (MW 1084), has a larger and more complex molecular structure providing sufficient affinity toward gelatin to form nanoparticles. Conformation of tannin molecules also affects affinity for gelatin. It has been reported that ellagitannin, compared to gallotannins, had intramolecular biphenyl linkages that can constrain aromatic rings in hydroxydiphenoyl groups, leading to the loss of conformational freedom (*151*). Such structural characteristics enhance binding between ellagitannin and gelatin, however, they may negatively impact affinity for other proteins, such as bovine serum albumin (*151*).

FTIR spectra of PPE-gelatin nanoparticle showed that peaks at 1665 and 1535 cm^{-1} were shifted toward lower wavenumbers from correspondent peaks in gelatin and PPE. The intensity of peaks at 1699 and 1558 cm^{-1} in gelatin FTIR spectra was lower than those in PPE-gelatin nanoparticle FTIR spectra, suggesting that carbonyl C=O stretching vibration in pomegranate ellagitannins was involved in PPE-gelatin nanoparticles. The major binding mechansim appeared to be hydrogen bonding, which was consistent with the appearance of peaks at 1665 and 1535 cm^{-1}, and with the disappearance of hydroxyl groups (peak in the range of 3500 - 3600 cm^{-1}) in gelatin FTIR spectra (*144-145, 149, 154*).

Formation of PPE-gelatin nanoparticles is also influenced by PPE-to-gelatin mass ratio (*74, 155*). When a small amount of tannins is added into a gelatin solution, tannin molecules deposit onto gelatin molecules via hydrogen binding and hydrophobic interactions. As the tannin content increases, single gelatin molecules adsorb more tannin molecules, which cause an increase in particle size. In this study, the particle size with PPE-to-gelatin mass ratios of 1:5, 5:5, and 7:5 was 102, 149, and 229 nm, respectively. The particle sizes measured by DLS appeared bigger than those in SEM photograph (**Figure 2-3**). This was because lyophilized dry particles were used in SEM analysis (*72*). Stability of the nanoparticle system in suspension is impacted by zeta-potential of nanoparticles (*156-157*). Nanoparticles with higher zeta-potentials are more stable in solution due to static repulsion of particles. In this study, zeta-potentials of the nanoparticle suspensions were around +18 mV. The resultant nanoparticles under these three mass ratios were stable opalescent suspensions in deionized water.

Uptake of nanoparticles *in vivo* depends on particle size, zeta-potential, and morphology of nanoparticles. In the gastrointestinal tract, nanoparticles are absorbed into epithelial cells by inter membranous diffusion and by endocytosis mediated by receptors on cell membranes(*13, 118*). Nanoparticle endocytosis was thought to be the major route. Nanoparticles with a particle size below 500 nm were effectively absorbed by enterocytes in the gastrointestinal tract (*118, 158-159*). PPE-gelatin nanoparticles fabricated in this study had a favorable particle size for absorption. Nanoparticles with spherical morphology was found to be captured more easily by receptors on epithelial cells than particles of different shapes (*160*). Surface charge (zeta-potential) of the nanoparticle is another factor that affects direct uptake (*13, 118, 161*). It was reported

that the mucus layer attached to the surface of epithelial cells has negative charges. When positively charged nanoparticles approach the mucus layer, weak ionic interaction is established, prolonging the retention time between nanoparticles and epithelial cells and eventually enhancing the entrapment of nanoparticles in epithelial cells (*13*). Nanoparticles in the present study had the positively charged surface (around +18 mV). Therefore, we anticipate that PPE-gelatin nanoparticles may increase the absorption of ellagitannin *in vivo*. This is of importance because only 3-6% of ellagitannins were found to be absorbed from pomegranate juice (*136, 162*).

Bioactivities of a component are often altered once it is embedded into nanoparticles (*81*). Pomegranate ellagitannins were known to induce cell-cycle arrest and apoptosis of cancer cells (*163*). Punicalagin A and B were known to activate caspase-3 pathway and cleave poly-(ADP-ribose) polymerases, resulting in DNA fragmentation in HL-60 cells and apoptosis (*163-164*). PPE-gelatin nanoparticles were less effective than PPE in inducing the early stage of apoptosis, whereas they had similar effects in inducing the late stage of apoptosis and necrosis. We speculated that cellular uptakes of nanoparticles may be a major reason for the observed differences in apoptotic effects. Our data suggested that PPE-gelatin nanoparticles have lower toxicity than pomegranate ellagitannins.

Summary

The PPE obtained from pomegranate pericarp contained punicalagin A and B, ellagic acid-hexoside, and ellagic acid. Punicalagins had the capacity of binding gelatin to form nanoparticles. The nanoparticles fabricated using three PPE-to-gelatin mass ratios had the particle sizes < 250 nm, zeta-potentials around +18 mv, spherical

morphology, and good loading capacity. PPE-gelatin nanoparticles had lower apoptotic effects on HL-60 cells compared to PPE solution.

Table 2-1. Particle size, zeta-potential, and production efficiency of nanoparticles fabricated using three PPE-to-gelatin mass ratios

Volume of PPE solution (mL)	Volume of gelatin solution (mL)	PPE-to-gelatin mass ratio	Particle size (DLS, nm)	Zeta-potential (mV)	Production efficiency (%)
1	5	1:5	102 ± 9 c	18.3 ± 1.2 a	18.5 ± 4.9 b
5	5	5:5	149 ± 2 b	17.8 ± 0.9 a	53.0 ± 4.2 a
7	5	7:5	229 ± 5 a	18.0 ± 1.3 a	62.0 ± 2.8 a

Data are mean ± standard deviation (n=3). Duplicate tests were done for production efficiency. Means within a column followed by the same letter are not significantly different at $p \leq 0.05$.

Table 2-2. Content and loading capacity of individual ellagitannin in nanoparticles fabricated using three PPE-gelatin mass ratios

Ellagitannin compound		Punicalagin A	Punicalagin B	Ellagic acid-hexoside	Ellagic acid
Content in dry PPE powder (mg/g)		166.2 ± 3.0	324.6 ± 0.3	3.4 ± 0.6	7.5 ± 0.0
Loading capacity (%, w/w)	1:5	9.0 ± 2.6 b	9.0 ± 2.4 b	ND	ND
	5:5	14.8 ± 1.5 a	25.7 ± 2.2 a	ND	ND
	7:5	10.8 ± 0.1 ab	20.5 ± 0.1 a	ND	ND

Means within a column followed by the same letter are not significantly different at $p \leq 0.05$. ND, not detected. Results are represented as mean ± standard deviation of duplicate tests.

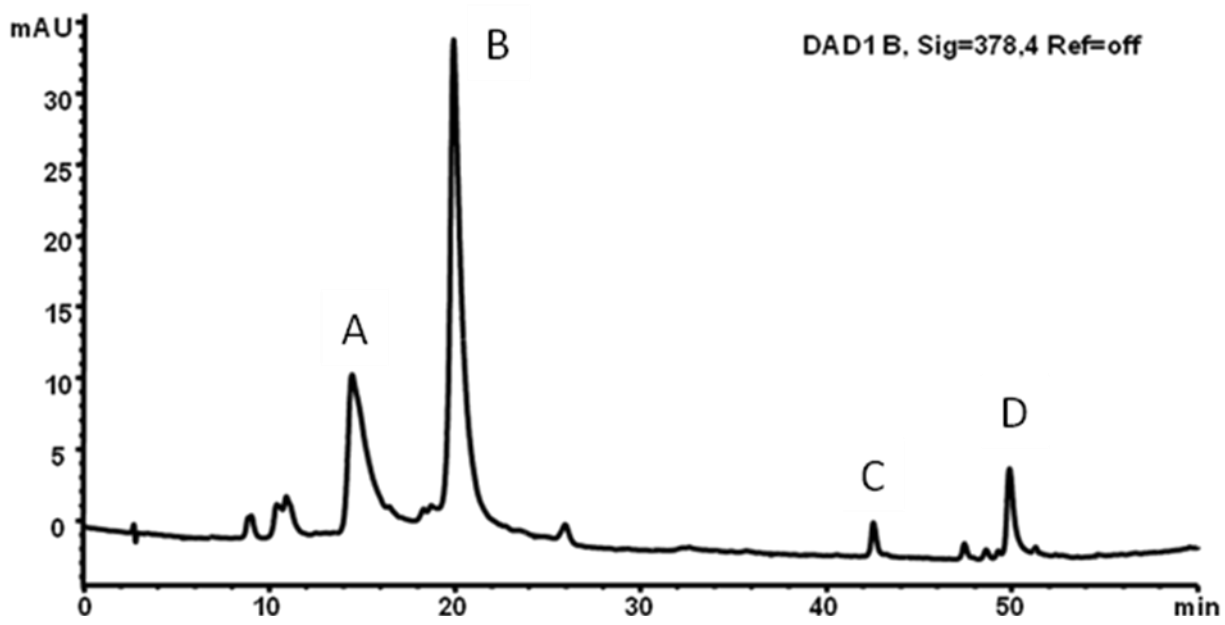

Figure 2-1. HPLC chromatogram of PPE solution. A) Punicalagin A. B) Punicalagin B. C) Ellagic acid-hexoside. D) Ellagic acid.

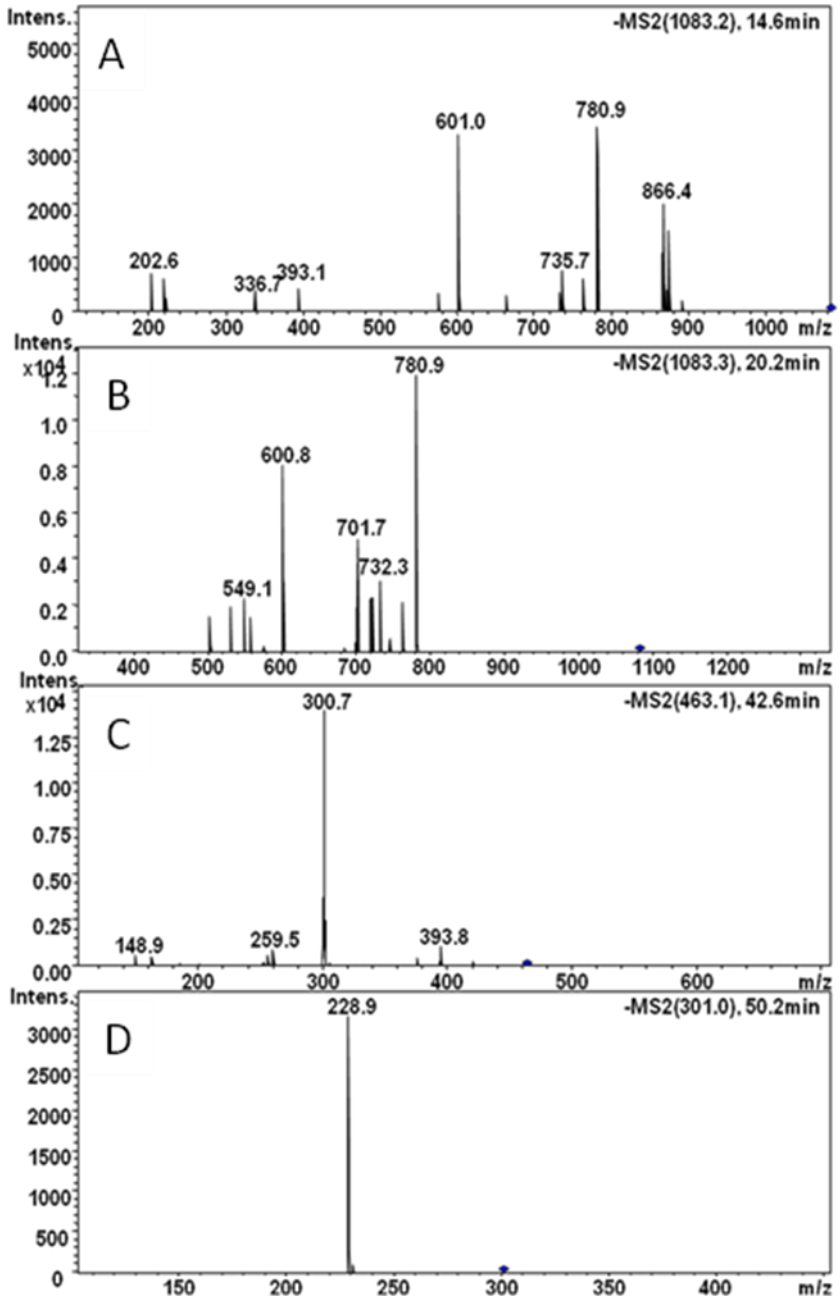

Figure 2-2. Product ion spectra (MS^2) of ellagitannins. A) Punicalagin A. B) Punicalagin B. C) Ellagic acid-hexoside. D) Ellagic acid.

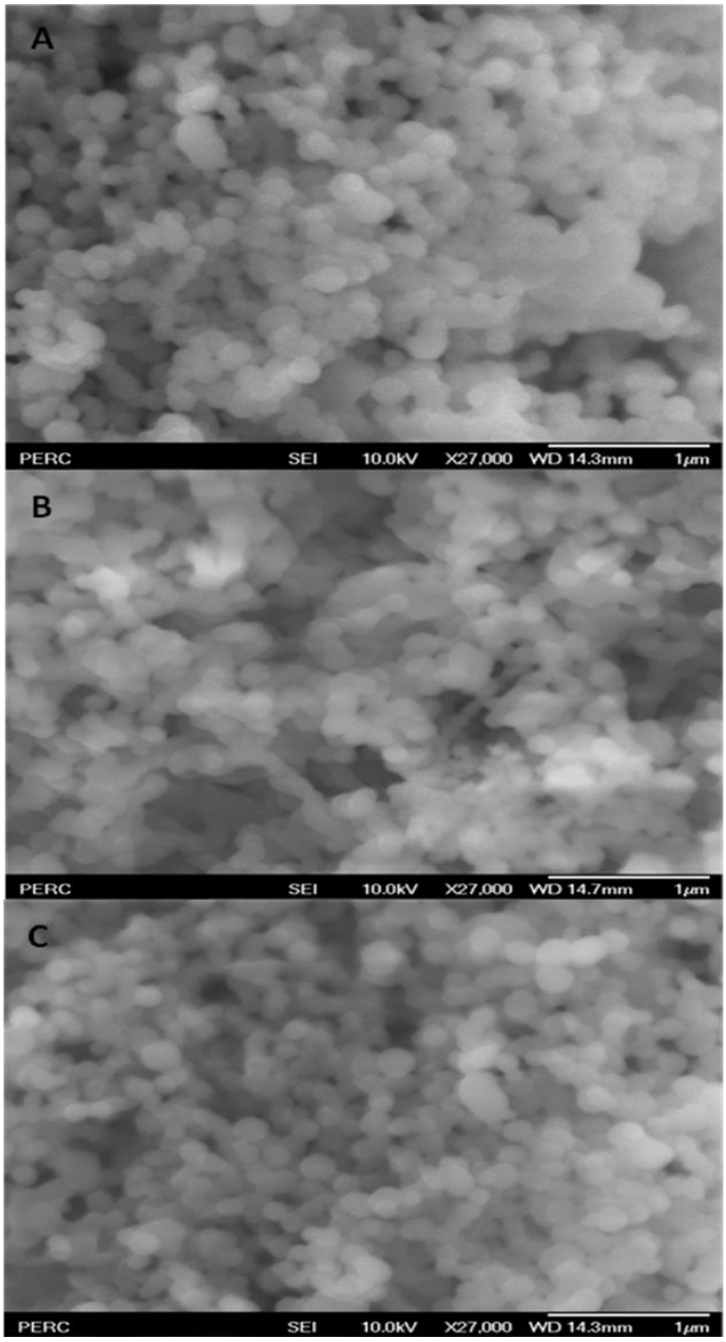

Figure 2-3. Morphology of PPE-gelatin nanoparticles using scanning electron microscopy (SEM). A) PPE-to-gelatin mass ratio of 1:5. B) PPE-to-gelatin mass ratio of 5:5. C) PPE-to-gelatin mass ratio of 7:5.

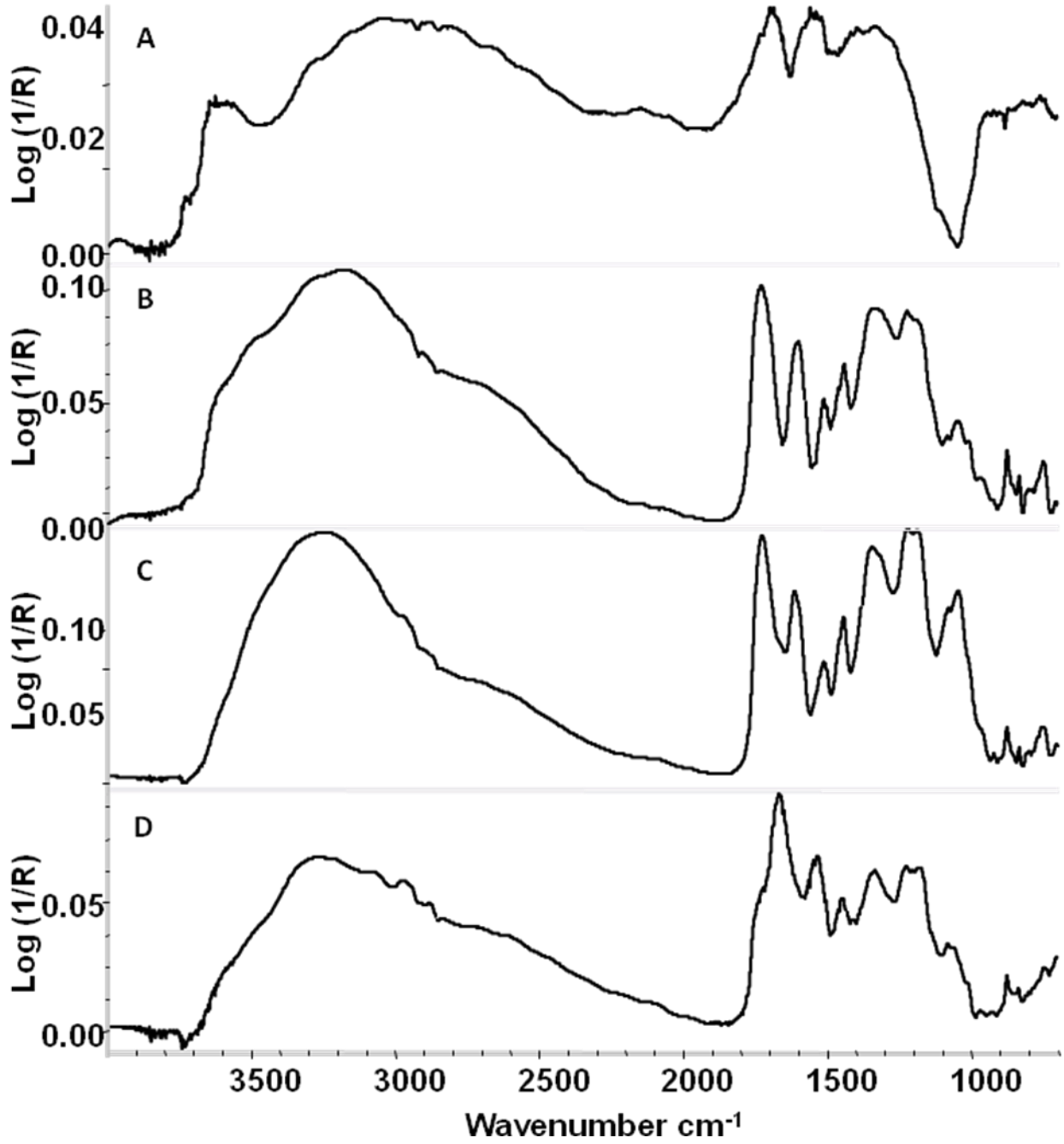

Figure 2-4. Fourier Transform Infrared (FTIR) spectra of PPE-gelatin nanoparticles. A) Gelatin. B) PPE. C) Freeze-dried supernatant. D) Freeze-dried PPE-gelatin nanoparticles.

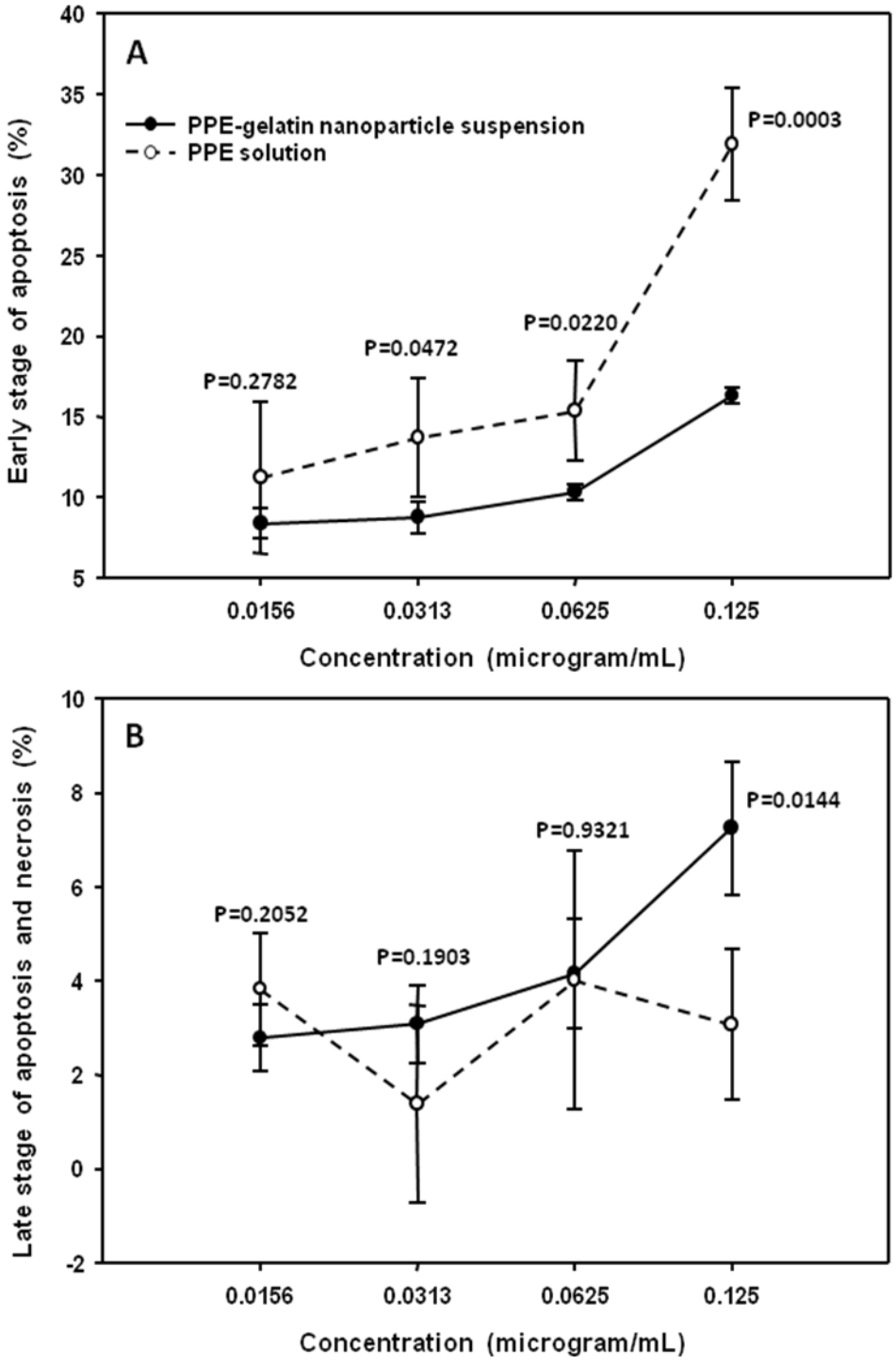

Figure 2-5. Apoptotic effect of PPE-gelatin nanoparticles suspension and PPE solution on HL-60 cancer cells. A) Early stage of apoptosis. B) Late stage of apoptosis and necrosis. PPE-gelatin nanoparticle suspension was fabricated using PPE-to-gelatin mass ratio 5:5. Data are mean ± standard deviation of triplicate tests.

CHAPTER 3
EFFECT OF MASS RATIO, PH, TEMPERATURE, AND REACTION TIME ON FABRICATION OF PARTIALLY PURIFIED POMEGRANATE ELLAGITANNIN (PPE)-GELATIN NANOPARTICLES

Background

Nanoparticle fabrication is of particular interest for nutritional sciences due to the unique benefits of nanosized carriers to increase oral bioavailability of loaded bioactive ingredients (*118, 165*). In the gastrointestinal tract, enterocytes and microfold cell in epithelial wall absorb nanoparticles by endocytosis (*13*). Nanoparticle endocytosis was affected by particle size, zeta-potential, and morphology. It was reported that particle sizes below 500 nm significantly improved the bioavailability of ingredients loaded on nanoparitlces (*118, 158-159*). Zeta-potentials, or surface charges, of nanoparticles affect the stability of nanoparticle suspension system and their absorption in the gastrointestinal tract. It was known that zeta-potential above ±30 mV enhanced the stability of nanoparticles in suspension (*156, 166-167*). Positive zeta-potential stimulated the entrapment of nanoparticles in epithelial walls due to ionic interactions between nanoparticles and the mucus layer on the surface of enterocytes and microfold cell, which prolongs retention time of nanoparticles on epithelial walls (*13*). Spherical nanoparticles can be recognized and captured by receptors on the surface of epithelial cells, causing increased absorption rate compared to nanoparticles of different morphologies (*118, 168*).

Nanoparticles are fabricated using two basic approaches: ‘top-down’ and ‘bottom-up’ (*118, 169*). The ‘top-down’ approach adopts shear or particle collisions as the energy sources to cut larger entities into nanoscale aggregates, whereas self-assembly of smaller molecules is the primary mechanism for the ‘bottom-up’ method.

Self-assembly between molecules takes advantage of intermolecular affinity (*74, 151*). Particle size, zeta-potential, and loading efficiency of self-assembled particles are controlled by reaction conditions. In this study, pomegranate partially purified ellagitannin (PPE)-gelatin nanoparticles were fabricated under different PPE-to-gelatin mass ratios, pH conditions, temperatures, and reaction times to study their effects on particle characteristics, including particle size, zeta-potential, and loading efficiency of ellagitannins. The objective of this study was to identify reaction conditions that can result in smaller particles sizes, positive zeta-potentials, and stable nanoparticle colloidal suspension.

Materials and Methods

Chemicals

Pomegranates were purchased from a local grocery store. Gelatin types A, formic acid, ethanol, and methanol were products of Fisher Scientific (Pittsburg, PA). Amberlite XAD-16N resin was a product of Rohn Haas (Midland, Michigan). Punicalagin and ellagic acid was purchased from Quality Phytochemicals LLC (Edison, NJ) and Sigma-Aldrich (St. Louis, MO), respectively. Partially purified pomegranate ellagitannins (PPE) were prepared according to the published methods with minor modification (*137, 170*). It contained 16.6% of punicalagin A, 32.6% of punicalagin B, 0.3% of ellagic acid-hexoside, and 0.8% of ellagic acid. Other compounds in PPE were not characterized.

Fabrication of PPE-gelatin Nanoparticles

Both gelatin type A (0.5 g) and PPE powder (0.5 g) were dissolved in de-ionized water (1000 mL) to a concentration of 0.5 mg/mL. The pH value of de-ionized water was 5.5 and it dropped to 5.3 and 4.2, respectively, after gelatin and PPE were dissolved. The PPE solution was mixed with the gelatin solution at different reaction conditions for

the self-assembly to occur. The resultant nanoparticle suspensions were centrifuged at 12,000 rpm for 5 min to separate suspension into supernatant and nanoparticles in sediment. Concentrations of punicalagin A and B in the supernatant were quantified using HPLC for loading efficiency assessment.

To study the effects of the PPE-to-gelatin mass ratios on nanoparticle fabrication, 1, 2, 3, 4, 5, 6, 7, 8, or 9 mL of the PPE solution was mixed with 5 mL of the gelatin solution. This gave PPE-to-gelatin mass ratio 1:5 to 9:5. Nanoparticles were fabricated at 25 ^{o}C for 2 days. To study the effects of pH on nanoparticle fabrication, HCl (3 mol/L) and NaOH (6 mol/L) solutions were added drop by drop to adjust pH value of gelatin solution to 1.0, 2.0, 3.0, 4.0, 5.3, 6.0, 7.0, or 11.0. PPE solution of 1, 5, or 7 mL was added into 5 mL of gelatin solution. Size, zeta-potentials, and loading efficiencies of resulting nanoparticles were measured after 2 days of reaction time. For the effects of temperature on nanoparticle fabrication, PPE solution of 1, 5, or 7 mL was mixed with 5 mL of gelatin solution. The suspensions were incubated at different temperatures from 5^{o}C to 50^{o}C for 2 days. Then, characteristics of these nanoparticles were measured. For the effects of reaction time, PPE solution of 1, 5, or 7 mL was added into 5 mL of gelatin solution at 25^{o}C. The characteristics of the nanoparticles were measured at 0.5, 1, 1.5, 2, 3, and 4 days, respectively. Except for gelatin solutions which were used to study pH effects, the pH of gelatin and PPE solutions were not adjusted (5.3 and 4.2, respectively).

Transmission Electron Microscopy (TEM)

PPE-gelatin nanoparticles were fabricated using PPE-to-gelatin mass ratio 5:5 at 25^{o}C for 48 hours. The morphology of dry PPE-gelatin nanoparticles was measured on a JEOL 200CX TEM (JEOL Inc., Tokyo, Japan).

Particle Size and Zeta-potential Measurements

Mean particle size and size distribution of fresh suspensions was measured by dynamic light scattering (DLS) using Nanotrac ULTRA with an external probe (Microtrac Inc., Largo, FL). Samples were measured in triplicate tests and six readings were obtained for each replicate to calculate the average particle size.

Zeta-potentials were determined using Brookhaven ZetaPlus (Brookhaven Instrument Corp., Holtsville, NY). The following parameters were used for zeta-potential measurement: zeta-potential model, Smoluchoswki; media, aqueous; temperature, 22.0^{o}C; viscosity, 0.955 cP; refractive index, 1.334; dielectric constant, 79.63. Triplicate tests were conducted for each sample and ten readings were obtained for each replicate to calculate the average zeta-potential.

Loading Efficiency Assessment

An Agilent 1200 HPLC system consisting of an autosampler, a binary pump, a column compartment, a diode array detector (Agilent Technologies, Palo Alto, CA) was interfaced to a HCT ion trap mass spectrometer (Bruker Daltonics, Billerica, MA). PPE solution and supernatant from PPE-gelatin nanoparticle suspension were filtered through 0.45 µm filter units and 30 µL were injected without further purification, respectively. An Agilent Zorbax ODS column (4.6 mm × 25 cm) was used for separation of ellagitannins. The binary mobile phase consisted of (A) formic acid: water (2:98 v/v) and (B) formic acid: methanol (2:98 v/v). A 65-min gradient was as follows: 0−30 min, 1−20% B linear; 30-45 min, 20- 40% B; 45-60 min, 40-95% B; 60-65 min, 95-1% B; followed by 5 min of re-equilibration of the column before the next run. The detection wavelength on the diode array detector was 378 nm. Electrospray ionization in negative mode was performed using nebulizer 65 psi, dry gas 11 L/min, drying temperature

350^{o}C, and capillary 4000 V. The full scan mass spectra were measured from *m/z* 100-2000. The retention time for punicalagin A, punicalagin B, ellagic acid-hexoside, and ellagic acid were 14.48, 19.93, 42.50, and 49.83 min. Punicalagin A and B were quantified using external standard. Data were collected and calculated using Chemstation software (Version B. 01.03, Agilent Technologies, Palo Alto, CA). The loading efficiency was calculated as (the amount of ellagitannin embedded into PPE-gelatin nanoparticles) / (the amount of ellagitannin used for nanoparticle fabrication).

Data Analyses

Samples were analyzed in triplicate tests and the average values were used. Data was expressed as mean ± standard deviation. Figures were drafted using Sigma-Plot (Version 10.0, Systat Software, Chicago, IL).

Results

Transmission Electron Microscopy (TEM)

Self-assembly between PPE and gelatin in aqueous solution resulted in the formation of nanoparticles. Nanoparticles fabricated using PPE-to-gelatin mass ratio 5:5 had a spherical morphology (**Figure 3-1**).

Effects of PPE-to-gelatin Mass Ratios

The average sizes of the nanoparticles fabricated using the PPE-to-gelatin mass ratios from 1:5 to 6:5 were in a range of 122 nm to 129 nm. A noticeable increase of nanoparticle size was observed as the PPE-to-gelatin mass ratio increased to 7:5 and 8:5, but the sizes were still below 273 nm. The average size dramatically increased to 621 nm at a mass ratio of 9:5. Turbidity in the suspension started to appear at this mass ratio. This observation suggested that there was a critical point when using PPE and gelatin to prepare nanoparticles. At such a point, the binding sites on the gelatin

molecule were saturated by ellagitannins. Adding more tannin molecules caused precipitation due to the particle aggregation. As a result, the colloidal system lost stability and precipitation started to occur. The critical point for PPE and gelatin appeared to be the mass ratio between 8:5 and 9:5.

Zeta-potentials of the nanoparticles increased and reached a peak of +21.7 mV at a PPE-to-gelatin mass ratio of 3:5. It dropped to +15.8 mV and +14.5 mV when the ratio increased to 8:5 and 9:5, respectively (**Figure 3-2B**).

Loading efficiency of punicalagin A was 39.3% at a mass ratio of 2:5 and increased to reach a peak of 78.2% at a mass ratio of 8:5 (**Figure 3-2C**). A similar trend was observed for punicalagin B. Its loading efficiency elevated from 29.6% to 74.5% when the ratio increased from 1:5 to 8:5 (**Figure 3-2D**).

Effects of PH

When gelatin solution in the pH condition of 1.0, 2.0, 3.0 or 11.0 was used for fabrication, particle sizes around 0 nm were observed at three mass ratios. This indicated that no nanoparticles were formed in these pH conditions and the PPE and gelatin existed in a true solution instead of a colloidal suspension (**Figure 3-3A**). At pH 4.0, the sizes of nanoparticles fabricated at the mass ratio 1:5, 5:5, and 7:5 were 21, 44, and 67 nm, respectively. At pH 5.3, the sizes were 122, 129, and 194 nm, respectively. However, the average sizes at the mass ratio 5:5 and 7:5 dramatically increased to 752 nm and 1307 nm at pH above 6.0, respectively. The pH range of 4.0 to 5.3 gave rise to nanoparticles with smaller sizes.

Zeta-potentials of PPE-gelatin nanoparticles were significantly affected by pH (**Figure 3-3B**). Zeta-potentials of the nanoparticles using gelatin solution at pH 4.0 and 5.3 showed +26.1 and +14.7 mV at a mass ratio of 1:5, +23.8 and +17.3 mV at a mass

ratio of 5:5, and +15.0 and +17.0 mV at a mass ratio of 7:5, respectively. Particles fabricated at pH 6.0 and 7.0 had the zeta-potentials of -1.5 and +1.1 mV at a mass ratio of 1:5, -1.3 and +1.0 mV at a mass ratio of 5:5, and +0.9 and -0.7 mV at a mass ratio of 7:5, respectively. Such low zeta-potentials suggested that surface charges of nanoparticles were close to neutral. Low zeta-potential decreases the stability of nanoparticles in colloidal system. Nanoparticles that were fabricated using gelatin solution with pH from 4.0 to 5.3 showed higher surface charges and better stability.

In the pH range from 4.0 to 7.0, increases were observed in loading efficiency of punicalagin A and B from nanoparticles fabricated under these mass ratios. For punicalagin A, its loading efficiency in nanoparticles increased from 48.8% to 54.0% at a mass ratio of 1:5, from 29.5% to 84.3% at a mass ratio of 5:5, and from 44.1% to 70.7% at a mass ratio of 7:5, respectively. Punicalagin B was embedded into nanoparticles, from 10.6% to 21.1%, from 23.1% to 73.9%, and from 33.9% to 63.5%, respectively.

Effects of Temperatures

At a mass ratio of 1:5, nanoparticles fabricated at different temperatures (25-50^{o}C) had similar particle sizes from 114 to 122 nm (**Figure 3-4A**). Highest particle sizes were observed at 5^{o}C in the nanoparticles using mass ratios of 5:5 and 7:5. The sizes decreased to below 316 nm when the temperatures were 25^{o}C and higher.

Nanoparticles fabricated below 25^{o}C at these mass ratios showed stable positive-charge properties (**Figure 3-4B**). Nanoparticles formed at 5, 10, 15, and 25^{o}C had the zeta-potentials from +14.7 to +17.2 mV at a mass ratio of 1:5, from +17.3 to +19.3 mV at a mass ratio of 5:5, and +14.2 to +17.0 mV at a mass ratio of 7:5. However, the fluctuations in zeta-potentials were observed above 25^{o}C. Zeta-potentials

of nanoparticles fabricated at a mass ratio of 7:5 dropped dramatically from +17.0 to -0.9 mV.

Increase of temperature from 5^{o}C to 50^{o}C slightly increased loading efficiency of punicalagin A and B. The increase was more pronounced for punicalagin A at a mass ratio of 1:5.

Effects of Reaction Time

Nanoparticles were fabricated at a mass ratio of 1:5 after 12 hours, and particle sizes remained similar to 4 days (138 nm) (**Figure 3-5A**). At a mass ratio of 5:5, nanoparticles with a size of 75 nm were fabricated after 12 h of interaction, and size of 96 nm was observed by 4 days. Nanoparticles at a mass ratio of 7:5 had a size of 125 nm after 12 h. However, it dramatically increased to 194 nm after 2 days and 923 nm after 4 days, respectively.

Particle surface-charge showed little change at different reaction time (**Figure 3-5B**). Zeta-potentials of the nanoparticles, in reaction time from 0.5 to 4 days, fluctuated between +14.7 and +18.4 mV at a mass ratio of 1:5, between +17.3 and +19.7 mV at a mass ratio of 5:5, and between +15.5 to +17.6 mV at a mass ratio of 7:5, respectively.

In nanoparticles made at a mass ratio of 1:5, loading efficiency of punicalagin A and B remained 68.6% and 38.0% by 4 days, respectively. Nanoparticles made at a mass ratio of 5:5 had a loading efficiency of 67.4% for punicalagin A and 57.2% for punicalagin B at 12 h of interaction, and loading efficiency of 88.3% and 78.9% was obtained after 4 days, respectively. From 78.3% to 85.8% of punicalagin A, and from 70.3% to 73.1% of punicalagin B was observed in loading efficiency from 0.5 to 4 day, respectively.

Discussion

Fabrication of tannin-protein nanoparticles depends on affinity between tannin and protein molecules. The structure of the protein molecule determines the degree of affinity (*150-151, 171*). It was known that the protein with compact tertiary structure provides less hydrophobic sites, constraining interaction with tannin molecules and thus resulting in poor affinity for tannin molecules (*151*). However, gelatin is a proline-rich protein with extended random coil conformation. Hence, gelatin provides more interaction sites for tannin molecules, eventually promoting higher affinity for tannin molecules (*150, 171*). Assembly of tannin-protein particles is also directly determined by the structures of tannin molecules. Tannin molecular weight is a critical factor. Tannins with higher molecular weights possess larger structure and more hydrophobic sites, which results in increased affinity toward protein (*172*). Among four ellagitannins were identified in PPE, punicalagin A and B were predominant in amount and also had much higher molecular weight (1084) than ellagic acid-hexoside (464) and ellagic acid (302) (*170*). Punicalagins were able to bind with gelatin to form nanoparticles, whereas ellagic acid-hexoside or ellagic acid could not.

Self-assembly of tannin and protein molecules is based on interaction among them via hydrogen bonding and hydrophobic interaction as driving forces (*173-174*). The same amount of gelatin was used in the reaction system to provide the same number of hydrophobic sites. Different amounts of the PPE were added into the system to test effects of mass ratio. When a small amount of tannins was added in the system, limited numbers of phenolic hydroxyl groups from tannin molecules were present to interact with excessive amount of protein molecules. In this case, one tannin molecule can bind with two or more gelatin molecules. After more PPE was added, more

hydroxylic groups from the tannins were brought into the system, increasing interaction between tannin and gelatin molecules. As a result, a single protein molecule could carry more tannin molecules and higher loading efficiency was observed. However, when the amount of PPE reached the critical point, interaction sites on gelatin molecules became saturated by tannin molecules. PPE that exceeded this stoichiometric value formed an extended network of hydrogen bonds among nanoparticles, which resulted in their aggregation in suspension (*74, 155*). Therefore, fabrication of nanoparticles should be conducted below the critical point. Nanoparticles at mass ratios below 6:5 had similar particle sizes. However, lower loading efficiencies were observed in lower mass ratios, such as 2:5, 3:5, which indicated that one tannin molecule might assemble with two or three gelatin molecules during the fabrication process. Larger particle sizes were observed from the particles under the mass ratios above 8:5, which suggests that the aggregation occurred when ellagitannin molecules exceeded the saturated value of the network of hydrogen bonds among the nanoparticles. It was proposed that nanoparticles with zeta-potential above ±30 mV provided the best stability. Lower zeta-potentials means weak repulsion between particles and can promote aggregation and precipitation of nanoparticles (*156*). Particles fabricated using the mass ratio above 8:5 suggested nanoparticles had very low zeta potentials. This may promote aggregation of particles and increased particle sizes.

The pH is a critical factor that affects the structures, the conformations, and charge properties of gelatins and tannins. Ellagitannins can be hydrolyzed into ellagic acid in extreme pH conditions (*175-176*). Hydrolyzed ellagitannins will lose the capacity to bind with gelatin. This may explain the absence of nanoparticles when using gelatin

solution in the pH conditions of 1.0, 2.0, 3.0, and 11.0. Gelatins at different pH conditions possess different number of ionizable sites (*177*). Gelatin at its isoelectric point provides the most binding sites, which will promote self-assembly between gelatin and tannin (*74*). However, stability of nanoparticle suspension relies critically on charge repulsions among nanoparticles. Zero repulsions among particles are anticipated when zeta-potentials of nanoparticles are neutral, promoting the aggregation of particles and thus leading to precipitation (*156, 166-167*). The isoelectric point of gelatin is around pH 6.0 to 7.0. Our study showed that particles fabricated using gelatin solution in the pH conditions from 4.0 to 5.3 had small particle sizes and positive zeta-potential. However, dramatic increases of particle sizes were observed at pH 6.0 and 7.0. This was consistent with weak zeta-potentials and the declined repulsion among the particles.

Excessively high temperature alters the structural conformations of ellagitannins and gelatins (*177-178*). In our study, PPE-gelatin nanoparticles were able to be fabricated at 50^{o}C, suggesting that this temperature has little negative influence on molecular binding. It was known that the coil conformation of gelatin became looser and more extended with the increase of temperature (*74*). Higher temperature exposes more hydrophobic groups from gelatins to bind with more ellagitannin molecules. As a result, loading efficiency of tannin molecules was increased (*74, 177*). Particles fabricated under the mass ratios of 1:5, 5:5, and 7:5, within the temperature from 25 to 50^{o}C, had small particle sizes and high loading efficiency, respectively. When interaction happens at lower temperatures, compact coil conformation of gelatin provides less hydrophobic sites for interaction with tannin molecules. As a result, larger

particles were formed. Particles sizes prepared from the mass ratios of 5:5 and 7:5 were above 500 nm when the temperature was below 25^{o}C.

When PPE and gelatin were mixed, interaction between them occurs rapidly till their hydrophobic sites are saturated (*151, 171*). The suspension will be stable if no more tannins molecules participate in it to induce particle aggregation. In our study, nanoparticle suspensions at the mass ratios of 1:5 and 5:5 had favorable nanoparticle characteristics after 0.5 day and remained stable untill 4 days. Nanoparticle suspension from the mass ratio of 7:5 had constant particle characteristics by 2 day reaction, but increased particle sizes with large variation were observed after 4 days. It indicated that assembly of particles was promoted and eventually led to precipitation.

Summary

PPE-to-gelatin mass ratio determined characteristics and stability of nanoparticle suspensions. The critical point for PPE-gelatin nanoparticles was at a mass ratio of 8:5. Nanoparticles prepared in a pH range from 4 to 5.3 had particle sizes and zeta-potentials that favor higher bioavailability of loaded ellagitannins. Reaction temperatures from 25 to 50^{o}C had the positive influence on nanoparticle characteristics. Self-assembly occurred rapidly between gelatin and ellagitannin and fabrication was done after 12 hours and remained stable after 4 days.

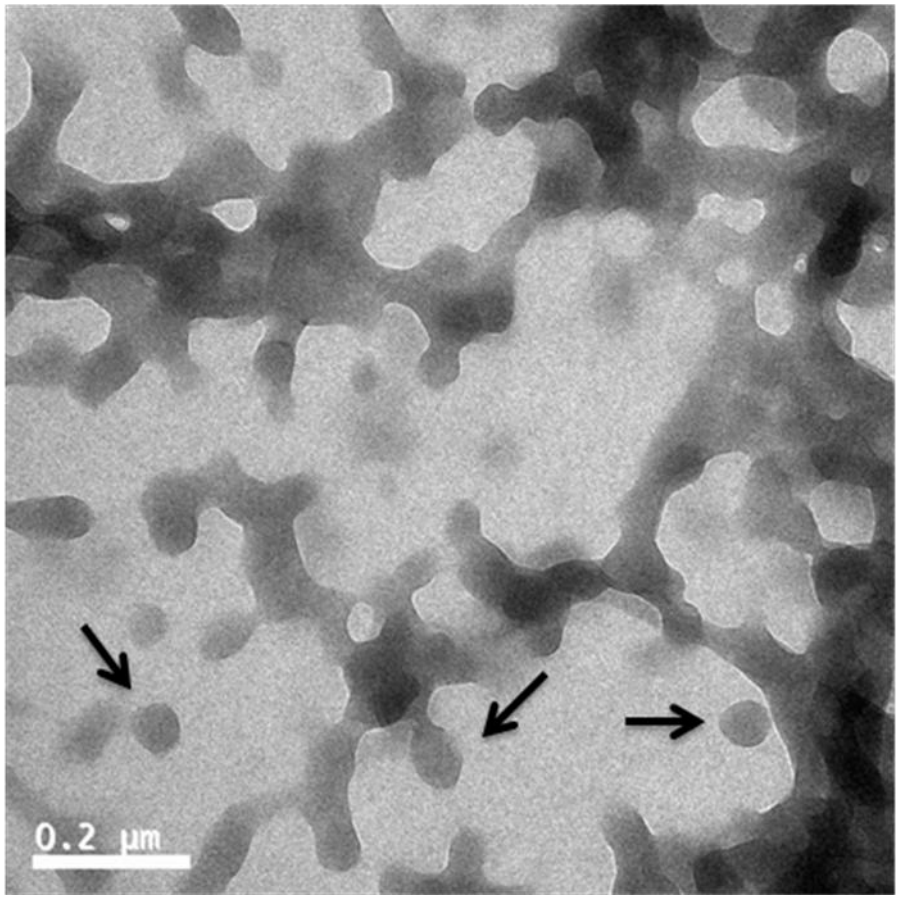

Figure 3-1. Morphology of PPE-gelatin nanoparticle using transmission electron microscopy (TEM). PPE-gelatin nanoparticles were fabricated using PPE-to-gelatin mass ratio of 5:5 at 25^{o}C for 48 h. The pH of gelatin and PPE water solutions were 5.3 and 4.2, respectively. Nanoparticles in colloidal suspension are denoted by arrows.

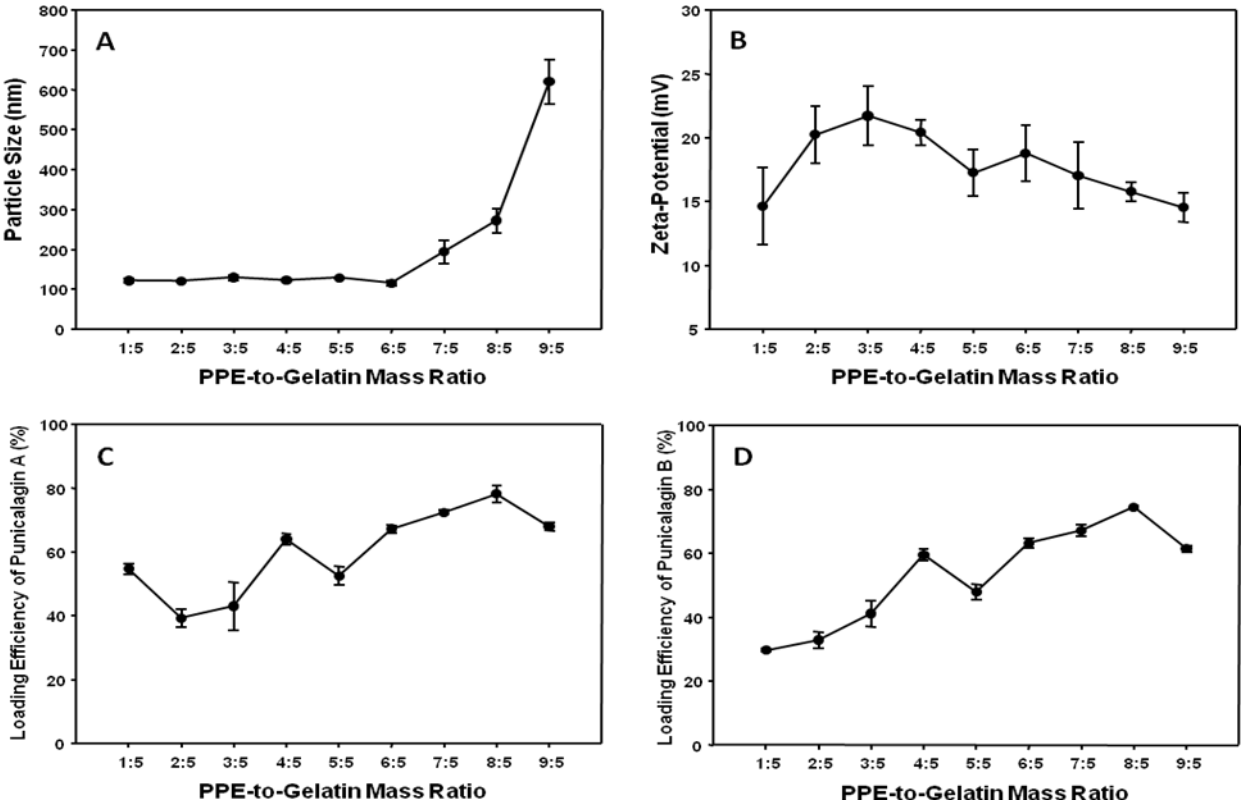

Figure 3-2. PPE-gelatin nanoparticle characteristics under the conditions of PPE-to-gelatin mass ratio from 1:5 to 9:5 at 25^{o}C for 2 days. A) Particle size. B) Zeta-potential. C) Loading efficiency of punicalagin A. D) Loading efficiency of punicalagin B. The pH of gelatin and PPE water solutions were 5.3 and 4.2, respectively.

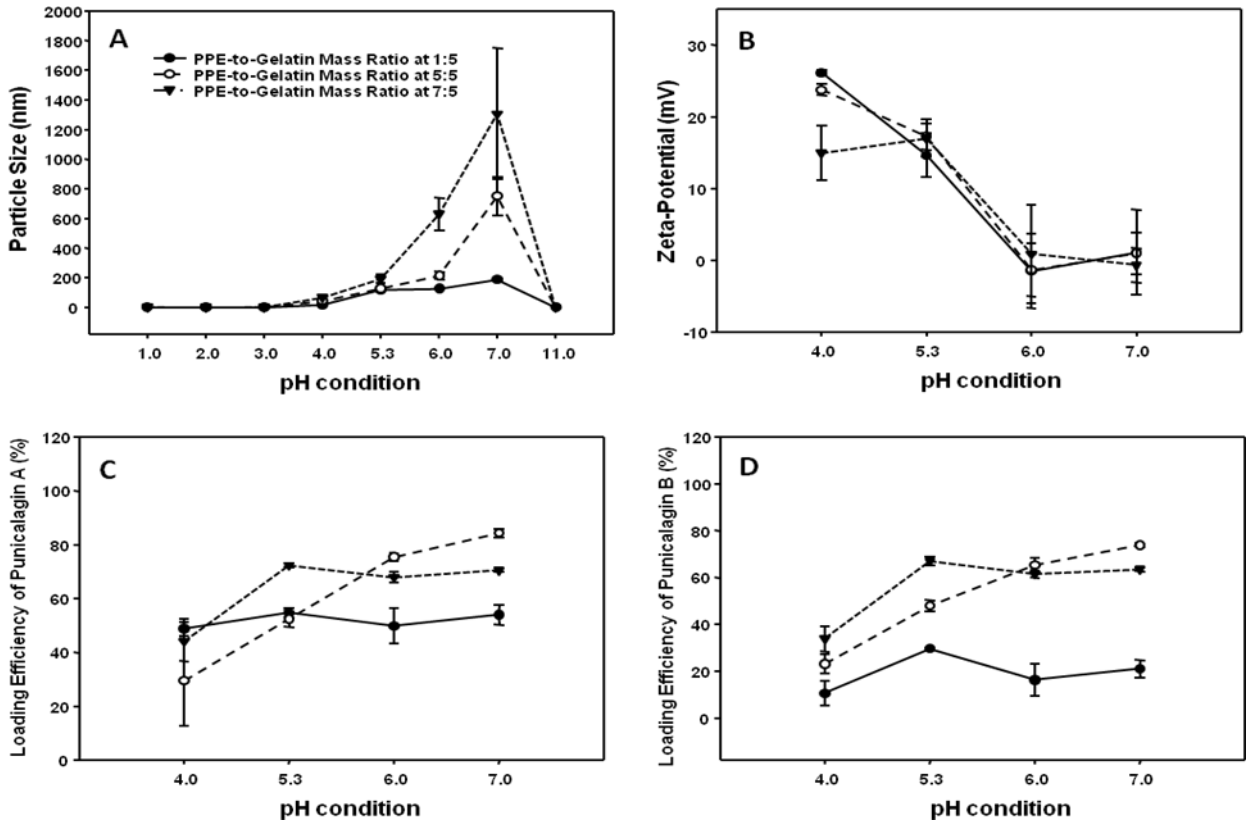

Figure 3-3. PPE-gelatin nanoparticle characteristics under the conditions of PPE-to-gelatin mass ratio at 1:5, 5:5, and 7:5, pH of gelatin solution were 1.0, 2.0, 3.0, 4.0, 5.3, 6.0, 7.0, and 11.0, temperature at 25^{o}C, and reaction time of 2 days. A) Particle size. B) Zeta-potential. C) Loading efficiency of punicalagin A. D) Loading efficiency of punicalagin B. The pH of gelatin and PPE water solution were 5.3 and 4.2, respectively.

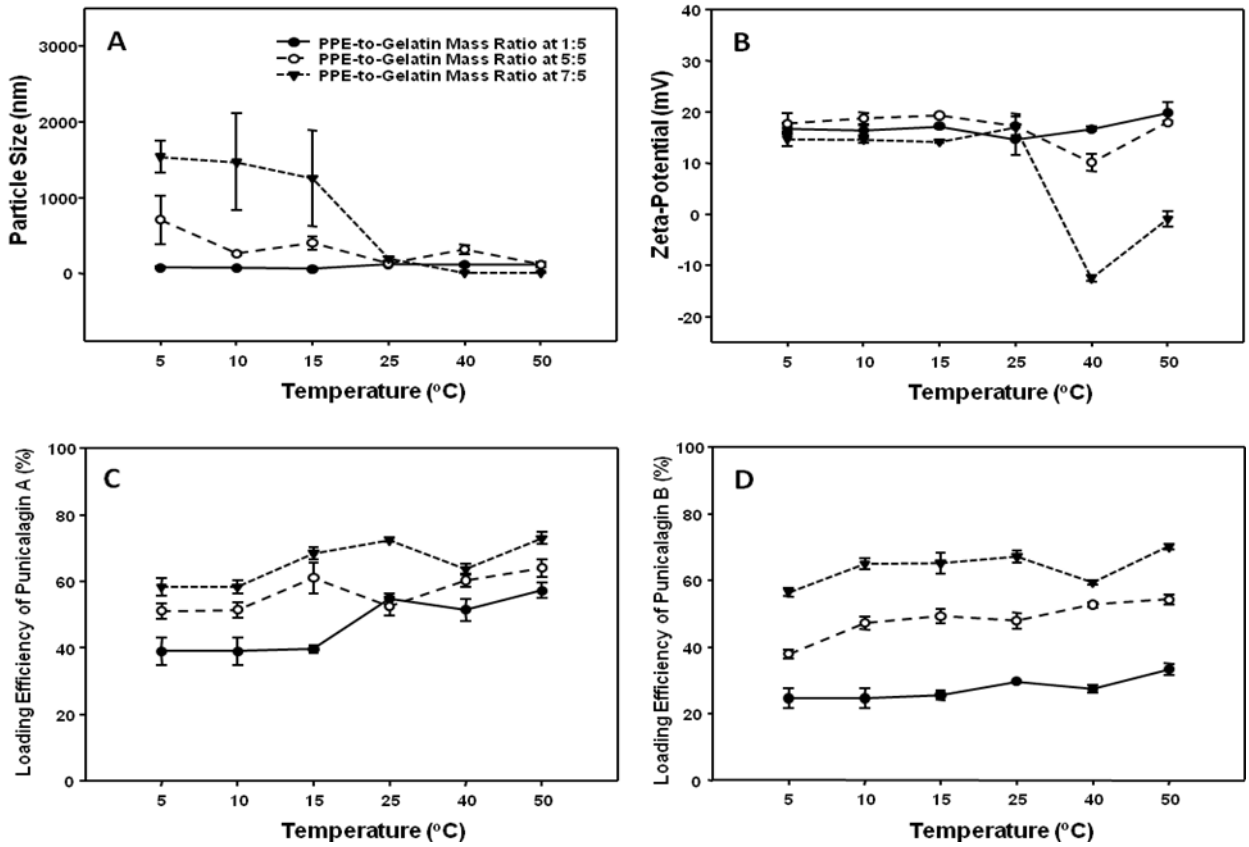

Figure 3-4. PPE-gelatin nanoparticle characteristics under PPE-to-gelatin mass ratio at 1:5, 5:5, and 7:5 at 5, 10, 15, 25, 40, or 50^{o}C for 2 days. A) Particle size. B) Zeta-potential. C) Loading efficiency of punicalagin A. D) Loading efficiency of punicalagin B. The pH of gelatin and PPE water solutions were 5.3 and 4.2, respectively.

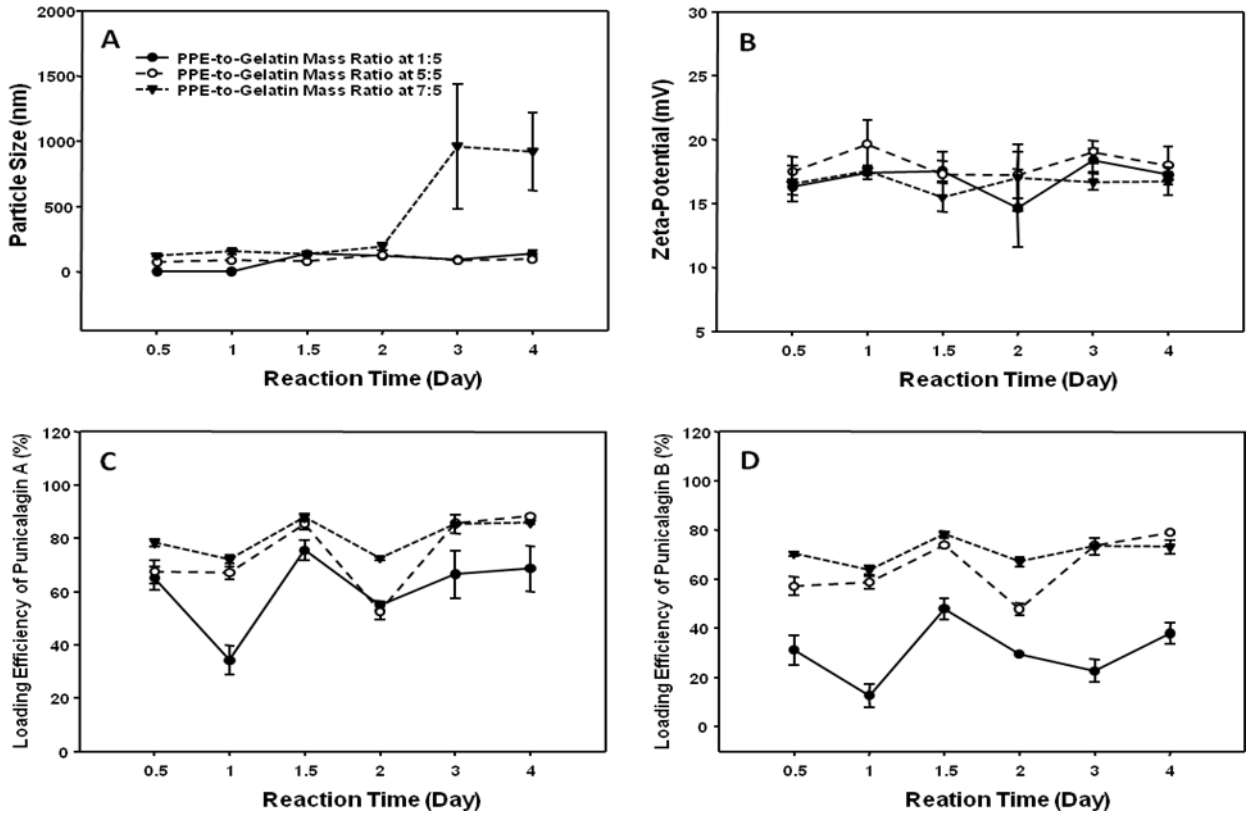

Figure 3-5. PPE-gelatin nanoparticle characteristics under PPE-to-gelatin mass ratio at 1:5, 5:5, and 7:5, at 25^{o}C for 0.5, 1, 1.5, 2, 3, or 4 days. A) Particle size. B) Zeta-potential. C) Loading efficiency of punicalagin A. D) Loading efficiency of punicalagin B. The pH of gelatin and PPE water solutions were 5.3 and 4.2, respectively.

CHAPTER 4
FABRICATION OF COATED BOVINE SERUM ALBUMIN (BSA)-EPIGALLOCATECHIN GALLATE (EGCG) NANOPARTICLES AND THEIR TRANSPORT ACROSS MONOLAYERS OF HUMAN INTESTINAL EPITHELIAL CACO-2 CELLS

Background

(-)-Epigallocatechin gallate (EGCG) is a major flavan-3-ol in green tea (*179*). EGCG has been reported to reduce plaques related to dementia and inhibit growth of brain, prostate, cervical, and bladder cancers by inducing apoptosis (*180-184*). The absorption rates of EGCG were less than 5% in humans and below 1% in rats after oral administration (*185-188*). Such low bioavailability of EGCG limits its bioactivity *in vivo*.

Nanoparticles are defined as particles below 1000 nm in size by biological sciences (*132*). Nanoparticles have the potential to increase absorption of bioactive compounds through several mechanisms. The low absorption rate of EGCG is attributed to its poor permeability across intestinal epithelium because passive diffusion is thought to be its only absorption route (*68, 189*). A number of nanoparticles, such as chitosan nanoparticles and poly(lactic-co-glycolic acid) nanoparticles, are known to enhance absorption of bioactive compounds by opening tight junctions or improving their transcellular absorption by nanoparticle endocytosis (*13, 118, 121*). Secondly, low bioavailability of EGCG is also caused by its poor stability in the gastrointestinal tract since EGCG was readily oxidized or degraded under acidic (pH below 1.5) or neutral pH conditions (*55*) . It was suggested that chitosan nanoparticles protected EGCG from degradation in the gastrointestinal tract (*190-191*). Lastly, nanoparticles may increase solubility of hydrophobic compounds to enhance the absorption in small intestine (*192*). For example, cyclodextrin has been widely used as a carrier to increase the solubility of type II drugs for the enhancement of absorption (*192*).

Besides nanoparticles, absorption enhancers are also suggested to improve absorption of bioactive compounds. Chitosan is an absorption enhancer that is known to promote absorption of drugs by disrupting tight junctions among epithelial cells or enhancing cellular uptake on epithelial cells (*193-195*). Poly-lysine has a structure similar to many cell penetrating peptides and it has the capacity to increase endocytotic cellular uptake of drugs (*196-199*).

The objectives of this study were to fabricate absorption-enhancer coated nanoparticles and to investigate the impact of coating on size, surface chemistry, and zeta-potential of nanoparticles. We hypothesized that coating the EGCG loaded BSA nanoparticles with absorption enhancer may improve the stability and/or the absorption of EGCG.

Materials and Methods

Chemicals

(-)-Epigallocatechin gallate (EGCG) was purchased from Quality Phytochemicals LLC (Edison, NJ). Poly-ε-lysine was a gift from Zhejiang Silver-elephant Bioengineering Co (Taizhou, Zhejiang, China). Bovine serum albumin (BSA), chitosan (5-20mPa.s), glutaraldehyde, simulated gastric fluid (SGF, pH adjusted to 4.5 to simulate fed state), simulated intestinal fluid (SIF, pH adjusted to 6.5) without pancreatin, SIF with pancreatin, and pepsin were purchased from Fisher Scientific (Pittsburg, PA). Fluorescein isothiocyanate (FITC) labeled BSA was purchased from Fisher Scientific (Pittsburg, PA). Alexa^{TM} 594-concanavalin A was purchased from Molecular Probes (Grand Island, NY). Caco-2 cells were obtained from American Type Culture Collection (Manassas, VA).

Fabrication of BSA Nanoparticles

BSA nanoparticles were fabricated using a desolvation method. Briefly, 5 mL of 5 mg/mL BSA water solution was transferred to a beaker under a stirring speed of 750 rpm at room temperature. Ten mL pure ethanol was added drop-wise to BSA solution till a white-milk suspension was formed. The suspension was stirred for additional 10 min before 200 μL of glutaraldehyde was added drop-wise to the suspension. The suspension was stirred for 1 more hour. Afterwards, the suspension was centrifuged at 13,300 rpm for 10 min to remove the supernatant. The sediment was washed by deionized water three times and then re-suspended in 5 mL of deionized water.

Loading EGCG into BSA Nanoparticles

BSA nanoparticles suspension (5mL) was stirred at 750 rpm. EGCG water solution (15 mL, 1mg/mL) was added drop-wise to the suspension and the suspension was stirred at the same speed for 30 min.

Coating the BSA-EGCG Nanoparticles

Poly-ε-lysine solution (2mL, 2 mg/mL) or chitosan solution (2 mL, 1 mg/mL) was added drop-wise to 20 mL of BSA-EGCG nanoparticles suspension at 750 rpm for 60 min.

Scanning Electron Microscopy (SEM)

BSA-EGCG nanoparticles (BEN), poly-ε-lysine coated BSA-EGCG nanoparticles (PBEN), and chitosan coated BSA-EGCG nanoparticles (CBEN) suspensions were lyophilized for 24 hours. Morphology of dry BEN, PBEN, and CBEN were measured using Field Emission Scanning Electron Microscope (Model JSM-633OF, JEOL Ltd, Tokyo, Japan).

Loading Efficiency and Loading Capacity Assessments

The nanoparticle suspensions were centrifuged at 13,300 rpm for 10 min to collect the supernatant. The supernatant was analyzed using HPLC to measure the EGCG content. The loading efficiency and the loading capacity were calculated using the equations below:

Loading efficiency = (EGCG amount loaded into nanoparticles/EGCG amount used for nanoparticle fabrication) × 100%.

Loading capacity = (EGCG amount loaded into nanoparticles/Dry nanoparticle amount) × 100%.

Nanoparticles Characterization under Different pH Conditions

The nanoparticles were characterized under different pH conditions following a published paper with minor modifications (*200*). Briefly, BEN, PBEN, or CBEN water suspension was adjusted to pH of 1.5, 3.5, 4.5, 5.0, 5.5, 6.0, 6.5, and 7.0 using a diluted HCl or NaOH solution. Mean particle size and zeta-potential were measured on Zetatrac (Microtrac Inc., Largo, FL). Samples were measured in duplicate tests at 25^{o}C and three readings were obtained for each replicate to calculate the average particle size and zeta-potential.

Release of EGCG in Simulated Digestive Fluids

The release profile of EGCG was measured in simulated gastric fluid (SGF) and in simulated intestinal fluid (SIF) with or without digestive enzymes (*201*). Briefly, dry nanoparticles were suspended in 5 mL of SGF (pH 4.5) with or without 0.1% pepsin (w/v) and incubated at 37^{o}C for 0.5 h. Subsequently, 1 mL of the sample was centrifuged at 13,300 rpm for 10 min. The supernatant (0.5 mL) obtained was mixed with 0.05 mL of ascorbic acid solution (1% ascorbic acid in 0.28% H_3PO_4 water solution)

to reach pH 2.5, and then analyzed on HPLC. The dry nanoparticles were suspended in 5 mL of SIF (pH 6.5) without or with 1.0% pancreatin (w/v) and incubated at 37^{o}C for 2 hours. Then, 1 mL of the sample was centrifuged at 13,300 rpm for 10 min. The supernatant (0.5 mL) obtained was mixed with 0.4 mL of 1% ascorbic acid solution, followed by HPLC analysis. An Agilent Zorbax SB C18 column (4.6 mm × 250 mm) was used to analyze EGCG. The binary mobile phase consisted of 0.04 % acetic acid: water (A) and acetonitrile (B). A 22-min gradient was used as follows: 0−20 min, 10−30% B linear; 20-22 min, 30-10% B linear; followed by 2 min of re-equilibration of the column before the next run. The detection wavelength on the diode array detector was 280 nm. The injection volume was 20 µL with a flow rate of 1 mL/min. Each sample was analyzed in duplicate tests. The cumulative EGCG release was calculated using the following equation:

Cumulative EGCG release (%) = *(EGCG amount in supernatant/EGCG amount in dry nanoparticles) ×100%*

Storage Stability of Loaded EGCG in Nanoparticles

EGCG (1 mg) or the dry nanoparticles with equal amounts of EGCG were kept for 0, 3, 6, 9, 12, or 24 hours at 60^{o}C. At each time point, the samples were mixed with 1 mL of ethanol/water solution (9:1 v/v) to extract EGCG. After centrifuging at 13,300 rpm for 10 min, the supernatant was removed and analyzed on HPLC. Each treatment was carried out in duplicate tests. EGCG remaining percentage was calculated using the following equation:

EGCG remaining percentage (%) = *(EGCG amount in supernatant/Initial EGCG amount) × 100%*

EGCG Absorption on Caco-2 Cell Monolayers

Caco-2 cells were seeded at 6-well transwell plates with an internal diameter of 24 mm and membrane growth area of 4.67 cm^2 (Corning Inc, Lowell, MA). The cells were cultured using Dulbecco's modified eagle media containing 20% fetal bovine serum, 1% penicillin-streptomycin, and 1% non-essential amino acids. The cells were grown to confluence and allowed to mature for 17 days at 37^oC and 5% CO_2. The cell culture media was changed every 1-2 days. The permeability study was carried out in triplicate tests after the transepithelial electrical resistance (TEER) was above 600 $\Omega \times cm^2$, measured using an epithelial volt-ohm meter (Millicell ERS-2, Millipore Corp, Billerica, MA). The permeability study followed a published paper with minor modifications (*68*). Dry EGCG, BEN, PBEN, or CBEN was added into Hank's balanced salt solution (HBSS, pH adjusted to 6.0) to control EGCG concentration at 0.023 mg/mL. One and half milliliter of each sample was transferred to the apical chamber of the transwells plate and 2.6 mL of the fresh buffer was added to the basolateral chamber. After incubation at 37^oC for 30, 60, 90, and 120 min, the transepithelial electric resistance (TEER) was measured. Subsequently, 0.5 mL of the samples was taken from the basolateral chamber, acidified with ascorbic acid solution to adjust to pH 2.5 and stored in -80^oC until analyses. The fresh buffer (0.5 mL) was re-filled to the basolateral chamber. The samples were analyzed by HPLC-ESI-MS^n using a published method with minor modifications (*68*). An Agilent Zorbax SB C18 column (4.6 mm × 250 mm) was used. The binary mobile phase consisted of 0.04 % acetic acid: water (A) and acetonitrile (B). A 22-min gradient was used as follows: 0−20 min, 10−30% B linear; 20-22 min, 30-10% B linear; followed by 2 min of re-equilibration of the column before the next run. The injection volume was 20 µL with a flow rate of 1 mL/min. Electrospray

ionization in negative mode was performed using nebulizer 65 psi, drying gas 11 L/min, drying temperature 350^{o}C, and capillary 4000 V. The MRM was used to monitor the transition of deprotonated EGCG *m/z* 457 $[M - H]^-$ to the product ion *m/z* 169. EGCG was used as an external standard. Quantification was conducted using QuantAnalysis (Version 2.0, Bruker Daltonics Inc, Billerica, MA). The apparent permeability coefficient (P_{app}) of EGCG was calculated using the following equation:

$$P_{app} = (dQ/dt) \times (1/AC_0)$$

Where dQ/dt is the permeability rate (μg/s), C_0 is the initial concentration in the apical chamber (μg/mL), and A is the surface area of filter (cm^2), which was 4.67 cm^2 in this study.

Confocal Laser Scanning Microscopy

Fluorescein isothiocyanate (FITC) labeled BSA was used to fabricate FITC labeled BSA nanoparticles. The fabrication procedures followed the same procedure of fabrication of BEN, PBEN, and CBEN. Caco-2 cells were seeded on a four-well chambered coverglass (Fisher Scientific Inc., Pittsburg, PA) and incubated at 37°C in 95% air and 5% CO_2 environment until the monolayer was formed. On the day of experiment, the growth medium was replaced by HBSS buffer (pH 6.0). After equilibration in the buffer at 37°C for 30 min, the buffer was replaced with FITC labeled BEN, FITC labeled PBEN, and FITC labeled CBEN suspension. Then, the monolayers were further incubated for 60 min. At the end of experiment, the cells were washed six times with the buffer to remove the excess nanoparticles. Subsequently, the cells were fixed in 2% paraformaldehyde for 1 hour, and then washed with the buffer an additional three times. Afterward, Alexa^{TM} 594-concanavalin A was used to stain the cell membrane for 30 min and then washed with buffer three times. Finally, the monolayers

were kept in the buffer until they were examined on a confocal laser scanning microscope (Leica TCS SP2 AOBS system, Germany) equipped with Leica LCS imaging software.

Statistical Analyses

Data was expressed as mean ± standard deviation. Student's t test was used to compare mean values between two groups. One-way analyses of variance with all paired Tukey HSD comparison of the means were performed using JMP software (Version 8.0, SAS Institute Inc., Cary, NC). A difference with $p \leq 0.05$ was considered significant.

Results

Particle Morphology, EGCG Loading Efficiency and Loading Capacity

Lyophilized nanoparticles were measured by SEM (**Figure 4-1**). BEN, PBEN, and CBEN showed a spherical morphology with the particle sizes between 100 and 200 nm. The loading efficiency of EGCG on BEN was 32.3% (**Table 4-1**). Poly-ε-lysine coating increased EGCG loading efficiency to 35.4%. Coating with chitosan did not change the loading efficiency. The loading capacity of EGCG in BEN was 18.9% (w/w) and remained unchanged after BEN was coated with poly-ε-lysine or chitosan (17.0% and 16.0%, respectively).

Impact of Coating on Particle Size and Zeta-potential

The sizes of the nanoparticles in suspension appeared to be pH-dependent (**Figure 4-2**). The impact of coatings on particle size also depended on pH. BEN had an average size of 304 nm at pH 1.5 and 301 nm at pH 3.5 (**Figure 4-2A**). This particle size dramatically increased to 2828 nm at pH 4.5 and 2460 nm at pH 5.0 due to the particle aggregation. The particle sizes dropped back to between 170 nm and 300 nm at

a pH range 5.5-7.0. Poly-ε-lysine coating prevented the particle aggregation at and below pH 6.0. The average sizes of PBEN at pH 1.5, 3.5, 4.5, 5.0, 5.5, and 6.0 were 297 nm, 264 nm, 286 nm, 296 nm, 265 nm, and 358 nm, respectively. At pH 6.5 and 7.0, the size of PBEN increased to 5800 nm and 5330 nm, respectively. A similar phenomenon was also observed for CBEN. CBEN had an average size of 322 nm, 269 nm, 247 nm, 359 nm, 381 nm, and 383 nm at pH of 1.5, 3.5, 4.5, 5.0, 5.5, and 6.0, whereas the average size increased to 1315 nm and 2700 nm at pH 6.5 and 7.0, respectively.

Coating also altered the zeta-potential of the particles (**Figure 4-2B**). BEN showed positive surface charges over +20 mV at pH 1.5 and 3.5. The zeta-potentials of BEN were -28.1 mV, -11.5 mV, -19.9 mV, -21.6 mV, -42.9 mV, and -34.2 mV at pH 4.5, 5.0, 5.5, 6.0, 6.5, and 7.0, respectively. Poly-ε-lysine coating caused the nanoparticles to possess positive charge of 41.2 mV, 55.0 mV, 23.0 mV, 40.3 mV, 39.9 mV, and 38.5 mV at pH 1.5, 3.5, 4.5, 5.0, 5.5, and 6.0, respectively. However, the zeta-potentials of PBEN drastically dropped to 4.4 mV and 4.0 mV at pH 6.5 and 7.0, respectively. CBEN showed the zeta-potentials of 45.0 mV, 43.3 mV, 27.8 mV, 12.6 mV, 10.5 mV, and 14.6 mV at pH 1.5, 3.5, 4.5, 5.0, 5.5, and 6.0. However, adjusting pH to 6.5 and 7.0 reduced the zeta-potentials of the particles to 2.4 mV and 2.8 mV, respectively. The decreases in zeta-potentials coincided with particle aggregation and the increase in particle sizes.

Impact of Nano-encapsulation and Particle Coating on EGCG Release in Simulated Digestive Fluids

Release of EGCG from the nanoparticles was assessed in simulated gastrointestinal fluids with or without digestive enzymes (**Figure 4-3**). After incubation of the nanoparticles in pepsin-free simulated gastric fluid for 0.5 hour, around 25% of

EGCG was released from all tested nanoparticles with no significant differences on EGCG release observed among uncoated and coated nanoparticles (**Figure 4-3A**). Adding pepsin in simulated gastric fluid caused more EGCG to be released from BEN, PBEN, and CBEN. BEN released 52.7% of EGCG in SGF with pepsin after 0.5 hour, whereas the release percentage of EGCG from PBEN and CBEN were 33.0% and 37.1%, respectively. The release percentages of EGCG from the coated nanoparticles were significant lower than that from BEN.

A similar phenomenon on EGCG release from the nanoparticles was observed in SIF with or without pancreatin (**Figure 4-3B**). BEN released 38.1% of EGCG in pancreatin-free simulated intestine fluid after 2 hours. The release of EGCG from PBEN and CBEN was 29.1% and 24.3%, respectively. The releases of EGCG were significantly increased after pancreatin was added to intestinal fluid for BEN and CBEN. Release of EGCG from PBEN in SIF with pancreatin was 44.6 % compared to 29.1% of EGCG release in SIF without pancreatin. However, no statistical difference was observed. Coating inhibited EGCG release in SIF with pancreatin. BEN released 68.5% of EGCG in 2 hours. PBEN released 44.6% of EGCG, which was significantly less than that from BEN. The release of EGCG from CBEN was 54.2%, which was not significantly different from BEN.

Impact of Nano-encapsulation and Particle Coating on EGCG Stability

EGCG loaded in the nanoparticles degraded faster than pure EGCG at 60^{o}C (**Figure 4-4**). About 10%-20% of EGCG in all the nanoparticles was degraded at 3 hours, whereas pure EGCG showed no degradation. At 6 hours, about 40% of EGCG in BEN remained. Particle coating increased EGCG remaining percentage to 60%. In contrast, 91% of EGCG remained in pure EGCG sample. Such trend continued to 24

hours. However, the positive effects of coating on EGCG stability were no longer significant after 6 hours.

Impact of Nano-encapsulation and Particle Coating on EGCG Transport on Caco-2 Monolayers

The apparent permeability coefficient (P_{app}) of EGCG in the solution was 3.83 × 10^{-7} cm/s at 30 min and the P_{app} of EGCG remained similar during the incubation period (**Figure 4-5A**). However, the highest P_{app} of EGCG in all the nanoparticles appeared at 30 min and then a decreasing trend of P_{app} of EGCG was observed. P_{app} of EGCG in CBEN (11.17 × 10^{-7} cm/s) was significantly higher than that of EGCG solution at 30 min and it was similar to that of BEN and PBEN. P_{app} of EGCG in CBEN and PBEN were higher at 120 min compared with EGCG solution.

The transepithelial electric resistance (TEER) of Caco-2 monolayer treated by EGCG solution did not significantly decrease during the incubation period (**Figure 4-5B**). The TEER percentage of the initial value was 95.6% at 30 min and remained to be 93.0% after 90 min. No significant differences on TEER percentage were observed in EGCG solution, BEN, or PBEN at 30, 60, or 90 min. However, CBEN significantly decreased the TEER percentage of Caco-2 monolayer to 77.8% at 30 min and to 70.2% at 120 min.

Impact of Nano-encapsulation and Particle Coating on Nanoparticle Cellular Uptake by Caco-2 Cells

The cellular uptake of FITC labeled BEN, PBEN, and CBEN by Caco-2 cells was visualized using confocal laser scanning microscopy (**Figure 4-6**). Results showed that the fluorescence was observed in Caco-2 cells treated by FITC labeled BEN (**Figure 4-6B**), which indicates that FITC labeled BEN were taken up by cells after 60 min incubation time. Similar observations on BSA nanoparticle cellular uptake were reported

in the previous studies (*202-204*). Compared with FITC labeled BEN, FITC labeled PBEN and CBEN showed more intense fluorescence, suggesting that poly-ε-lysine and chitosan coatings enhanced the cellular uptake of the nanoparticles. The enhancement of cellular uptake of nanoparticles coated with poly-lysine or chitosan were also reported in earlier studies (*205-207*).

Discussion

After fabrication of BSA nanoparticles with a desolvation method, EGCG was loaded onto these nanoparticles using the polyphenol-protein affinity. EGCG binds with BSA via hydrogen bonds and hydrophobic interactions (*170, 208*). Poly-ε-lysine and chitosan were coated on the surface of BSA-EGCG nanoparticles via electrostatic interactions. Both poly-ε-lysine and chitosan had a large number of $–NH_2$ groups. These groups ionized into $–NH_3^+$ in water. BSA nanoparticles had negative charges in water (pH 5.5) because the isoelectric point of BSA is 4.7. These positively charged poly-ε-lysine or chitosan interacted with negatively charged BSA nanoparticles by electrostatic interactions. Moreover, the affinity between poly-ε-lysine or chitosan and BSA can also be attributed to hydrogen bonds and hydrophobic interactions (*209-210*). EGCG was loaded on BSA nanoparticles before the coating step, therefore loading efficiency or loading capacity of EGCG was not changed by the addition of the coating. The scanning electron microscope revealed that BEN, PBEN, and CBEN had the spherical morphology. Dynamic light scattering measures the sizes of nanospheres with higher accuracy than nano-materials of other morphology (*77*).

The pH environment in the human gastrointestinal tract varies from acidic to neutral. Therefore it is critical to understand the change of particle sizes and zeta-potentials under different pH conditions. Protein nanoparticles in suspension are

stabilized primarily by inter-particle electrostatic repulsion, which is measured by zeta-potential (*75*). Protein nanoparticles tend to aggregate at pH near its isoelectric point due to reduced zeta-potential (*75*). The isoelectric point of BSA protein is around 4.7 and inter-particle repulsions were significantly reduced in pH between 4.5 and 5.0, causing the aggregation of BEN at these pH values (*211*). Poly-ε-lysine and chitosan coatings altered both the size and zeta-potential of BEN at the pH range 1.5-7.0. Both PBEN and CBEN prevented particle aggregation at and below pH 6.0. However, when pH was 6.5 and 7.0, PBEN dramatically increased the particle size to above 5000 nm due to particle aggregation. CBEN had a particle size 1300 nm and 2600 nm at pH 6.5 and 7.0. These aggregations were also accompanied with the decrease of zeta-potentials.

The gastrointestinal tract consists of different pH areas, starting from 6.5-7.0 in the mouth, to 1.5 to 5.0 in the stomach, and then to 5.0 to 7.0 in the intestine. Poly-ε-lysine or chitosan coatings were expected to stabilize BSA-EGCG nanoparticles in the stomach and the upper portion of the small intestine (duodenum) where the pH changes from 1.5 to 6.0. However, particle aggregation is speculated to occur in the jejunum and ileum where the pH is about 7.0. Zeta-potentials of the nanoparticles under different pH conditions also impact the interaction of particles with mucus and epithelial cells in intestine. Goblet cells secrete mucus to form barrier layers in intestinal epithelium. Negatively charged nanoparticles are repulsed by mucus layers (*212*). Positively charged nanoparticles exhibited absorption rates by adhering to the negatively charged mucus layer of small intestine (*212*).

There are two factors that may affect the releases of loaded EGCG from protein nanoparticles. First, EGCG can be released from the nanoparticles by diffusion. In the present study, about 25% of EGCG was released from all the nanoparticles in SGF without pepsin. BEN released about 40% of EGCG in SIF without pancreatin, whereas less than 30% of EGCG was released from PBEN and CBEN (**Figure 4-3**). Protein nanoparticles may also be digested by proteinases in the gastrointestinal tract. Digestion causes protein nanoparticles to lose structural integrity and the subsequent release of loaded EGCG. The SGF with pepsin and the SIF with pancreatin caused BEN to release about 50% and 70% of loaded EGCG, respectively. Higher percentage releases of EGCG were also observed in the coated nanoparticles with the presence of enzymes in simulated digestive fluids. The additional release of EGCG was primarily attributed to the digestion of BSA protein by proteinases. However, coatings on the surface of the nanoparticles delayed EGCG release. Coating provided an additional barrier for diffusion. It may also decrease accessibility or digestibility of BSA by proteinases. Less than 40% or 55% of EGCG was released from the coated nanoparticles in SGF and SIF with proteinases compared to about 50% and 70% of EGCG released from BEN. Thus, coatings appeared to protect the nanoparticles against release of EGCG in the gastrointestinal tract, which might improve the stability of EGCG in the gastrointestinal tract and potentially enhance the absorption of EGCG (*213-214*).

Because nanoparticles have very high surface area/mass ratio, compounds loaded on nanoparticles are more susceptible to oxidation. Indeed, degradation of EGCG on nanoparticle at 60^{o}C was accelerated compared with pure EGCG (**Figure 4-**

4). Coatings created an additional barrier on the nanoparticles and protected EGCG against degradation at the early stage of the storage period.

Caco-2 monolayers were widely used to evaluate the intestinal absorption of EGCG and other flavonoids (*215-216*). The P_{app} of EGCG in the present study was between 2.86×10^{-7} cm/s and 4.27×10^{-7} cm/s (**Figure 4-5A**), which was consistent with previous studies (*68, 195*). The slight decrease on TEER of Caco-2 monolayer treated by EGCG during the incubation period suggested that EGCG concentration had no adverse effect on Caco-2 monolayers (**Figure 4-5B**). Nanoparticles have been proposed to enhance absorption of bioactive compounds through two mechanisms. Tight junctions connect cells in the Caco-2 monolayers. Nanoparticles with the average size below 20 nm are known to reversibly disrupt tight junctions. This will facilitate paracellular absorption of bioactive compounds released from nanoparticles. The decrease of TEER reflected the disruption of tight junctions on Caco-2 monolayers. Furthermore, Caco-2 cells may take up nanoparticles through clathrin-mediated or caveolae-mediated endocytosis. Nanoparticles internalized into Caco-2 cells via endocytosis can be transported into endosome and lysosome. Acid and enzymes in lysosome degrade nanoparticle and release the loaded bioactive compounds (*118, 217*). In the study, TEER percentage of the Caco-2 monolayer treated by BEN did not show significant differences compared to that of EGCG solution, suggesting that the BEN did not disrupt the tight junctions among the Caco-2 cells during the incubation period. The P_{app} of EGCG in BEN showed a decreasing trend from 9.22×10^{-7} cm/s to 3.73×10^{-7} cm/s during the incubation period. Confocal microscopic results suggested that BEN were taken up by Caco-2 cells (**Figure 4-6B**). Both poly-ε-lysine and chitosan

have been used as absorption enhancers to increase the absorption of drugs (*193, 196, 218*). Poly-ε-lysine has a structure similar to cell penetrating peptides that may improve the transport of bioactive compounds by enhancing endocytosis (*196*). The highest P_{app} value of EGCG in PBEN was 9.41×10^{-7} cm/s at 30 min. After 120 min, the P_{app} of EGCG was 5.43×10^{-7} cm/s in PBEN, which was higher than that in EGCG solution. In the meantime, TEER percentage of Caco-2 monolayer treated by PBEN was similar to those by EGCG solution at 90 min. Thus, we speculate that poly-ε-lysine enhanced the cellular uptake of nanoparticles in Caco-2 cells and increased the absorption of EGCG on Caco-2 monolayers. The confocal microscopy indicated that poly-ε-lysine coating enhanced the cellular uptake of the FITC labeled nanoparticles by Caco-2 cells (**Figure 4-6C**). Chitosan coating significantly increased the P_{app} of EGCG (11.17×10^{-7} cm/s) on Caco-2 monolayers at 30 min compared to EGCG solution. Furthermore, the P_{app} of EGCG remained 6.27×10^{-7} cm/s at 120 min. CBEN also caused a greater drop of TEER compared with that of EGCG solution during the incubation period. Two mechanisms were proposed to explain the enhancement of EGCG absorption by CBEN. First, chitosan had the capacity to open up tight junction among Caco-2 cells. Therefore, EGCG released from nanoparticles may transport across monolayers through paracellular way (*190, 193, 218*). Second, chitosan coating may enhance cellular uptake of nanoparticles, which was suggested by the cellular uptake of FITC labeled CBEN by Caco-2 cells (**Figure 4-6D**).

Summary

BEN with poly-ε-lysine and chitosan coatings had the spherical morphology, and the loading efficiency and capacity of EGCG were 35.4% and 32.7%, and 17.0% and 16.0%, respectively. These coatings significantly stabilized the characterization of BEN

in the pH range from 1.5 to 6.0. Higher release of EGCG was observed in all the nanoparticles incubated in simulated gastric and intestinal fluids with proteinases. However, the coatings delayed the release of EGCG from the nanoparticles. The storage stability study showed faster degradation of EGCG in all the nanoparticles compared to free EGCG. CBEN significantly enhanced EGCG absorption on Caco-2 monolayer, which was attributed to the enhancement of cellular uptake of CBEN by Caco-2 cells.

Table 4-1. Loading efficiency and loading capacity of EGCG in BSA-EGCG nanoparticles (BEN), poly-ε-lysine coated BSA-EGCG nanoparticles (PBEN), and chitosan coated BSA-EGCG nanoparticles (CBEN)

Nanoparticles	Loading efficiency (%)	Loading capacity (w/w %)
BSA-EGCG nanoparticles (BEN)	32.3 ± 1.0 b	18.9 ± 0.9 a
Poly-ε-lysine coated BSA-EGCG nanoparticles (PBEN)	35.4 ± 1.4 a	17.0 ± 1.0 a
Chitosan coated BSA-EGCG nanoparticles (CBEN)	32.7 ± 0.9 ab	16.0 ± 1.3 a

Data are mean ± standard deviation of triplicate tests. Different letters in the column represent significant difference at $p \leq 0.05$.

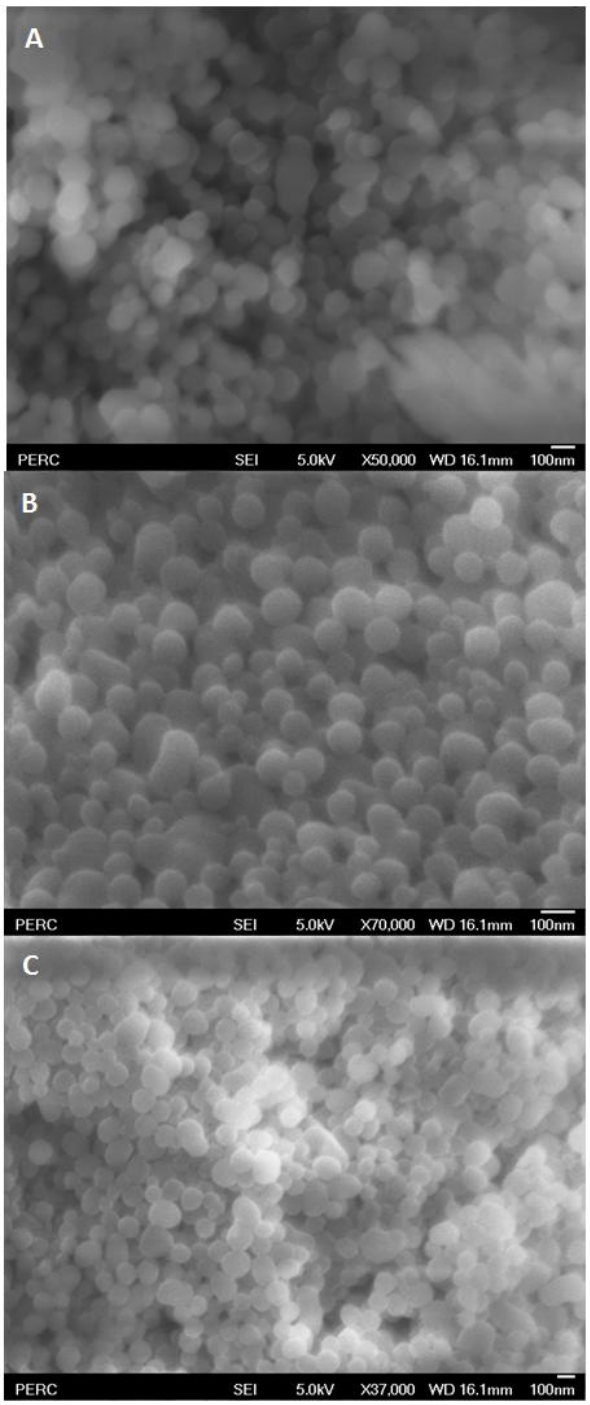

Figure 4-1. Scanning electron microscopy images. A) BSA-EGCG nanoparticles (BEN). B) Poly-ε-lysine coated BSA-EGCG nanoparticles (PBEN). C) Chitosan coated BSA-EGCG nanoparticles (CBEN).

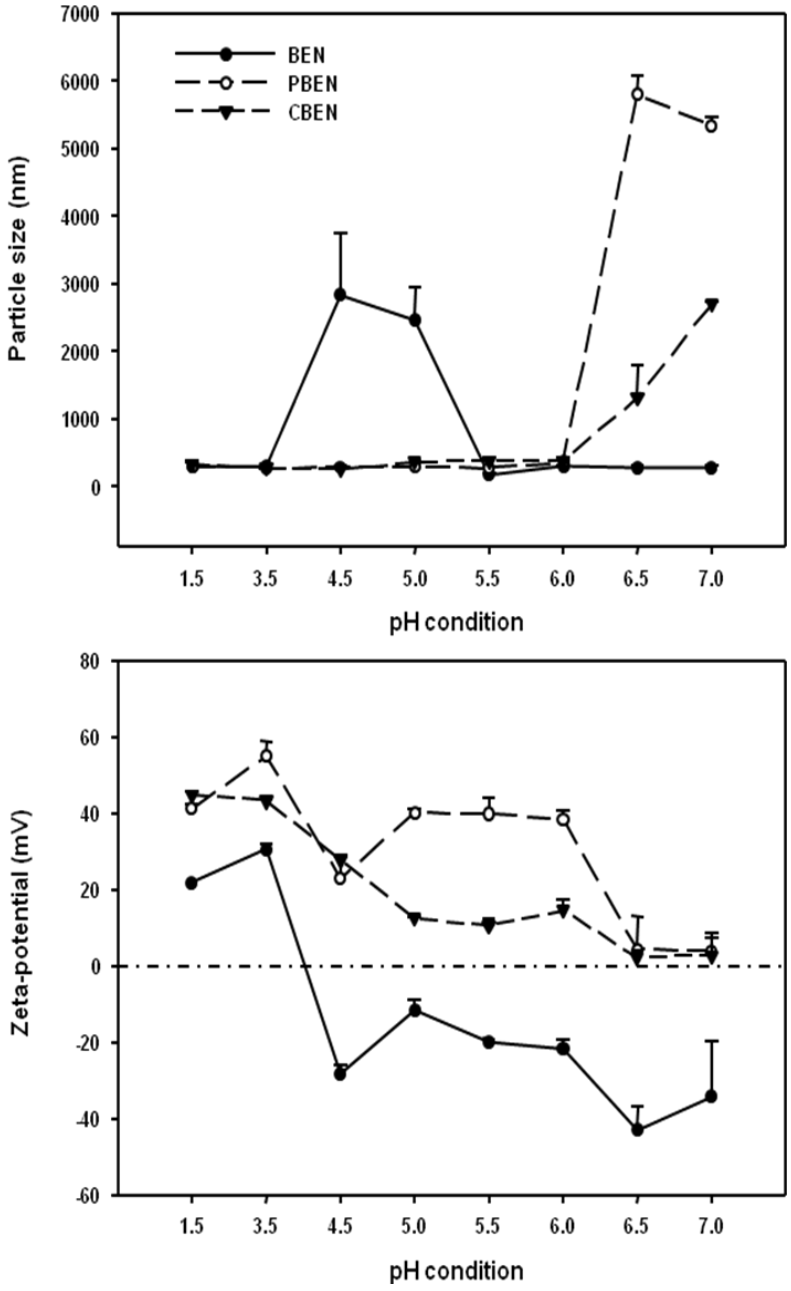

Figure 4-2. Particles size and zeta-potential of BSA-EGCG nanoparticles (BEN), poly-ε-lysine coated BSA-EGCG nanoparticles (PBEN), and chitosan coated BSA-EGCG nanoparticles (CBEN) in the pH range from 1.5 to 7.0. A) Particles size. B) Zeta-potential. Data are mean ± standard deviation of duplicate tests.

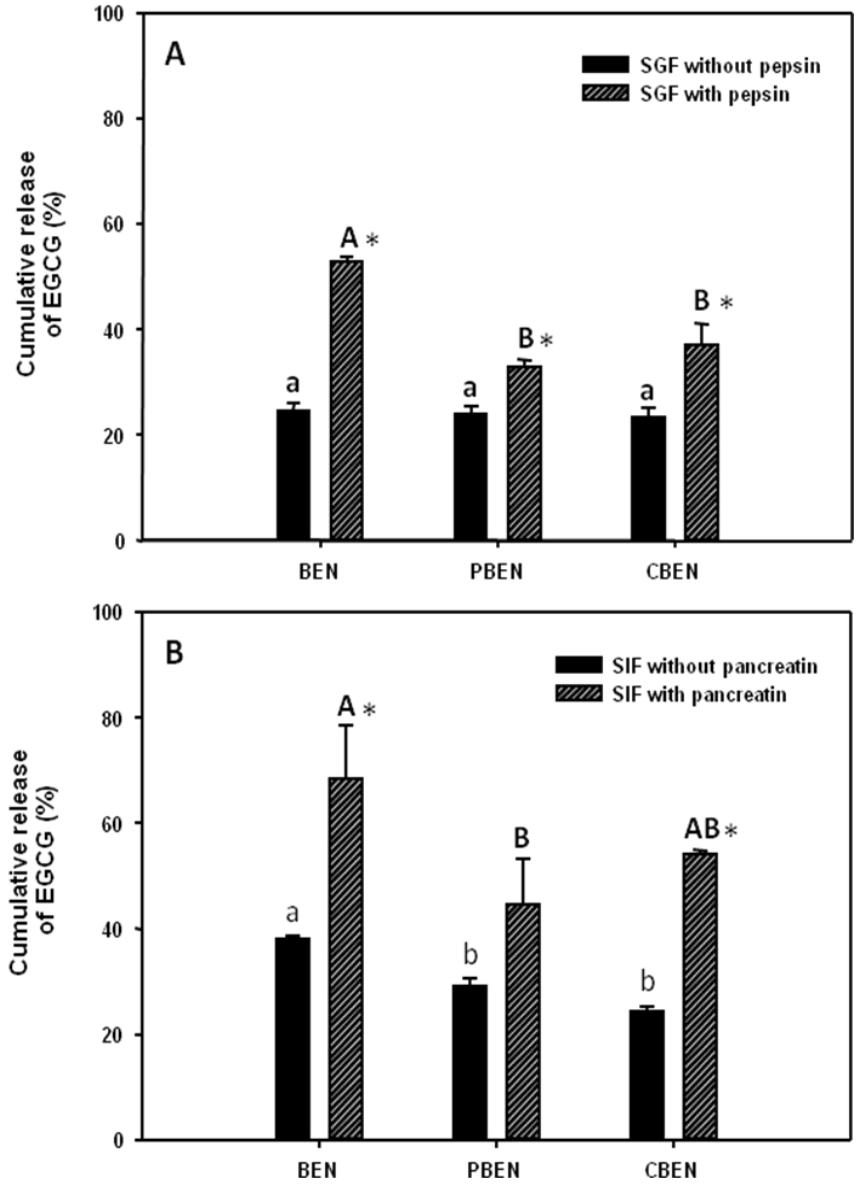

Figure 4-3. Cumulative release of EGCG from nanoparticles in simulated fluids with and without digestive enzymes at 37°C. A) Simulated gastric fluid (SGF) with and without pepsin for 0.5 hour. B) Simulated intestinal fluid (SIF) with and without pancreatin for 2 hours. Data are mean ± standard deviation of duplicate tests. Different low-case letters indicate significant differences in SGF or SIF without digestive enzyme. Different upper-case letters indicate significant differences in SGF or SIF with digestive enzyme. * indicates significant differences of two groups using t-test (with digestive enzyme *versus* without digestive enzyme).

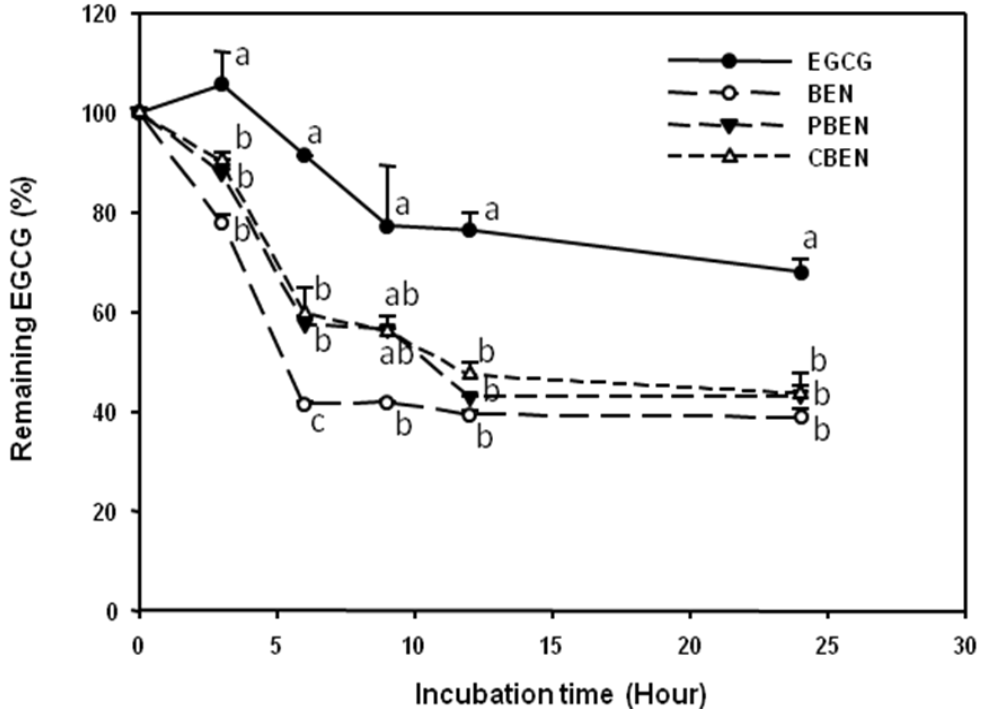

Figure 4-4. Stability of EGCG, EGCG in dry BSA-EGCG nanoparticles (BEN), poly-ε-lysine coated BSA-EGCG nanoparticles (PBEN), and chitosan coated BSA-EGCG nanoparticles (CBEN) at 60^{o}C for 0, 3, 6, 9, 12, and 24 hours. Data are mean ± standard deviation of duplicate tests. Different letters at each incubation time period represent significant differences.

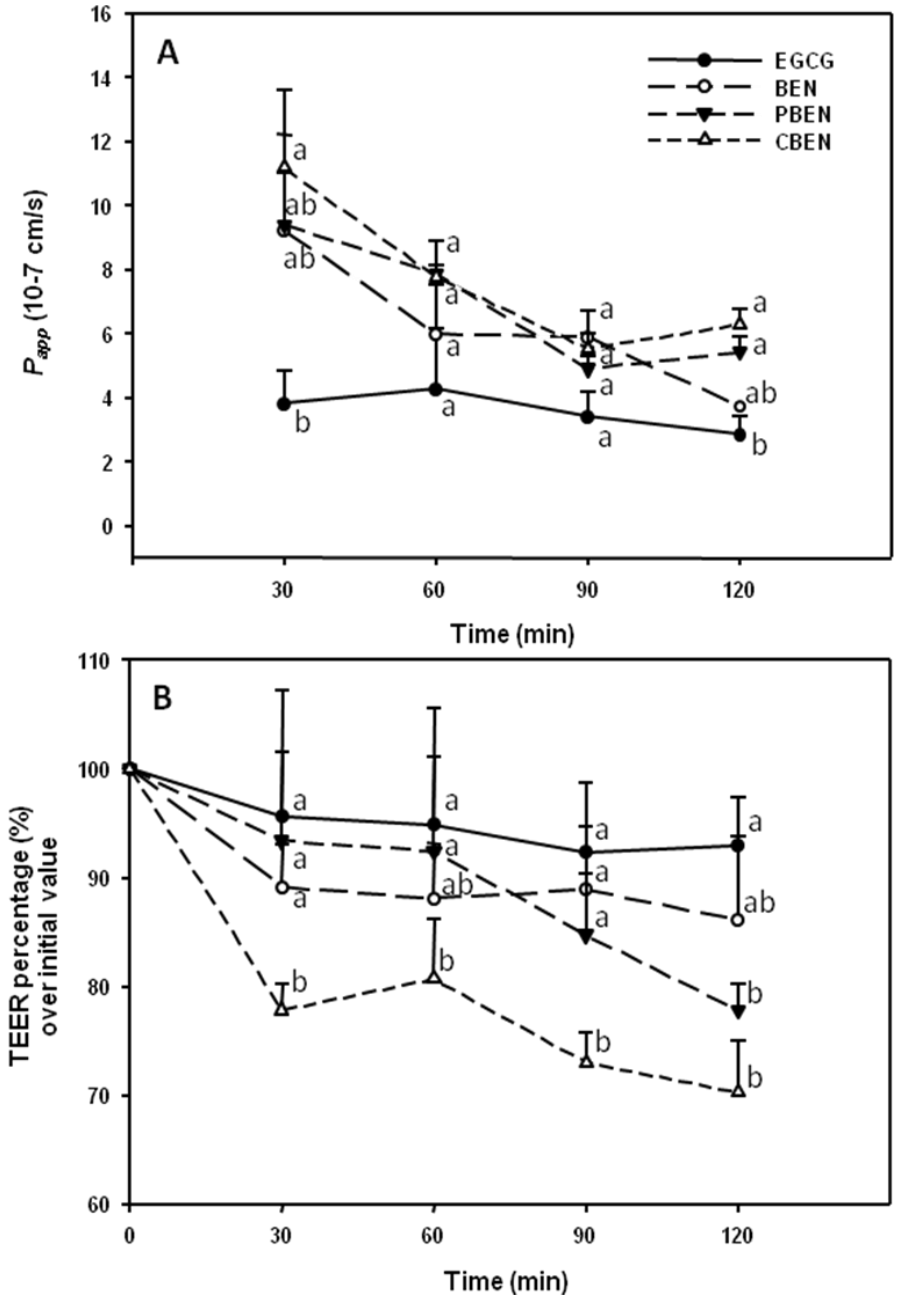

Figure 4-5. Apparent permeability coefficient (P_{app}) and transepithelial electric resistance (TEER) of EGCG in solution, BSA-EGCG nanoparticles (BEN), poly-ε-lysine coated BSA-EGCG nanoparticles (PBEN), and chitosan coated BSA-EGCG nanoparticles (CBEN) at 37^{o}C for 30, 60, 90, and 120 min. A) P_{app}. B) TEER. Data are mean ± standard deviation of triplicate tests. Different letters at each incubation period represent significant differences.

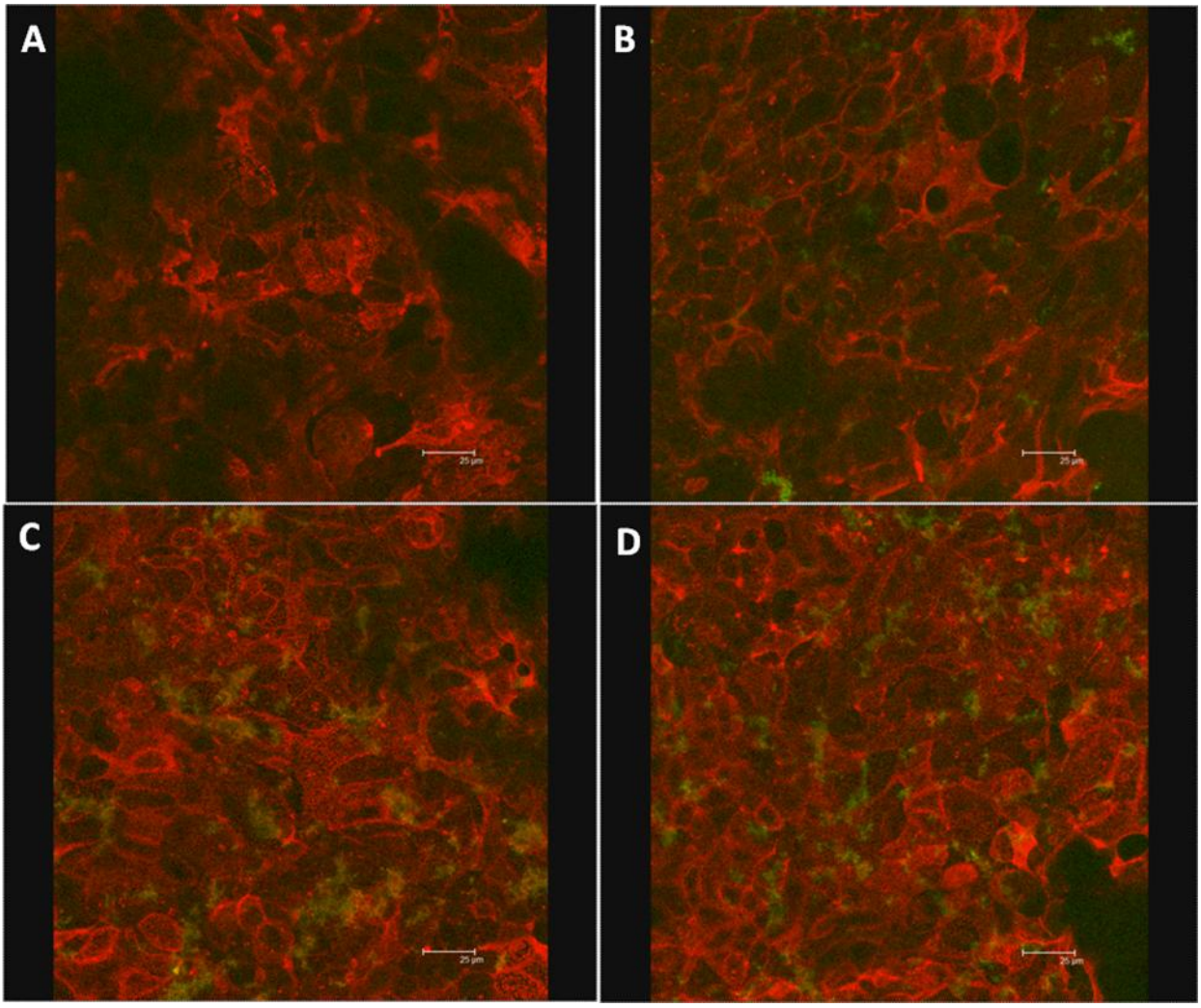

Figure 4-6. FITC labeled BSA-EGCG nanoparticles (FITC labeled BEN), FITC labeled poly-ε-lysine coated BSA-EGCG nanoparticles (FITC labeled PBEN), and FITC labeled chitosan coated BSA-EGCG nanoparticles (FITC labeled CBEN) cellular uptake by Caco-2 cells for 60 min at 37^{o}C. A) Control. B) FITC labeled BEN. C) FITC labeled PBEN. D) FITC labeled CBEN. Red: cell membrane stained with Alexa^{TM} 594-concanavalin A; Green: FITC labeled nanoparticles.

CHAPTER 5
FABRICATION OF SELF-ASSEMBLED (-)-EPIGALLOCATECHIN GALLATE (EGCG) OVALBUMIN-DEXTRAN CONJUGATE NANOPARTICLES AND THEIR TRANSPORT ACROSS MONOLAYERS OF HUMAN INTESTINAL EPITHELIAL CACO-2 CELLS

Background

(-)-Epigallocatechin gallate (EGCG) has been of particular interest in both food and pharmaceutical sciences since it was reported to possess anticancer properties against brain, prostate, cervical, and bladder tumors (*180-184*). However, its low absorption rate limits its bioactivity *in vivo* because EGCG is absorbed via passive diffusion coupled with active efflux (*185-188*). Nanoparticle delivery systems have been widely used to enhance absorption of bioactive compounds because nanoparticles can penetrate small intestinal epithelium by the paracellular and/or endocytotic pathway (*13, 118, 121*).

Protein is a major material that has been widely used for nano-carrier formation (*82, 170, 202*). However, protein-based nanoparticles have several drawbacks. First, proteins are sensitive to pH conditions and tend to precipitate at a pH around their isoelectric points (*74-75*). Second, ionic effect on proteins can also cause the aggregation of proteins (*219*). More importantly, digestive enzymes in the gastrointestinal tract can readily hydrolyze protein to polypeptides and amino acids, which causes burst release of bioactive compounds and subsequent drug degradation and poor absorption (*201*).

Ovalbumin is a major protein in egg white. It can be easily extracted and purified (*220*). Ovalbumin has been reported to resist pepsin digestion (*221*). Dextran consists of a complex branched polysaccharide and has been reported to decrease vascular thrombosis, prolong antithrombitic and colloidal effect, and provide anticoagulation

benefits (*222-224*). Dextran is not digestible by α-amylase in the small intestine and can only be degraded by some microbial enzymes in the large intestine (*225*).

The Maillard reaction conjugates reducing sugars and amines (*226-228*). In the present study, we applied the Maillard reaction to conjugate ovalbumin and dextran to form the ovalbumin-dextran conjugates. Then, EGCG and ovalbumin-dextran conjugates were self-assembled using a heating process to form EGCG ovalbumin-dextran conjugate nanoparticles. Glutaraldehyde was used to crosslink EGCG ovalbumin-dextran conjugate nanoparticles. The aim of this study was to fabricate protein-polysaccharide nanoparticles with improved stability in the gastrointestinal tract and to enhance the absorption of loaded EGCG.

Materials and Methods

Chemicals

(-)-Epigallocatechin gallate (EGCG) was purchased from Quality Phytochemicals LLC (Edison, NJ). Ovalbumin (98% purity) was obtained from Sigma Adrich (St. Louis, MO). Dextran (low fraction, molecular weight of 60 to 90 kDa), simulated gastric fluid (SGF, pH adjusted to 4.0), simulated intestinal fluid (SIF, pH adjusted to 6.0) with pancreatin, and pepsin were purchased from Fisher Scientific (Pittsburg, PA). Caco-2 cells were obtained from American Type Culture Collection (Manassas, VA).

Preparations of Ovalbumin-dextran Conjugates

Ovalbumin (250 mg) and an equal amount of dextran were mixed and dissolved in 100 mL of water. The pH of the solution was adjusted to pH 8.0 using 0.1 N NaOH. Afterwards, this solution was lyophilized to form a fine powder. The dry powder was heated at 60^{o}C with 79% relative humidity in a desiccator containing saturated KBr

solution for 2 days to form the ovalbumin-dextran conjugates. The conjugates were stored at -20^{o}C and used without any further purification.

SDS-PAGE Analysis of Ovalbumin-dextran Conjugates

The formation of ovalbumin-dextran conjugates was confirmed using SDS-PAGE on a gel electrophoresis apparatus to detect the molecular weight distributions of ovalbumin and the ovalbumin-dextran conjugates. Separating gels made of 10% polyacrylamide were used to separate proteins. Stacking gel made of 5% polyacrylamide and 0.1% SDS was used to load the samples. Samples were treated with 100 mM dithiothreitol and boiled for 5 min before loading. After electrophoresis, the gel was stained for protein and carbohydrate using Coomassie Blue R-250 and Fuchsin solution, respectively. The protein and carbohydrate stain was destained with 10% acetic acid (v/v) containing 10% methanol (v/v), and 7.5% acetic acid (v/v) water solution, respectively. The ovalbumin content in each lane was analyzed using UN-SCAN-IT gel analysis software (Version 6.1, Silk Scientific, Inc., Orem, Utah).

Preparations of EGCG Ovalbumin-dextran Conjugate Nanoparticles and Crosslinked EGCG Ovalbumin-dextran Conjugate Nanoparticles

Briefly, 50 mg of ovalbumin-dextran conjugate and 25 mg of EGCG were dissolved in 10 mL of deionized water (mass ratio of ovalbumin to EGCG was 1:1). After adjusting pH to 5.2, the solution was incubated at 80^{o}C for 60 min to form EGCG ovalbumin-dextran conjugate nanoparticles. The resulting nanoparticle suspension was stored at 4^{o}C before analysis.

Crosslinked EGCG ovalbumin-dextran conjugate nanoparticles were prepared by adding 5 µL of glutaraldehyde to 1 mL of nanoparticle suspension. The crosslinking

process was carried out at room temperature for 24 hours under stirring speed of 750 rpm.

Particle Size and Particle Morphology

Particle size was measured in aqueous suspension. One mL of EGCG ovalbumin-dextran conjugate nanoparticles or crosslinked EGCG ovalbumin-dextran conjugate nanoparticles were centrifuged at 13,300 rpm for 5 min and the sediments were re-suspended in 5 mL of de-ionized water. Mean particle size (number-weighted distribution) was measured on Zetatrac (Microtrac Inc., Largo, FL). Samples were measured in four replicates at 25^{o}C to calculate the average particle size.

The morphology of dry EGCG ovalbumin-dextran conjugate nanoparticles and crosslinked EGCG ovalbumin-dextran conjugate nanoparticles were measured using Field Emission Scanning Electron Microscope (Model JSM-633OF, JEOL Ltd, Tokyo, Japan).

Loading Efficiency and Loading Capacity Assessments

The nanoparticle suspensions were centrifuged at 13,300 rpm for 5 min to collect the supernatant. The supernatant was analyzed using HPLC for EGCG content. The loading efficiency and the loading capacity were calculated using the equations below:

$$Loading\ efficiency = \frac{EGCG\ amount\ loaded\ into\ nanoparticles}{EGCG\ amount\ used\ for\ nanoparticles\ fabrication} \times 100\%.$$

$$Loading\ capacity = \frac{EGCG\ amount\ loaded\ into\ nanoparticles}{dry\ nanoparticles\ amount} \times 100\%.$$

Nanoparticle Characterization under Different pH Conditions

Briefly, 1 mL of EGCG ovalbumin-dextran conjugate nanoparticles or crosslinked EGCG ovalbumin-dextran conjugate nanoparticles were centrifuged at 13,300 rpm for 5

min and the sediments were re-suspended in 5 mL of deionized water. The pH of the suspension was adjusted to 2.5, 3.0, 4.0, 5.0, 6.0, 7.0, and 7.5 using a diluted HCl or NaOH solution. Mean particle size (number-weighted distribution) and zeta-potential were measured on Zetatrac (Microtrac Inc., Largo, FL). Samples were measured in duplicate tests at 25^{o}C to calculate the average particle size and zeta-potential.

Nanoparticle Stability in Simulated Gastric or Intestinal Fluid

One mL of EGCG ovalbumin-dextran conjugate or crosslinked EGCG ovalbumin-dextran conjugate nanoparticles were centrifuged at 13,300 rpm for 5 min and the sediments were re-suspended in 5 mL of simulated gastric fluid (SGF, pH 4.0) or simulated intestinal fluid (SIF, pH 6.0) at 37^{o}C for 0.5, 1, 1.5, and 2 hour. At each time point, mean particle size (number-weighted distribution) was measured on Zetatrac (Microtrac Inc., Largo, FL). Samples were measured in duplicate tests to calculate the average particle size.

Release of EGCG in Simulated Digestive Fluids

The cumulative release of EGCG in the nanoparticles was measured in simulated gastric fluid (SGF) without or with pepsin and in simulated intestinal fluid (SIF) without or with pancreatin (*201*). Briefly, nanoparticles were suspended in 5 mL of SGF (pH 4.0) without or with 0.1% pepsin (w/v) and incubated at 37^{o}C for 0.5 h. Subsequently, 1 mL of the sample was centrifuged at 13,300 rpm for 5 min. Supernatant was measured by HPLC for EGCG content. The nanoparticles were suspended in 5 mL of SIF (pH 6.0) without or with 1.0% pancreatin (w/v) and incubated at 37^{o}C for 2 hours. Then, 1 mL of sample was centrifuged at 13,300 rpm for 5 min. The supernatant obtained was measured by HPLC analysis. Samples were measured in four replicates. An Agilent Zorbax SB C18 column (4.6 mm × 250 mm) was used to

analyze EGCG. The binary mobile phase consisted of 0.04 % acetic acid: water (A) and acetonitrile (B). A 22-min gradient was used as follows: 0−20 min, 10−30% B linear; 20-22 min, 30-10% B linear; followed by 2 min of re-equilibration of the column before the next run. The detection wavelength on the diode array detector was 280 nm. The injection volume was 5 µL with the flow rate at 1 mL/min. The cumulative EGCG release was calculated using the following equation:

$$\textit{Cumulative EGCG release (\%)} = \frac{\textit{EGCG amount in supernatant}}{\textit{EGCG amount in dry nanoparticles}} \times 100\%$$

EGCG Absorption on Caco-2 Cell Monolayers

Caco-2 cells were seeded at 6-well transwell plates with the internal diameter of 24 mm and membrane growth area of 4.67 cm^2 (Corning Inc, Lowell, MA). The cells were cultured using Dulbecco's modified eagle media containing 20% fetal bovine serum, 1% penicillin-streptomycin, and 1% non-essential amino acids. The cells were grown to confluence and allowed to mature for 17 days at 37^oC and 5% CO_2. The cell culture media were changed every 1-2 days. The permeability study was carried out in triplicate tests after the transepithelial electrical resistance (TEER) was 500-600 $\Omega \times cm^2$, measured using an epithelial volt-ohm meter (Millicell ERS-2, Millipore Corp, Billerica, MA). The permeability study followed a published paper with minor modifications (*68*). EGCG or EGCG ovalbumin-dextran conjugate nanoparticles were added into Hank's balanced salt solution (HBSS, pH adjusted to 6.0) to control EGCG concentration at 0.025 mg/mL. One and half milliliters of each sample was transferred to the apical chamber of the transwells and 2.6 mL of the fresh buffer was added to the basolateral chamber. After incubation at 37^oC for 30, 60, 90, and 120 min, the transepithelial electric resistance (TEER) was measured. Subsequently, 0.5 mL of the samples was

taken from the basolateral chamber, acidified with ascorbic acid solution to adjust pH to 2.5 and stored in -80^{o}C until analyses. The fresh buffer (0.5 mL) was re-filled to the basolateral chamber. The samples were analyzed by HPLC-ESI-MS^{n} using a published method with minor modifications (*68*). An Agilent Zorbax SB C18 column (4.6 mm × 250 mm) was used for compound separation. The binary mobile phase consisted of 0.04 % acetic acid: water (A) and acetonitrile (B). A 22-min gradient was as follows: 0−20 min, 10−30% B linear; 20-22 min, 30-10% B linear; followed by 2 min of re-equilibration of the column before the next run. The injection volume was 20 µL with a flow rate at 1 mL/min. Electrospray ionization in negative mode was performed using nebulizer 65 psi, drying gas 11 L/min, drying temperature 350^{o}C, and capillary 4000 V. The MRM was used to monitor the transition of deprotonated EGCG *m/z* 457 $[M - H]^-$ to the product ion *m/z* 169. EGCG was used as an external standard. Quantification was conducted using QuantAnalysis (Version 2.0, Bruker Daltonics Inc, Billerica, MA). The apparent permeability coefficient (P_{app}) of EGCG was calculated using the following equation:

$$P_{app} = \frac{dQ}{dt} x \frac{1}{AC_0}$$

Where dQ/dt is the permeability rate (µg/s), C_0 is the initial concentration in the apical chamber (µg/mL), and A is the surface area of filter (cm^2), which was 4.67 cm^2 in this study.

Statistical Analyses

Data was expressed as mean ± standard deviation. Student's t test was used to compare mean values between two groups using JMP software (Version 8.0, SAS Institute Inc., Cary, NC). A difference with $p \leq 0.05$ was considered significant.

Results

Synthesis of Ovalbumin-dextran Conjugates

After electrophoresis, ovalbumin showed a single band whereas dextran did not show any bands (**Figure 5-1A**). The ovalbumin/dextran physical mixture only showed the same band as the ovalbumin sample, indicating that no reaction occurred between ovalbumin and dextran. After the ovalbumin and dextran mixture was incubated at 60^{o}C under relative humidity of 79% in a desiccator containing saturated KBr solution for 2 days, a new smear band appeared, and the ovalbumin single band became smaller. This suggested that ovalbumin-dextran conjugate was generated. In **Figure 5-1B**, the ovalbumin and the ovalbumin/dextran physical mixture showed the single band in carbohydrate staining gel because ovalbumin is a glycoprotein. No band appeared on the dextran sample because dextran did not enter the gel due to lack of any charge. However, ovalbumin-dextran conjugate samples showed the smear band and the ovalbumin band became lighter, which further confirmed that dextran was covalently conjugated with ovalbumin. The content of ovalbumin conjugated with dextran was calculated using UN-SCAN-IT gel analysis software. Results suggested that 27% of ovalbumin reacted with dextran to form the conjugates.

Particle Size, Morphology, EGCG Loading Efficiency and Loading Capacity

After re-suspending nanoparticles in the water, both EGCG ovalbumin-dextran conjugate nanoparticles and crosslinked EGCG ovalbumin-dextran conjugate nanoparticles showed average particle sizes of 285 nm and 339 nm, respectively (**Figure 5-2)**. Both dry EGCG ovalbumin-dextran conjugate nanoparticles and crosslinked EGCG ovalbumin-dextran conjugate nanoparticles showed the spherical morphology, visualized by SEM.The sizes measured by Zetatrac were bigger than those

measured by SEM because the dry particles were used in SEM assessment (*170*). The loading efficiency of EGCG in EGCG ovalbumin-dextran conjugate nanoparticles and crosslinked EGCG ovalbumin-dextran conjugate nanoparticles was 23.4% and 30.0%, respectively (**Table 5-1**). The loading capacity of EGCG in the nanoparticles was 19.6% and 20.9%, respectively. No significant differences were observed in either loading efficiency or loading capacity between EGCG ovalbumin-dextran conjugate nanoparticles and crosslinked EGCG ovalbumin-dextran conjugate nanoparticles.

Nanoparticle Characterization under Different pH Conditions

EGCG ovalbumin-dextran conjugate nanoparticles showed a particle size of 210 nm in the aqueous suspension at pH 2.5, and the size remained at 323 nm and 308 nm when pH was adjusted to 3.0 and 4.0, respectively (**Figure 5-3A**). The particle size increased to 634 nm when the pH of EGCG ovalbumin-dextran conjugate nanoparticle suspension was 5.0, and then dropped to between 168 nm and 211 nm in a pH range from 6.0 to 7.5. Crosslinked EGCG ovalbumin-dextran conjugate nanoparticles showed particle sizes of 173 nm, 336 nm, and 347 nm at pH 2.5, 3.0, and 4.0, respectively. When the pH of the nanoparticle suspension was adjusted to 5.0, crosslinked EGCG ovalbumin-dextran conjugate nanoparticles had a size of 325 nm, and the size remained between 244 nm and 340 nm in a pH range of 6.0 to 7.5.

EGCG ovalbumin-dextran conjugate nanoparticles and crosslinked EGCG ovalbumin-dextran conjugate nanoparticles had comparable zeta-potentials in a pH range from 2.5 to 7.5 (**Figure 5-3B**). Both EGCG ovalbumin-dextran conjugate nanoparticles and crosslinked EGCG ovalbumin-dextran conjugate nanoparticles showed a zeta-potential of around 10 mV at pH of 2.5 and 3.0. Lower surface charges were observed in EGCG ovalbumin-dextran conjugate nanoparticles (zeta-potential of

between 6.71 mV and -1.37 mV) and crosslinked EGCG ovalbumin-dextran conjugate nanoparticles (zeta-potential of between 1.45 mV to -6.07 mV) in the pH range of 4.0 to 6.0. This was because such pH ranges were close to the isoelectric point of ovalbumin (around 4.5 to 4.8). When pH was above 7, both nanoparticles had the zeta-potential around -10 mV.

Stability of Nanoparticles in Simulated Digestive Fluids

The initial particle size of EGCG ovalbumin-dextran conjuagate nanoparticles and crosslinked EGCG ovalbumin-dextran conjugate nanoparticles re-suspended in simulated gastric fluid (SGF) was 261 nm and 380 nm, respectively (**Figure 5-4A**). Incubating these two nanoparticles in SGF at 37^{o}C for 2 hours did not cause a significant change in particle sizes. The particle size of EGCG ovalbumin-dextran conjugate nanoparticles was 183 nm, 349 nm, 294 nm, and 299 nm at 0.5, 1, 1.5, and 2 hours, respectively. Similarly, crosslinked EGCG ovalbumin-dextran conjugate nanoparticles showed average particle sizes of 478 nm, 294 nm, 527 nm, and 439 nm after 0.5, 1, 1.5, and 2 hour of incubation, respectively.

Both EGCG ovalbumin-dextran conjugate nanoparticles and crosslinked EGCG ovalbumin-dextran conjugate nanoparticles appeared stable in the simulated intestinal fluid (SIF) at 37^{o}C for 2 hours (**Figure 5-4B**). After EGCG ovalbumin-dextran conjugate nanoparticles and crosslinked EGCG ovalbumin-dextran conjugated nanoparticles were re-suspended in SIF, their particle sizes were 232 nm and 206 nm, respectively. After a 0.5 hour incubation, the sizes of these nanoparticles were 217 nm and 280 nm, and the sizes remained at 291 nm and 265 nm at 2 hours.

EGCG Release from Nanoparticles in Simulated Digestive Fluids

After incubation of the nanoparticles in simulated gastric fluid (SGF) for 0.5 hour, 12.3% and 8.3% of EGCG was released from EGCG ovalbumin-dextran conjugate nanoparticles and crosslinked EGCG ovalbumin-dextran conjugate nanoparticles, respectively (**Figure 5-5A**). Introducing pepsin into the SGF led to a significantly faster release of EGCG from the nanoparticles in SGF. They released 17.2% and 14.9% of EGCG, respectively. Similarly, 27.1% and 21.9% of EGCG was release from EGCG ovalbumin-dextran conjugate nanoparticles and crosslinked EGCG ovalbumin-dextran conjugate nanoparticles in simulated intestinal fluid (SIF) for 2 hours, respectively (**Figure 5-5B**). In SIF with pancreatin for 2 hours, EGCG ovalbumin-dextran conjugate nanoparticles and crosslinked EGCG ovalbumin-dextran conjugate nanoparticles released 37.9% and 32.5% of EGCG, respectively. Crosslinked EGCG ovalbumin-dextran conjugate nanoparticles retarded the EGCG release compared to EGCG ovalbumin-dextran conjugate nanoparticles in SIF without and with pancreatin.

EGCG Transport on Caco-2 Monolayers

The transepithelial electric resistance (TEER) percentage of Caco-2 monolayers treated by HBSS buffer (Blank) dropped to 100.6%, 95.6%, 94.1%, and 89.9% of initial value at 30, 60, 90, and 120 min, respectively (**Figure 5-6A**). No significant decreases on TEER of Caco-2 monolayers treated by EGCG were observed compared to the blank. The TEER of Caco-2 monolayers treated by EGCG was 98.1%, 95.1%, 91.7% and 85.0% of initial value, respectively. EGCG ovalbumin-dextran conjugate nanoparticles caused the decrease of TEER to 95.2%, 90.9%, 89.3%, and 79.8% of initial value at 30, 60, 90, and 120 min, respectively. However, there were no significant

differences on TEER of Caco-2 monolayers treated by the nanoparticles, EGCG, or blank.

The apparent permeability coefficient (P_{app}) of EGCG from the apical to the basolateral side on the Caco-2 monolayers was investigated after incubating EGCG solution or EGCG ovalbumin-dextran conjugate nanoparticles with Caco-2 monolayers for up to 120 min (**Figure 5-6B**). The P_{app} of EGCG in EGCG solution was between 0.28-0.42 × 10^{-6} cm/s during the incubation period. However, the P_{app} of EGCG in the nanoparticles was between 0.52-0.78 × 10^{-6} cm/s, and significantly higher than those of the EGCG solution.

Discussion

The Maillard reaction forms covalent bonds between carbonyl groups and amino groups (*226*). The ovalbumin-dextran conjugates were generated by controlling the Maillard reaction at an early stage, the Amadori rearrangement (*227-229*). SDS-PAGE showed that a new smear band appeared in both protein staining and carbohydrate staining gel after incubating the ovalbumin and dextran mixture at 60^{o}C under a relative humidity of 79% in a desiccator containing saturated KBr solution for 2 days. In the meantime, the ovalbumin band became smaller compared to unconjugated ovalbumin (**Figure 5-1**). This confirmed the generation of conjugates. The gel analysis revealed that about 27% of ovalbumin reacted with dextran to form the conjugates.

After mixing the ovalbumin-dextran conjugates with EGCG and adjusting the pH of the solution to 5.2, heating the mixture at 80^{o}C for 60 min caused the formation of a white milky suspension. The heating step induced the gelation of ovalbumin, which led to the heat-induced unfolding of ovalbumin (*230*). The protein-protein interactions (hydrogen bonding, electrostatic and hydrophobic interactions, disulfide-sulphydryl

interchange) and protein-EGCG interactions (hydrogen bonding and hydrophobic interactions) caused the self-assembly of EGCG and ovalbumin-dextran conjugates. This resulted in encapsulation of EGCG in the nanoparticles (*82, 170, 230*). Conjugation of ovalbumin with dextran increased the hydrophilic property of ovalbumin-dextran conjugates, which helped to stabilize the nanoparticles in the aqueous suspension. Glutaraldehyde was added to the nanoparticle suspension to crosslink the ovalbumin proteins, which further stabilized the structure of EGCG ovalbumin-dextran conjugate nanoparticles. The loading efficiency and the loading capacity of EGCG in EGCG ovalbumin-dextran conjugate nanoparticles and crosslinked EGCG ovalbumin-dextran conjugate nanoparticles were not significantly affected by additional crosslinking because glutaraldehyde was added after the heating step (**Table 5-1**). The formation of EGCG ovalbumin-dextran conjugate nanoparticles is illustrated in **Figure 5-7**. We hypothesized that the core of the nanoparticles was formed by the hydrophobic peptides of ovalbumin and the hydrophilic dextran was on the surface of the nanoparticles as the shell. Our data showed that the heating process degraded about 2.4% EGCG. Therefore, the degradation of EGCG is not a concern.

The pH in the human gastrointestinal tract varies drastically in different segments. For example, pH in mouth, stomach, small intestine, and large intestine were 6.5-7.0, 1.5 (fast)-5.0 (fed), 5.0-7.0, and 7.0-7.4, respectively (*13, 118*). The size and surface charge of protein-based nanoparticles depends on pH conditions. Weakened repulsion among the nanoparticles caused particle precipitation when the pH was around the isoelectric point of the selected protein (*75*). Therefore, it is important to know the change of particle size and zeta-potential under different pH conditions. In the

present study, both EGCG ovalbumin-dextran conjugate nanoparticles and crosslinked EGCG ovalbumin-dextran conjugate nanoparticles remained at nano-scale sizes in a pH range from 2.5 to 7.5 (**Figure 5-3**). Dextran has been reported to enhance colloidal stability (*223, 231-232*). Thus, hydrophilic dextran on the surface of the nanoparticles may retard the aggregation of ovalbumin proteins. Zeta-potential of the nanoparticles is primarily determined by the protein and zeta-potential varies according to pH conditions. Both EGCG ovalbumin-dextran conjugate and crosslinked EGCG ovalbumin-dextran conjugate nanoparticles showed positive zeta-potentials in a pH range from 2.5 to 3.0, whereas negative charges were observed when pH was above 7.0. It was noticed that both nanoparticles had weaker zeta-potentials (-6.07 mV to 6.76 mV) at pH 4.0-6. Mucus layers in the small intestine serve as a barrier between drugs and intestinal epithelia and they possess a negative charge (*212*). Thus, nanoparticles with strong negative or positive charges may be repulsed or adsorbed by mucus layers to hinder their contact with epithelial cells, whereas weakly charged nanoparticles may readily penetrate the mucus layers. EGCG ovalbumin-dextran conjugate nanoparticles and crosslinked EGCG ovalbumin-dextran conjugate nanoparticles had weak zeta-potentials at pH 5.0-6.0, which may enhance the penetration of nanoparticles through the mucus layers to reach epithelial cells in the upper portion of the small intestine.

It takes about 0.5 to 2 hours and 2 to 4 hours for ingested food to pass the stomach and small intestine, respectively (*13, 118*). Thus, the stability of nanoparticles in the stomach and small intestine are critical. The majority of ingested nanoparticles should maintain nano-size to enhance the absorption of loaded drugs. In simulated gastric fluid (SGF, pH 4.0, fed state) for 2 hours, EGCG ovalbumin-dextran conjugate

nanoparticles showed an average particle size between 183 nm and 349 nm, whereas the sizes of crosslinked EGCG ovalbumin-dextran conjugate nanoparticles were between 294 nm and 527 nm. More importantly, both nanoparticles showed particle sizes below 300 nm in simulated intestinal fluid (SIF, pH 6.0, upper portion of small intestine) for up to 2 hours. This was explained by the capacity of dextran to stabilize the nanoparticles in the gastrointestinal tract with high salt concentration and different pH (*232*). Nanoparticles with better stability in the gastrointestinal tract may increase permeation of EGCG in the small intestine.

Release of bioactive compounds from nanoparticles in the gastrointestinal tract is attributed to the diffusion of bioactive compounds in the gastrointestinal fluid. More importantly, degradation of nanoparticles by digestive enzymes in the gastrointestinal tract may cause the burst release of bioactive compounds (*201, 210*). For example, pepsin in the stomach, and trypsin, chymotrypsin, elastase, and carboxypeptidas A and B in the small intestine, can hydrolyze protein to amino acids, whereas α-amylase can hydrolyze 1,4-α-D-glucosidic linkages of polysaccharides. Dextran consists of straight chains with α-1,6 glycosidic linkages between glucoses and branches with α-1,3 linkages. This structure makes dextran resistant to hydrolysis by amylase in the gastrointestinal tract (*225*). In the present study, the release of EGCG from both of the nanoparticles in simulated fluids with presence of digestive enzymes was more than that with absence of digestive enzymes. This suggests that ovalbumin was hydrolyzed by proteinases in both SGF and SIF. It should be noted that EGCG ovalbumin-dextran conjugate nanoparticles and crosslinked EGCG ovalbumin-dextran conjugate nanoparticles showed similar EGCG release percentage in the simulated fluid with

digestive enzymes. This may be because the dextran on the surface of the nanoparticles protected the protein from digestion by hindering the contact between ovalbumin and proteinase. Also, ovalbumin was reported to be resistant against pepsin digestion in the stomach at fed state (*221*). Conformation change of ovalbumin after thermal processing provided resistance against trypsin, chymotrypsin, and elastate in the small intestine (*220, 233*). Furthermore, crosslinked EGCG ovalbumin-dextran conjugate nanoparticles decreased the EGCG release compared to EGCG ovalbumin-dextran conjugate nanoparticles in simulated fluids without and with digestive enzymes, which indicated the crosslinking process further improved the integrity of the nanoparticles in the presence of proteinases.

Caco-2 cell monolayers have been widely used to estimate the permeability of phenolic compounds *in vitro* (*215-216*). Monolayers were formed after the TEER was between 150 and 1600 $\Omega \times cm^2$ (*234*). The TEER value of Caco-2 monolayers in the present study was 500-600 $\Omega \times cm^2$. A significant decrease of TEER indicated that the tight junctions of the monolayers were disrupted or monolayer integrity was compromised. Nanoparticles with a size <20 nm have the capacity to reversibly open tight junctions among cells and facilitate the permeation of loaded drugs via the paracellular pathway (*118*). In this study, TEER values of Caco-2 monolayers were similar among the blank, EGCG solution, and EGCG ovalbumin-dextran conjugate nanoparticles. This suggested that the concentration of EGCG had little adverse effect on the integrity of the monolayer, and the nanoparticles did not open tight junctions of the monolayer to facilitate the permeation of EGCG by paracellular pathway.

The main mechanism for nanoparticles to enhance the permeability of bioactive compounds was the cellular uptake of the nanoparticles via endocytosis, including clathrin- and/or caveolae-mediated endocytosis (*118, 121-122*). It has been proposed that clathrin-mediated endocytosis allowed the nanoparticles with an average size below 300 nm to penetrate the membrane of the cells, whereas nanoparticles with a size below 500 nm could be internalized into cells by caveolae-mediated endocytosis (*127*). Upon internalization, nanoparticles can either be delivered into the endo/lysosome for the degradation to release the bioactive compounds, or escape the endo/lysosome to arrive at the basolateral side by extocytosis (*13, 118*). In the present study, the P_{app} of EGCG in EGCG solution was 0.28–0.42 × 10^{-6} cm/s, which was comparable with previous studies (*68, 195*). EGCG ovalbumin-dextran conjugate nanoparticles significantly improved the P_{app} of EGCG to 0.54–0.78 × 10^{-6} cm/s. We hypothesized that the internalization of the nanoparticles by Caco-2 cells was mediated by clathrin-mediated endocytosis since EGCG ovalbumin-dextran conjugate nanoparticles had a size below 300 nm in SIF (pH 6.0).

Summary

Ovalbumin and dextran were conjugated using the Maillard reaction. EGCG ovalbumin-dextran conjugate nanoparticles and crosslinked EGCG ovalbumin-dextran conjugate nanoparticles were formed by self-assembly under a heating process. These particles showed a spherical morphology measured by SEM and the sizes were 285 nm and 339 nm in aqueous suspension. The loading efficiency of EGCG in these conjugate nanoparticles was 23.4% and 30.0%, whereas the loading capacity was 19.6% and 20.9%, respectively. EGCG ovalbumin-dextran conjugate nanoparticles and crosslinked EGCG ovalbumin-dextran conjugate nanoparticles remained at nano-scale sizes in the

pH range from 2.5 to 7.5, and they showed stable particle sizes in SGF and SIF at 37^{o}C for 2 hours. The limited release of EGCG from these two nanoparticles in SGF and SIF without and with digestive enzymes was observed. EGCG in EGCG ovalbumin-dextran conjugate nanoparticles possessed the higher apparent permeability coefficient (P_{app}) on Caco-2 monolayers compared to EGCG solution.

Table 5-1. Loading efficiency and loading capacity of EGCG in EGCG ovalbumin-dextran conjugate nanoparticles and crosslinked EGCG ovalbumin-dextran conjugate nanoparticles

Nanoparticles	Loading efficiency (%)	Loading capacity (w/w %)
EGCG ovalbumin-dextran conjugate nanoparticles	23.4 ± 2.9	19.6 ± 3.2
Crosslinked EGCG ovalbumin-dextran conjugate nanoparticles	30.0 ± 4.9	20.9 ± 3.8

Data are mean ± standard deviation of four replicate tests. No significant differences are observed between the samples using student t test at $p \leq 0.05$.

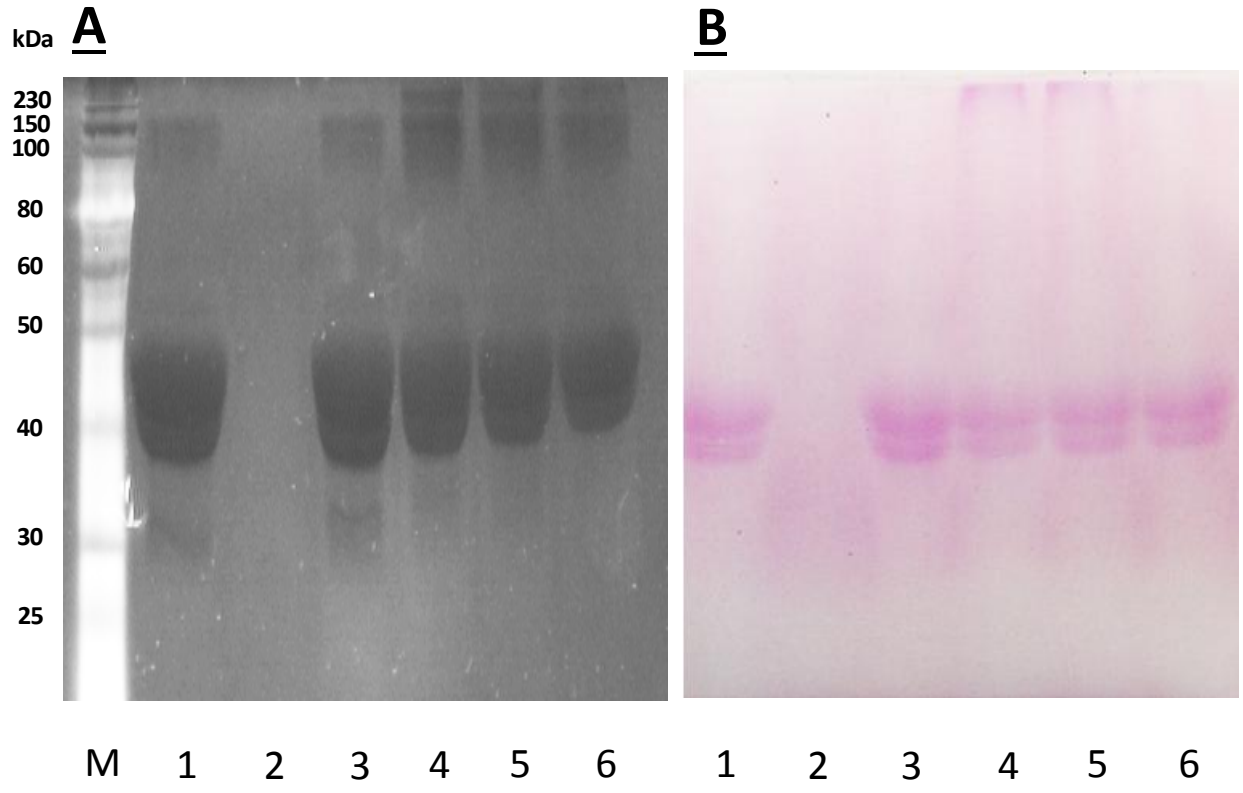

Figure 5-1. SDS-PAGE analysis of ovalbumin, dextran, ovalbumin/dextran physical mixture, and ovalbumin-dextran conjugates. A) Ovalbumin stain. B) Carbohydrate stain. Lane M represents molecular weight marker. Lane 1, 2, and 3 represent ovalbumin, dextran, and ovalbumin/dextran physical mixture, respectively. Lane 4, 5, and 6 represent triplicates of ovalbumin-dextran conjugates. The amount of ovalbumin in each lane was 22 µg. The amount of dextran was 22 µg.

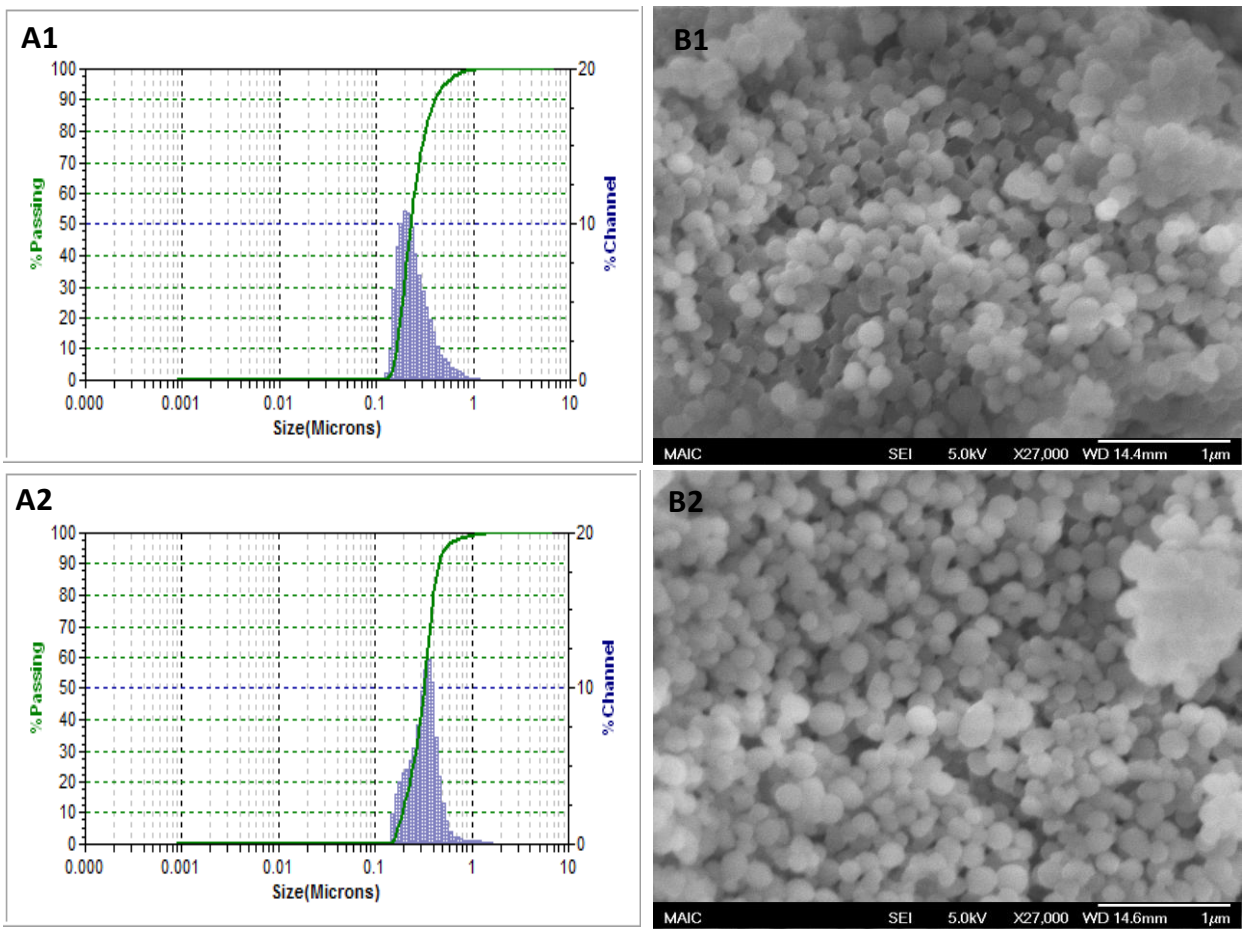

Figure 5-2. Particle size of and particle morphology of EGCG ovalbumin-dextran conjugate nanoparticles and crosslinked EGCG ovalbumin-dextran conjugate nanoparticles. A1) Particle size of EGCG ovalbumin-dextran conjugate nanoparticles. A2) Particle size of crosslinked EGCG ovalbumin-dextran conjugate nanoparticles. B1) Particle morphology of EGCG ovalbumin-dextran conjugate nanoparticles. B2) Particle morphology of EGCG ovalbumin-dextran conjugate nanoparticles.

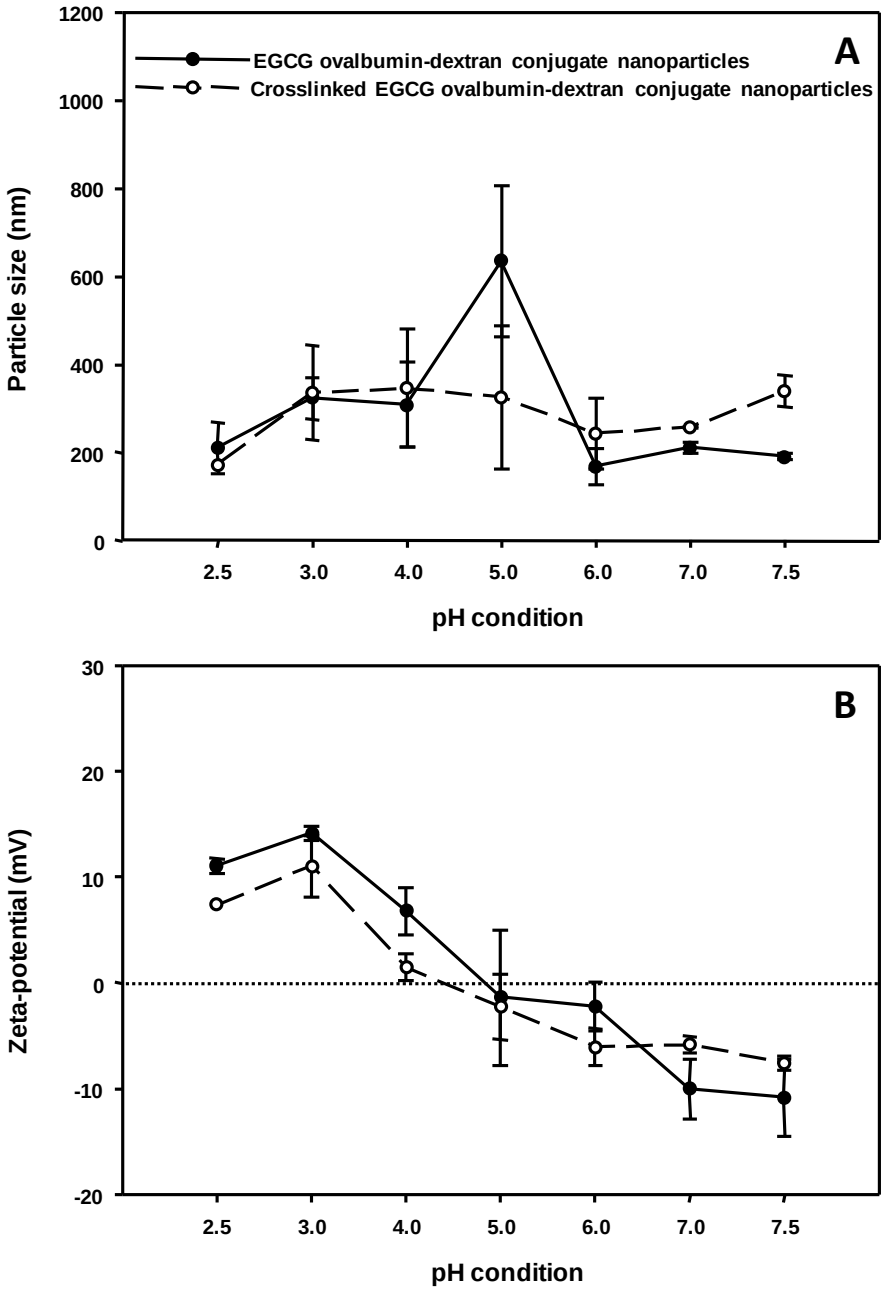

Figure 5-3. Particle size and zeta-potential of EGCG ovalbumin-dextran conjugate nanoparticles and crosslinked EGCG ovalbumin-dextran conjugate nanoparticles in the pH range from 2.5 to 7.5. A) Particle size. B) Zeta-potential. Data are mean ± standard deviation of duplicate tests.

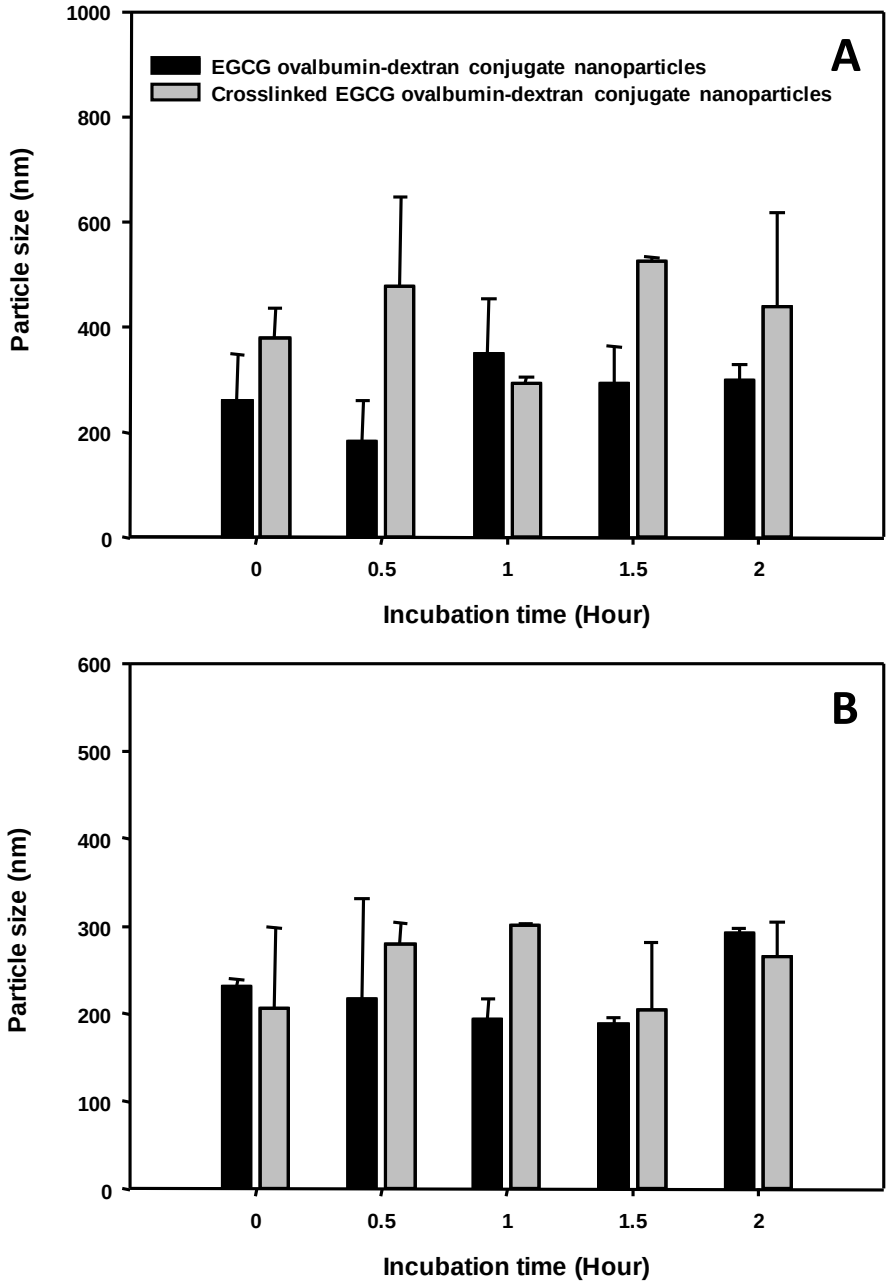

Figure 5-4. Particle size of EGCG ovalbumin-dextran conjugate nanoparticles and crosslinked EGCG ovalbumin-dextran conjugate nanoparticles in simulated fluids at 37^{o}C for 0, 0.5, 1, 1.5, and 2 hour. A) Simulated gastric fluid (SGF). B) Simulated intestinal fluid (SIF). Data are mean ± standard deviation of duplicate tests.

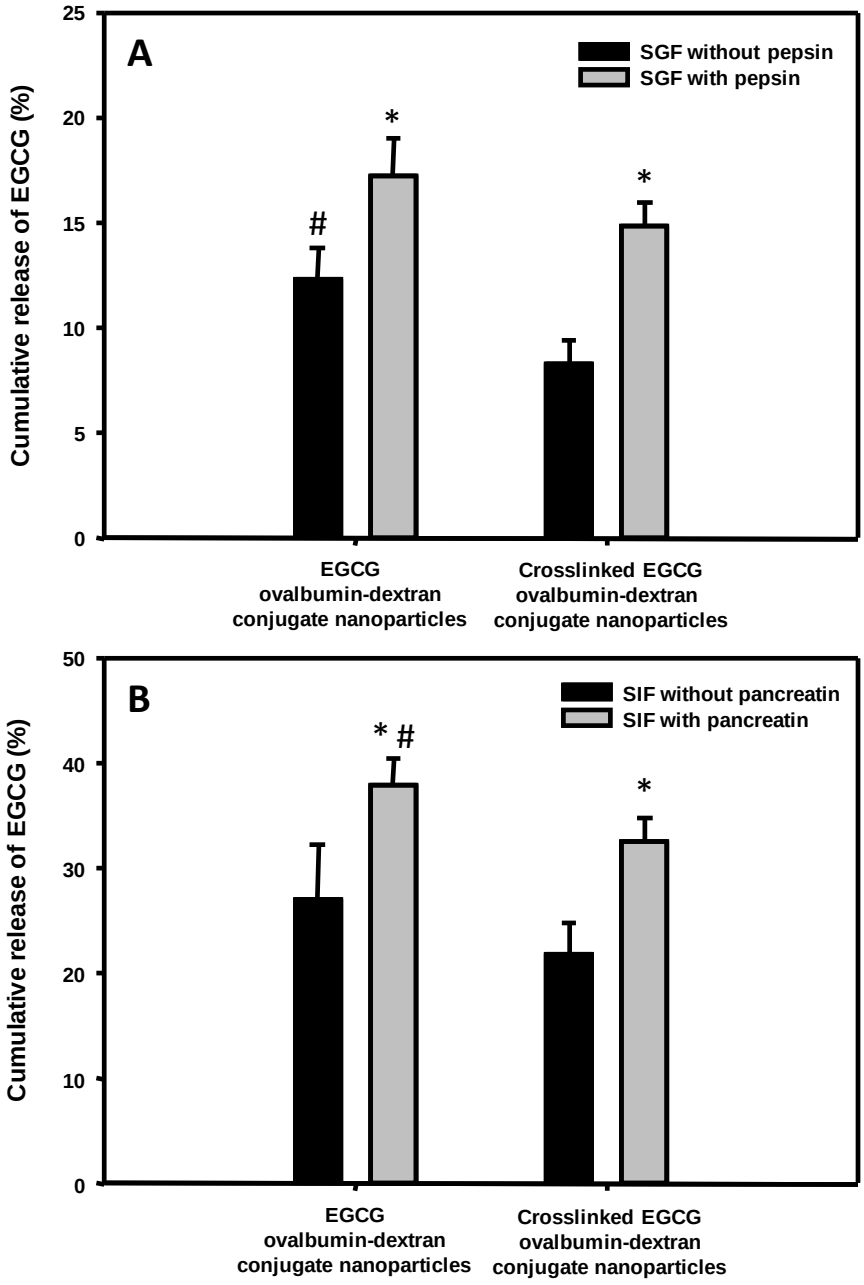

Figure 5-5. Cumulative release of EGCG from EGCG ovalbumin-dextran conjugate nanoparticles and crosslinked EGCG ovalbumin-dextran conjugate nanoparticles in simulated fluids without and with digestive enzymes at 37^{o}C. A) Simulated gastric fluid (SGF) without and with pepsin for 0.5 hour. B) Simulated intestinal fluid (SIF) without and with pancreatin for 2 hours. Data are mean ± standard deviation of four replicate tests. # denotes significant differences between EGCG ovalbumin-dextran conjugate nanoparticles and crosslinked EGCG ovalbumin-dextran conjugate nanoparticles using t-test at $p \leq 0.05$. ***** denotes significant differences between simulated fluid without enzyme and fluid with enzyme using t-test at $p \leq 0.05$.

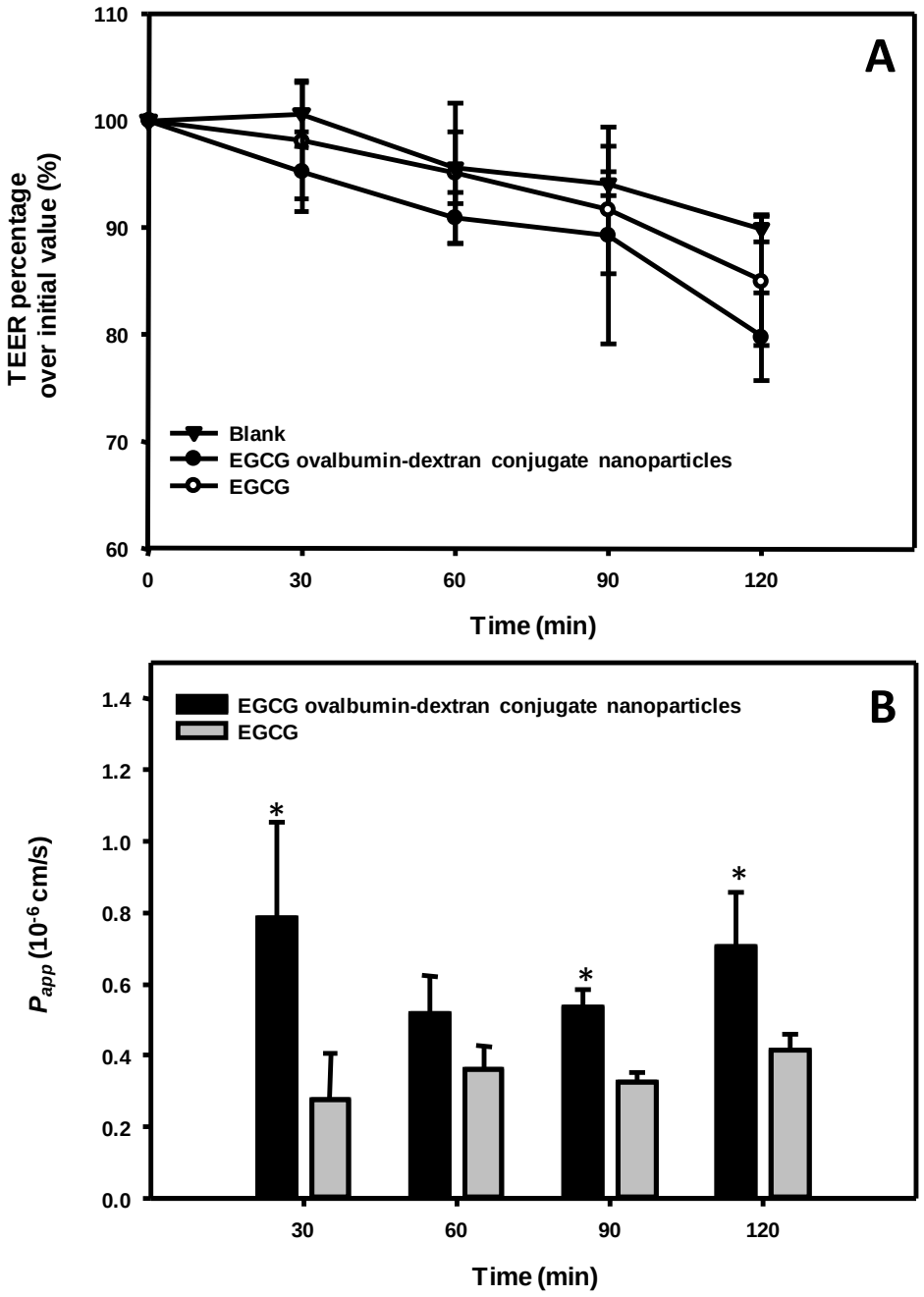

Figure 5-6. Transepithelial electric resistance (TEER) and apparent permeability coefficient (P_{app}) of EGCG in solution and EGCG ovalbumin-dextran conjugate nanoparticles at 37°C for 30, 60, 90, and 120 min. A) TEER. B) P_{app}. Data are mean ± standard deviation of triplicate tests. * at each incubation period represents significant differences at $p \leq 0.05$.

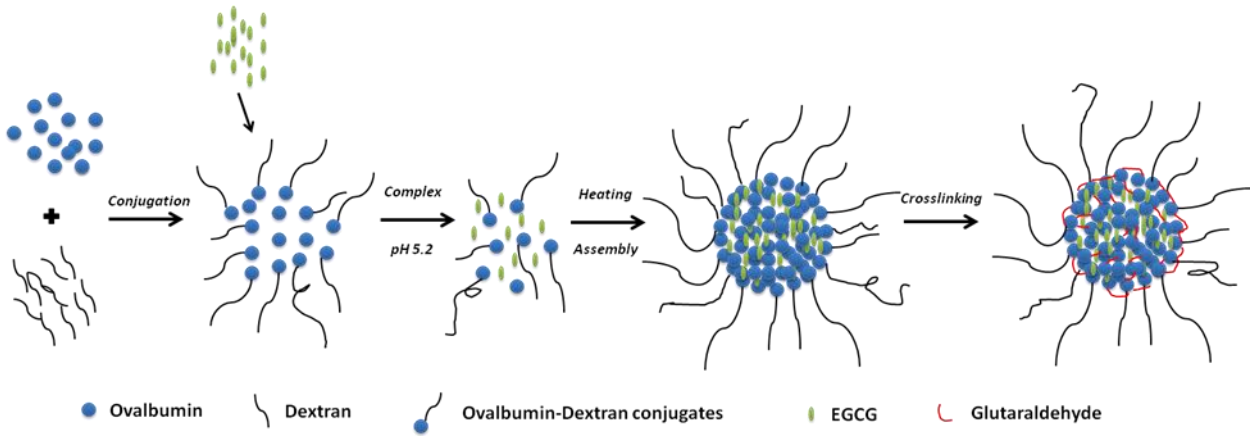

Figure 5-7. Illustration of formation of EGCG ovalbumin-dextran conjugate nanoparticles and crosslinked EGCG ovalbumin-dextran conjugate nanoparticles.

CHAPTER 6
CONCLUSIONS

The PPE obtained from pomegranate pericarp contained punicalagin A and B, ellagic acid-hexoside, and ellagic acid. Punicalagins had the capacity of binding gelatin to form nanoparticles. The nanoparticle fabricated using three PPE-to-gelatin mass ratios had the particle size < 250 nm, zeta-potential around +18 mv, spherical morphology, and good loading capacity. PPE-gelatin nanoparticles had lower apoptotic effects in HL-60 cells compared to PPE solution.

PPE-to-gelatin mass ratio was a major factor affecting characteristics and stability of nanoparticle suspension. The critical point for PPE-gelatin nanoparticles was at a mass ratio of 8:5. Nanoparticles prepared in a pH range from 4 to 5 had particle sizes and zeta-potentials that may favor the absorption of loaded ellagitannins. Reaction temperatures from 25 to 50^{o}C had a positive influence on nanoparticle characteristics. Self-assembly occurred rapidly between gelatin and ellagitannin and fabrication was done within 12 hours and remained stable for 4 days.

BEN with poly-ε-lysine and chitosan coatings had a spherical morphology, and the loading efficiency and capacity of EGCG were 35.4% and 32.7%, and 17.0% and 16.0%, respectively. These coatings significantly stabilized BEN in the pH range from 1.5 to 6.0. Faster release of EGCG was observed in all the nanoparticles incubated in simulated gastric and intestinal fluids with proteinases. However, the coatings delayed the release of EGCG from the nanoparticles. The storage stability study showed faster degradation of EGCG in all the nanoparticles compared to free EGCG. CBEN significantly enhanced EGCG absorption on Caco-2 monolayer, which was attributed to the enhancement of cellular uptake of CBEN by Caco-2 cells.

Ovalbumin and dextran were conjugated using the Maillard reaction. EGCG ovalbumin-dextran conjugate nanoparticles and crosslinked EGCG ovalbumin-dextran conjugate nanoparticles were formed by self-assembly under a heating process. These particles showed a spherical morphology measured by SEM and the sizes were 285 nm and 339 nm in aqueous suspension. The loading efficiency of EGCG in these two conjugated nanoparticles was 23.4% and 30.0%, whereas the loading capacity was 19.6% and 20.9%, respectively. EGCG ovalbumin-dextran conjugate nanoparticles and crosslinked EGCG ovalbumin-dextran conjugate nanoparticles remained at nano-scale sizes in the pH range from 2.5 to 7.5, and they showed stable particle sizes in SGF and SIF at 37^{o}C for 2 hours. Partial release of EGCG from these two nanoparticles in SGF and SIF without and with digestive enzymes was observed. EGCG in EGCG ovalbumin-dextran conjugate nanoparticles showed higher apparent permeability coefficient (P_{app}) on Caco-2 monolayers compared to EGCG solution.

LIST OF REFERENCES

(1) Kähkönen, M. P.; Hopia, A. I.; Vuorela, H. J.; Rauha, J.-P.; Pihlaja, K.; Kujala, T. S.; Heinonen, M., Antioxidant activity of plant extracts containing phenolic compounds. *Journal of Agricultural and Food Chemistry* **1999,** *47*, 3954-3962.

(2) Asen, S.; Stewart, R. N.; Norris, K. H., Co-pigmentation of anthocyanins in plant tissues and its effect on color. *Phytochemistry* **1972,** *11*, 1139-1144.

(3) Jackman, R. L.; Yada, R. Y.; Tung, M. A.; Speers, R. A., Athocyanins as food colorants —A review. *Journal of Food Biochemistry* **1987,** *11*, 201-247.

(4) Castañeda-Ovando, A.; Pacheco-Hernández, M. d. L.; Páez-Hernández, M. E.; Rodríguez, J. A.; Galán-Vidal, C. A., Chemical studies of anthocyanins: A review. *Food Chemistry* **2009,** *113*, 859-871.

(5) Lynn, D. G.; Chang, M., Phenolic signals in cohabitation: implications for plant development. *Annual Review of Plant Physiology and Plant Molecular Biology* **1990,** *41*, 497-526.

(6) Labrecque, L.; Lamy, S.; Chapus, A.; Mihoubi, S.; Durocher, Y.; Cass, B.; Bojanowski, M. W.; Gingras, D.; Béliveau, R., Combined inhibition of PDGF and VEGF receptors by ellagic acid, a dietary-derived phenolic compound. *Carcinogenesis* **2005,** *26*, 821-826.

(7) Rice-Evans, C.; Miller, N.; Paganga, G., Antioxidant properties of phenolic compounds. *Trends in Plant Science* **1997,** *2*, 152-159.

(8) Cai, Y.; Luo, Q.; Sun, M.; Corke, H., Antioxidant activity and phenolic compounds of 112 traditional Chinese medicinal plants associated with anticancer. *Life Sciences* **2004,** *74*, 2157-2184.

(9) Frankel, E. N.; German, J. B.; Kinsella, J. E.; Parks, E.; Kanner, J., Inhibition of oxidation of human low-density lipoprotein by phenolic substances in red wine. *The Lancet* **1993,** *341*, 454-457.

(10) Hollman, P. C. H.; Katan, M. B., Absorption, metabolism and health effects of dietary flavonoids in man. *Biomedicine & Pharmacotherapy* **1997,** *51*, 305-310.

(11) Kanaze, F. I.; Bounartzi, M. I.; Georgarakis, M.; Niopas, I., Pharmacokinetics of the citrus flavanone aglycones hesperetin and naringenin after single oral administration in human subjects. *Eur J Clin Nutr* **2006,** *61*, 472-477.

(12) Appeldoorn, M. M.; Vincken, J.-P.; Gruppen, H.; Hollman, P. C. H., Procyanidin dimers A1, A2, and B2 are absorbed without conjugation or methylation from the small intestine of rats. *The Journal of Nutrition* **2009,** *139*, 1469-1473.

(13) des Rieux, A.; Fievez, V.; Garinot, M.; Schneider, Y.-J.; Préat, V., Nanoparticles as potential oral delivery systems of proteins and vaccines: A mechanistic approach. *Journal of Controlled Release* **2006,** *116*, 1-27.

(14) Müller, R. H.; Mäder, K.; Gohla, S., Solid lipid nanoparticles (SLN) for controlled drug delivery – a review of the state of the art. *European Journal of Pharmaceutics and Biopharmaceutics* **2000,** *50*, 161-177.

(15) Crozier, A.; Jaganath, I. B.; Clifford, M. N., Dietary phenolics: chemistry, bioavailability and effects on health. *Natural Product Reports* **2009,** *26*, 1001-1043.

(16) Castillo-Muñoz, N.; Gómez-Alonso, S.; García-Romero, E.; Hermosín-Gutiérrez, I., Flavonol profiles of vitis vinifera red grapes and their single-cultivar wines. *Journal of Agricultural and Food Chemistry* **2007,** *55*, 992-1002.

(17) Li, Z.; Pan, Q.; Cui, X.; Duan, C., Optimization on anthocyanins extraction from wine grape skins using orthogonal test design. *Food Science and Biotechnology* **2010,** *19*, 1047-1053.

(18) Barnes, J. S.; Nguyen, H. P.; Shen, S.; Schug, K. A., General method for extraction of blueberry anthocyanins and identification using high performance liquid chromatography–electrospray ionization-ion trap-time of flight-mass spectrometry. *Journal of Chromatography A* **2009,** *1216*, 4728-4735.

(19) Souquet, J.-M.; Cheynier, V.; Brossaud, F.; Moutounet, M., Polymeric proanthocyanidins from grape skins. *Phytochemistry* **1996,** *43*, 509-512.

(20) Wang, H.; Murphy, P. A., Isoflavone content in commercial soybean foods. *Journal of Agricultural and Food Chemistry* **1994,** *42*, 1666-1673.

(21) Aoki, T.; Akashi, T.; Ayabe, S.-i., Flavonoids of leguminous plants: Structure, biological activity, and biosynthesis. *Journal of Plant Research* **2000,** *113*, 475-488.

(22) Ossipov, V.; Salminen, J.-P.; Ossipova, S.; Haukioja, E.; Pihlaja, K., Gallic acid and hydrolysable tannins are formed in birch leaves from an intermediate compound of the shikimate pathway. *Biochemical Systematics and Ecology* **2003,** *31*, 3-16.

(23) Jang, M.; Cai, L.; Udeani, G. O.; Slowing, K. V.; Thomas, C. F.; Beecher, C. W. W.; Fong, H. H. S.; Farnsworth, N. R.; Kinghorn, A. D.; Mehta, R. G.; Moon, R. C.; Pezzuto, J. M., Cancer chemopreventive activity of resveratrol, a natural product derived from grapes. *Science* **1997,** *275*, 218-220.

(24) Romero-Pérez, A. I.; Ibern-Gómez, M.; Lamuela-Raventós, R. M.; de la Torre-Boronat, M. C., Piceid, the major resveratrol derivative in grape juices. *Journal of Agricultural and Food Chemistry* **1999,** *47*, 1533-1536.

(25) Kundu, J. K.; Surh, Y.-J., Cancer chemopreventive and therapeutic potential of resveratrol: Mechanistic perspectives. *Cancer Letters* **2008,** *269*, 243-261.

(26) Baur, J. A.; Sinclair, D. A., Therapeutic potential of resveratrol: the in vivo evidence. *Nat Rev Drug Discov* **2006,** *5*, 493-506.

(27) Renaud, S.; de Lorgeril, M., Wine, alcohol, platelets, and the French paradox for coronary heart disease. *The Lancet* **1992,** *339*, 1523-1526.

(28) Wu, J. M.; Wang, Z. R.; Hsieh, T. C.; Bruder, J. L.; Zou, J. G.; Huang, Y. Z., Mechanism of cardioprotection by resveratrol, a phenolic antioxidant present in red wine (Review). *International journal of molecular medicine* **2001,** *8*, 3-17.

(29) Wang, Z.; Huang, Y.; Zou, J.; Cao, K.; Xu, Y.; Wu, J. M., Effects of red wine and wine polyphenol resveratrol on platelet aggregation in vivo and in vitro. *International Journal of Molecular Medicine* **2002,** *9*, 77-79.

(30) Sun, A. Y.; Simonyi, A.; Sun, G. Y., The “French paradox” and beyond: neuroprotective effects of polyphenols. *Free Radical Biology and Medicine* **2002,** *32*, 314-318.

(31) Vidavalur, R.; Otani, H.; Singal, P. K.; Maulik, N., Significance of wine and resveratrol in cardiovascular disease: French paradox revisited. *Experimental and Clinical Cardiology* **2006,** *11*, 217-225.

(32) Bertelli, A. A.; Giovannini, L.; Giannessi, D.; Migliori, M.; Bernini, W.; Fregoni, M.; Bertelli, A., Antiplatelet activity of synthetic and natural resveratrol in red wine. *International journal of tissue reactions* **1995,** *17*, 1-3.

(33) Martinez, J.; Moreno, J. J., Effect of resveratrol, a natural polyphenolic compound, on reactive oxygen species and prostaglandin production. *Biochemical Pharmacology* **2000,** *59*, 865-870.

(34) Lu, R.; Serrero, G., Resveratrol, a natural product derived from grape, exhibits antiestrogenic activity and inhibits the growth of human breast cancer cells. *Journal of Cellular Physiology* **1999,** *179*, 297-304.

(35) Lagouge, M.; Argmann, C.; Gerhart-Hines, Z.; Meziane, H.; Lerin, C.; Daussin, F.; Messadeq, N.; Milne, J.; Lambert, P.; Elliott, P.; Geny, B.; Laakso, M.; Puigserver, P.; Auwerx, J., Resveratrol improves mitochondrial function and protects against metabolic disease by activating SIRT1 and PGC-1. *Cell* **2006,** *127*, 1109-1122.

(36) Frankel, E. N.; Waterhouse, A. L.; Kinsella, J. E., Inhibition of human LDL oxidation by resveratrol. *The Lancet* **1993,** *341*, 1103-1104.

(37) Clément, M.-V.; Hirpara, J. L.; Chawdhury, S.-H.; Pervaiz, S., Chemopreventive agent resveratrol, a natural product derived from grapes, triggers CD95 signaling-dependent apoptosis in human tumor cells. *Blood* **1998,** *92*, 996-1002.

(38) Kaeberlein, M.; McDonagh, T.; Heltweg, B.; Hixon, J.; Westman, E. A.; Caldwell, S. D.; Napper, A.; Curtis, R.; DiStefano, P. S.; Fields, S.; Bedalov, A.; Kennedy, B. K., Substrate-specific activation of sirtuins by resveratrol. *Journal of Biological Chemistry* **2005,** *280*, 17038-17045.

(39) Yang, J.-H.; Hsia, T.-C.; Kuo, H.-M.; Chao, P.-D. L.; Chou, C.-C.; Wei, Y.-H.; Chung, J.-G., Inhibition of lung cancer cell growth by quercetin glucuronides via G2/M arrest and induction of apoptosis. *Drug Metabolism and Disposition* **2006,** *34*, 296-304.

(40) Morris, J. D. H.; Pramanik, R.; Zhang, X.; Carey, A.-M.; Ragavan, N.; Martin, F. L.; Muir, G. H., Selenium- or quercetin-induced retardation of DNA synthesis in primary prostate cells occurs in the presence of a concomitant reduction in androgen-receptor activity. *Cancer Letters* **2006,** *239*, 111-122.

(41) Granado-Serrano, A. B.; Martín, M. Á.; Bravo, L.; Goya, L.; Ramos, S., Quercetin attenuates TNF-induced inflammation in hepatic cells by inhibiting the NF-κB pathway. *Nutrition and Cancer* **2012,** *64*, 588-598.

(42) Vessal, M.; Hemmati, M.; Vasei, M., Antidiabetic effects of quercetin in streptozocin-induced diabetic rats. *Comparative Biochemistry and Physiology Part C: Toxicology & Pharmacology* **2003,** *135*, 357-364.

(43) Hsu, C.-P.; Shih, Y.-T.; Lin, B.-R.; Chiu, C.-F.; Lin, C.-C., Inhibitory effect and mechanisms of an anthocyanins- and anthocyanidins-rich extract from purple-shoot tea on colorectal carcinoma cell proliferation. *Journal of Agricultural and Food Chemistry* **2012,** *60*, 3686-3692.

(44) Devi, P. S.; Kumar, M. S.; Das, S. M., Evaluation of antiproliferative activity of red sorghum bran anthocyanin on a human breast cancer cell line (MCF-7). *International Journal of Breast Cancer* **2011,** *2011*.

(45) Murapa, P.; Dai, J.; Chung, M.; Mumper, R. J.; D'Orazio, J., Anthocyanin-rich fractions of blackberry extracts reduce UV-induced free radicals and oxidative damage in keratinocytes. *Phytotherapy Research* **2012,** *26*, 106-112.

(46) Bishayee, A.; Mbimba, T.; Thoppil, R. J.; Háznagy-Radnai, E.; Sipos, P.; Darvesh, A. S.; Folkesson, H. G.; Hohmann, J., Anthocyanin-rich black currant (Ribes nigrum L.) extract affords chemoprevention against diethylnitrosamine-induced hepatocellular carcinogenesis in rats. *The Journal of Nutritional Biochemistry* **2011,** *22*, 1035-1046.

(47) Sarkar, F. H.; Li, Y., Soy isoflavones and cancer prevention. *Cancer Investigation* **2003,** *21*, 744-757.

(48) Setchell, K. D., Phytoestrogens: the biochemistry, physiology, and implications for human health of soy isoflavones. *The American Journal of Clinical Nutrition* **1998,** *68*, 1333S-1346S.

(49) Hillman, G. G.; Singh-Gupta, V., Soy isoflavones sensitize cancer cells to radiotherapy. *Free Radical Biology and Medicine* **2011,** *51*, 289-298.

(50) Singh, B. N.; Shankar, S.; Srivastava, R. K., Green tea catechin, epigallocatechin-3-gallate (EGCG): Mechanisms, perspectives and clinical applications. *Biochemical Pharmacology* **2011,** *82*, 1807-1821.

(51) Chen, C.; Yu, R.; Owuor, E.; Tony Kong, A., Activation of antioxidant-response element (ARE), mitogen-activated protein kinases (MAPKs) and caspases by major green tea polyphenol components during cell survival and death. *Archives of Pharmacal Research* **2000,** *23*, 605-612.

(52) Kim, J.; Zhang, X.; Rieger-Christ, K. M.; Summerhayes, I. C.; Wazer, D. E.; Paulson, K. E.; Yee, A. S., Suppression of Wnt signaling by the green tea compound (–)-epigallocatechin 3-gallate (EGCG) in invasive breast cancer cells. *Journal of Biological Chemistry* **2006,** *281*, 10865-10875.

(53) Li, W.-g.; Li, Q.-h.; Tan, Z., Epigallocatechin gallate induces telomere fragmentation in HeLa and 293 but not in MRC-5 cells. *Life Sciences* **2005,** *76*, 1735-1746.

(54) McGhie, T. K.; Walton, M. C., The bioavailability and absorption of anthocyanins: Towards a better understanding. *Molecular Nutrition & Food Research* **2007,** *51*, 702-713.

(55) Zhu, Q. Y.; Zhang, A.; Tsang, D.; Huang, Y.; Chen, Z.-Y., Stability of green tea catechins. *Journal of Agricultural and Food Chemistry* **1997,** *45*, 4624-4628.

(56) Onoue, S.; Ochi, M.; Yamada, S., Development of (−)-epigallocatechin-3-gallate (EGCG)-loaded enteric microparticles with intestinal mucoadhesive property. *International Journal of Pharmaceutics* **2011,** *410*, 111-113.

(57) Konishi, Y., Transepithelial transport of microbial metabolites of quercetin in intestinal Caco-2 cell monolayers. *Journal of Agricultural and Food Chemistry* **2005,** *53*, 601-607.

(58) Cerda, B.; Periago, P.; Espin, J. C.; Tomas-Barberan, F. A., Identification of urolithin A as a metabolite produced by human colon microflora from ellagic acid and related compounds. *Journal of Agricultural and Food Chemistry* **2005,** *53*, 5571-5576.

(59) Stephanie, D.; Isabelle, M.; Jean-Francois, H.; Daniel, T.; Augustin, S., Transport of proanthocyanidin dimer, trimer, and polymer across monolayers of human intestinal epithelial Caco-2 cells. *Antioxidants & Redox Signaling* **2001,** *3*, 957-967.

(60) Kim, M.; Kometani, T.; Okada, S.; Shimuzu, M., Permeation of hesperidin glycosides across Caco-2 cell monolayers via the paracellular pathway. *Biosci Biotechnol Biochem* **1999,** *63*, 2183-2188.

(61) Boyer, J.; Brown, D.; Liu, R., In vitro digestion and lactase treatment influence uptake of quercetin and quercetin glucoside by the Caco-2 cell monolayer. *Nutrition Journal* **2005,** *4*, 1.

(62) Boyer, J.; Brown, D.; Liu, R. H., Uptake of quercetin and quercetin 3-glucoside from whole onion and apple peel extracts by Caco-2 cell monolayers. *Journal of Agricultural and Food Chemistry* **2004,** *52*, 7172-7179.

(63) Tian, X.-J.; Yang, X.-W.; Yang, X.; Wang, K., Studies of intestinal permeability of 36 flavonoids using Caco-2 cell monolayer model. *International Journal of Pharmaceutics* **2009,** *367*, 58-64.

(64) Kaldas, M. I.; Walle, U. K.; Walle, T., Resveratrol transport and metabolism by human intestinal Caco-2 cells. *J Pharm Pharmacol* **2003,** *55*, 307-312.

(65) Chukwumah, Y.; Walker, L.; Vogler, B.; Verghese, M., In vitro absorption of dietary trans-resveratrol from boiled and roasted peanuts in Caco-2 cells. *Journal of Agricultural and Food Chemistry* **2011,** *59*, 12323-12329.

(66) Murota, K.; Shimizu, S.; Miyamoto, S.; Izumi, T.; Obata, A.; Kikuchi, M.; Terao, J., Unique uptake and transport of isoflavone aglycones by human intestinal Caco-2 cells: Comparison of isoflavonoids and flavonoids. *The Journal of Nutrition* **2002,** *132*, 1956-1961.

(67) Planas, J. M.; Alfaras, I.; Colom, H.; Juan, M. E., The bioavailability and distribution of trans-resveratrol are constrained by ABC transporters. *Archives of Biochemistry and Biophysics* **2012,** *527*, 67-73.

(68) Zhang, L.; Zheng, Y.; Chow, M. S. S.; Zuo, Z., Investigation of intestinal absorption and disposition of green tea catechins by Caco-2 monolayer model. *International Journal of Pharmaceutics* **2004,** *287*, 1-12.

(69) Zhang, L.; Chow, M. S. S.; Zuo, Z., Effect of the co-occurring components from green tea on the intestinal absorption and disposition of green tea polyphenols in Caco-2 monolayer model. *Journal of Pharmacy and Pharmacology* **2006,** *58*, 37-44.

(70) Shimomura, M.; Sawadaishi, T., Bottom-up strategy of materials fabrication: a new trend in nanotechnology of soft materials. *Current Opinion in Colloid & Interface Science* **2001,** *6*, 11-16.

(71) Whitesides, G. M.; Grzybowski, B., Self-assembly at all scales. *Science* **2002,** *295*, 2418-2421.

(72) Zhong, Q.; Jin, M., Zein nanoparticles produced by liquid–liquid dispersion. *Food Hydrocolloids* **2009,** *23*, 2380-2387.

(73) Grzelczak, M.; Vermant, J.; Furst, E. M.; Liz-Marzán, L. M., Directed self-assembly of nanoparticles. *ACS Nano* **2010,** *4*, 3591-3605.

(74) Yi, K.; Cheng, G.; Xing, F., Gelatin/tannin complex nanospheres via molecular assembly. *Journal of Applied Polymer Science* **2006,** *101*, 3125-3130.

(75) Li, Z.; Gu, L., Effects of mass ratio, pH, temperature, and reaction time on fabrication of partially purified pomegranate ellagitannin−gelatin nanoparticles. *Journal of Agricultural and Food Chemistry* **2011,** *59*, 4225-4231.

(76) Chen, Y.-C.; Yu, S.-H.; Tsai, G.-J.; Tang, D.-W.; Mi, F.-L.; Peng, Y.-P., Novel Technology for the preparation of self-assembled catechin/gelatin nanoparticles and their characterization. *Journal of Agricultural and Food Chemistry* **2010,** *58*, 6728-6734.

(77) Bootz, A.; Vogel, V.; Schubert, D.; Kreuter, J., Comparison of scanning electron microscopy, dynamic light scattering and analytical ultracentrifugation for the sizing of poly(butyl cyanoacrylate) nanoparticles. *European Journal of Pharmaceutics and Biopharmaceutics* **2004,** *57*, 369-375.

(78) Pusey, P. N., Suppression of multiple scattering by photon cross-correlation techniques. *Current Opinion in Colloid & Interface Science* **1999,** *4*, 177-185.

(79) Filipe, V.; Hawe, A.; Jiskoot, W., Critical evaluation of nanoparticle tracking analysis (NTA) by nanoSight for the measurement of nanoparticles and protein aggregates. *Pharmaceutical Research* **2010,** *27*, 796-810.

(80) Williams, D. B.; Carter, C. B., *Transmission electron microscopy: A textbook for materials science*. second edition ed.; Springer: New York, 2009.

(81) Powers, K. W.; Brown, S. C.; Krishna, V. B.; Wasdo, S. C.; Moudgil, B. M.; Roberts, S. M., Research strategies for safety evaluation of nanomaterials. Part VI. Characterization of nanoscale particles for toxicological evaluation. *Toxicological Sciences* **2006,** *90*, 296-303.

(82) Zou, T.; Li, Z.; Percival, S. S.; Bonard, S.; Gu, L., Fabrication, characterization, and cytotoxicity evaluation of cranberry procyanidins-zein nanoparticles. *Food Hydrocolloids* **2012,** *27*, 293-300.

(83) Rejinold, N.; Muthunarayanana, M.; Chennazhi, K.; Nair, S.; Jayakumar, R., Curcumin loaded firbinogen nanoparticles for cancer drug delivery. *Journal of Biomedical Nanotechnology* **2011,** *7*, 521-534.

(84) Luz, P.; Magalhães, L.; Pereira, A.; Cunha, W.; Rodrigues, V.; Andrade e Silva, M., Curcumin-loaded into PLGA nanoparticles. *Parasitology Research* **2012,** *110*, 593-598.

(85) Mukerjee, A.; Vishwanatha, J. K., Formulation, characterization and evaluation of curcumin-loaded PLGA nanospheres for cancer therapy. *Anticancer Research* **2009,** *29*, 3867-3875.

(86) Anand, P.; Nair, H. B.; Sung, B.; Kunnumakkara, A. B.; Yadav, V. R.; Tekmal, R. R.; Aggarwal, B. B., Design of curcumin-loaded PLGA nanoparticles formulation with enhanced cellular uptake, and increased bioactivity in vitro and superior bioavailability in vivo. *Biochemical Pharmacology* **2010,** *79*, 330-338.

(87) Das, R. K.; Kasoju, N.; Bora, U., Encapsulation of curcumin in alginate-chitosan-pluronic composite nanoparticles for delivery to cancer cells. *Nanomedicine: Nanotechnology, Biology and Medicine* **2010,** *6*, 153-160.

(88) Duan, J.; Zhang, Y.; Han, S.; Chen, Y.; Li, B.; Liao, M.; Chen, W.; Deng, X.; Zhao, J.; Huang, B., Synthesis and in vitro/in vivo anti-cancer evaluation of curcumin-loaded chitosan/poly(butyl cyanoacrylate) nanoparticles. *International Journal of Pharmaceutics* **2010,** *400*, 211-220.

(89) Teng, Z.; Luo, Y.; Wang, Q., Nanoparticles synthesized from soy protein: Preparation, characterization, and application for nutraceutical encapsulation. *Journal of Agricultural and Food Chemistry* **2012,** *60*, 2712-2720.

(90) Kim, T. H.; Jiang, H. H.; Youn, Y. S.; Park, C. W.; Tak, K. K.; Lee, S.; Kim, H.; Jon, S.; Chen, X.; Lee, K. C., Preparation and characterization of water-soluble albumin-bound curcumin nanoparticles with improved antitumor activity. *International Journal of Pharmaceutics* **2011,** *403*, 285-291.

(91) Sang, S.; Lee, M.-J.; Hou, Z.; Ho, C.-T.; Yang, C. S., Stability of tea polyphenol (−)-epigallocatechin-3-gallate and formation of dimers and epimers under common experimental conditions. *Journal of Agricultural and Food Chemistry* **2005,** *53*, 9478-9484.

(92) Kim, M.-R.; Hong, J., Analysis of chemical interactions of (−)-epigallocatechin-3-gallate, a major green tea polyphenol, with commonly-consumed over-thecounter drugs. *Food Science and Biotechnology* **2010,** *19*, 559-564.

(93) Nellans, H. N., (B) Mechanisms of peptide and protein absorption: (1) Paracellular intestinal transport: modulation of absorption. *Advanced Drug Delivery Reviews* **1991,** *7*, 339-364.

(94) Sonaje, K.; Chuang, E.-Y.; Lin, K.-J.; Yen, T.-C.; Su, F.-Y.; Tseng, M. T.; Sung, H.-W., Opening of epithelial tight junctions and enhancement of paracellular permeation by chitosan: Microscopic, ultrastructural, and computed-tomographic observations. *Molecular Pharmaceutics* **2012,** *9*, 1271-1279.

(95) Jevprasesphant, R.; Penny, J.; Attwood, D.; McKeown, N. B.; D'Emanuele, A., Engineering of dendrimer surfaces to enhance transepithelial transport and reduce cytotoxicity. *Pharmaceutical Research* **2003,** *20*, 1543-1550.

(96) Zha, L. Y.; Xu, Z. R.; Wang, M. Q.; Gu, L. Y., Chromium nanoparticle exhibits higher absorption efficiency than chromium picolinate and chromium chloride in Caco-2 cell monolayers. *Journal of Animal Physiology and Animal Nutrition* **2008,** *92*, 131-140.

(97) Ward, P. D.; Tippin, T. K.; Thakker, D. R., Enhancing paracellular permeability by modulating epithelial tight junctions. *Pharmaceutical Science & Technology Today* **2000,** *3*, 346-358.

(98) Vllasaliu, D.; Exposito-Harris, R.; Heras, A.; Casettari, L.; Garnett, M.; Illum, L.; Stolnik, S., Tight junction modulation by chitosan nanoparticles: Comparison with chitosan solution. *International Journal of Pharmaceutics* **2010,** *400*, 183-193.

(99) Martien, R.; Loretz, B.; Sandbichler, A. M.; Schnürch, A. B., Thiolated chitosan nanoparticles: transfection study in the Caco-2 differentiated cell culture. *Nanotechnology* **2008,** *19*, 045101.

(100) Sadeghi, A. M. M.; Dorkoosh, F. A.; Avadi, M. R.; Weinhold, M.; Bayat, A.; Delie, F.; Gurny, R.; Larijani, B.; Rafiee-Tehrani, M.; Junginger, H. E., Permeation enhancer effect of chitosan and chitosan derivatives: Comparison of formulations as soluble polymers and nanoparticulate systems on insulin absorption in Caco-2 cells. *European Journal of Pharmaceutics and Biopharmaceutics* **2008,** *70*, 270-278.

(101) Bravo-Osuna, I.; Vauthier, C.; Chacun, H.; Ponchel, G., Specific permeability modulation of intestinal paracellular pathway by chitosan-poly(isobutylcyanoacrylate) core-shell nanoparticles. *European Journal of Pharmaceutics and Biopharmaceutics* **2008,** *69*, 436-444.

(102) Kudsiova, L.; Lawrence, M. J., A comparison of the effect of chitosan and chitosan-coated vesicles on monolayer integrity and permeability across Caco-2 and 16HBE14o-cells. *Journal of Pharmaceutical Sciences* **2008,** *97*, 3998-4010.

(103) Yeh, T.-H.; Hsu, L.-W.; Tseng, M. T.; Lee, P.-L.; Sonjae, K.; Ho, Y.-C.; Sung, H.-W., Mechanism and consequence of chitosan-mediated reversible epithelial tight junction opening. *Biomaterials* **2011,** *32*, 6164-6173.

(104) Junginger, H. E.; Verhoef, J. C., Macromolecules as safe penetration enhancers for hydrophilic drugs—a fiction? *Pharmaceutical Science & Technology Today* **1998,** *1*, 370-376.

(105) Borchard, G.; Lueβen, H. L.; de Boer, A. G.; Verhoef, J. C.; Lehr, C.-M.; Junginger, H. E., The potential of mucoadhesive polymers in enhancing intestinal peptide drug absorption. III: Effects of chitosan-glutamate and carbomer on epithelial tight junctions in vitro. *Journal of Controlled Release* **1996,** *39*, 131-138.

(106) Leroux, J.-C.; Gravel, P.; Balant, L.; Volet, B.; Anner, B. M.; Allémann, E.; Doelker, E.; Gurny, R., Internalization of poly(D,L-1actic acid) nanoparticles by isolated human leukocytes and analysis of plasma proteins adsorbed onto the particles. *Journal of Biomedical Materials Research* **1994,** *28*, 471-481.

(107) Xing, X.; He, X.; Peng, J.; Wang, K.; Tan, W., Uptake of silica-coated nanoparticles by HeLa cells. *Journal of Nanoscience and Nanotechnology* **2005,** *5*, 1688-1693.

(108) Kim, H.; Gil, S.; Andrieux, K.; Nicolas, V.; Appel, M.; Chacun, H.; Desmaële, D.; Taran, F.; Georgin, D.; Couvreur, P., Low-density lipoprotein receptor-mediated endocytosis of PEGylated nanoparticles in rat brain endothelial cells. *Cellular and Molecular Life Sciences* **2007,** *64*, 356-364.

(109) Benfer, M.; Kissel, T., Cellular uptake mechanism and knockdown activity of siRNA-loaded biodegradable DEAPA-PVA-g-PLGA nanoparticles. *European Journal of Pharmaceutics and Biopharmaceutics* **2012,** *80*, 247-256.

(110) Panyam, J.; Labhasetwar, V., Dynamics of endocytosis and exocytosis of poly(D,L-Lactide-co-Glycolide) nanoparticles in vascular smooth muscle cells. *Pharmaceutical Research* **2003,** *20*, 212-220.

(111) Chang, J.; Jallouli, Y.; Kroubi, M.; Yuan, X.-b.; Feng, W.; Kang, C.-s.; Pu, P.-y.; Betbeder, D., Characterization of endocytosis of transferrin-coated PLGA nanoparticles by the blood–brain barrier. *International Journal of Pharmaceutics* **2009,** *379*, 285-292.

(112) Ofokansi, K.; Winter, G.; Fricker, G.; Coester, C., Matrix-loaded biodegradable gelatin nanoparticles as new approach to improve drug loading and delivery. *European Journal of Pharmaceutics and Biopharmaceutics* **2010,** *76*, 1-9.

(113) Tseng, C.-L.; Wang, T.-W.; Dong, G.-C.; Yueh-Hsiu Wu, S.; Young, T.-H.; Shieh, M.-J.; Lou, P.-J.; Lin, F.-H., Development of gelatin nanoparticles with biotinylated EGF conjugation for lung cancer targeting. *Biomaterials* **2007,** *28*, 3996-4005.

(114) Smith, P. J.; Giroud, M.; Wiggins, H. L.; Gower, F.; Thorley, J. A.; Stolpe, B.; Mazzolini, J.; Dyson, R. J.; Rappoport, J. Z., Cellular entry of nanoparticles via serum sensitive clathrin-mediated endocytosis, and plasma membrane permeabilization. *International Journal of Nanomedicine* **2012,** *7*, 2045-2055.

(115) Mercer, J.; Helenius, A., Virus entry by macropinocytosis. *Nat Cell Biol* **2009,** *11*, 510-520.

(116) Sahay, G.; Alakhova, D. Y.; Kabanov, A. V., Endocytosis of nanomedicines. *Journal of Controlled Release* **2010,** *145*, 182-195.

(117) O' Neill, M. J.; Guo, J.; Byrne, C.; Darcy, R.; O' Driscoll, C. M., Mechanistic studies on the uptake and intracellular trafficking of novel cyclodextrin transfection complexes by intestinal epithelial cells. *International Journal of Pharmaceutics* **2011,** *413*, 174-183.

(118) Acosta, E., Bioavailability of nanoparticles in nutrient and nutraceutical delivery. *Curr. Opin. Colloid Interface Sci.* **2009,** *14*, 3–15.

(119) Ogunkoya, Y.; Nickel, B.; Gay, V.; Murray, S., Using quantum dots to visualize clathrin associations. *Biotechnic & Histochemistry* **2009,** *84*, 109-115.

(120) Ehrlich, M.; Boll, W.; van Oijen, A.; Hariharan, R.; Chandran, K.; Nibert, M. L.; Kirchhausen, T., Endocytosis by random initiation and stabilization of clathrin-coated pits. *Cell* **2004,** *118*, 591-605.

(121) Roger, E.; Lagarce, F.; Garcion, E.; Benoit, J.-P., Biopharmaceutical parameters to consider in order to alter the fate of nanocarriers after oral delivery. *Nanomedicine* **2010,** *5*, 287-306.

(122) Wang, J.; Byrne, J. D.; Napier, M. E.; DeSimone, J. M., More Effective nanomedicines through particle design. *Small* **2011,** *7*, 1919-1931.

(123) Kiss, A. L., Caveolae and the regulation of endocytosis
caveolins and caveolae. In Jasmin, J.-F.; Frank, P. G.; Lisanti, M. P., Eds. Springer US: 2012; Vol. 729, pp 14-28.

(124) Reilly, M. J.; Larsen, J. D.; Sullivan, M. O., Polyplexes traffic through caveolae to the golgi and endoplasmic reticulum en route to the nucleus. *Molecular Pharmaceutics* **2012,** *9*, 1280-1290.

(125) Schnitzer, J. E.; Oh, P.; Pinney, E.; Allard, J., Filipin-sensitive caveolae-mediated transport in endothelium: reduced transcytosis, scavenger endocytosis, and capillary permeability of select macromolecules. *The Journal of Cell Biology* **1994,** *127*, 1217-1232.

(126) Hao, X.; Wu, J.; Shan, Y.; Cai, M.; Shang, X.; Jiang, J.; Wang, H., Caveolae-mediated endocytosis of biocompatible gold nanoparticles in living Hela cells. *Journal of Physics: Condensed Matter* **2012,** *24*, 164207.

(127) Rejman, J.; Oberle, V.; Zuhorn, I. S.; Hoekstra, D., Size-dependent internalization of particles via the pathways of clathrin- and caveolae-mediated endocytosis. *Biochem. J.* **2004,** *377*, 159-169.

(128) Jin, H.; Lovell, J. F.; Chen, J.; Lin, Q.; Ding, L.; Ng, K. K.; Pandey, R. K.; Manoharan, M.; Zhang, Z.; Zheng, G., Mechanistic insights into LDL nanoparticle-mediated siRNA delivery. *Bioconjugate Chemistry* **2011,** *23*, 33-41.

(129) Ma, X.; Wu, Y.; Jin, S.; Tian, Y.; Zhang, X.; Zhao, Y.; Yu, L.; Liang, X.-J., Gold nanoparticles induce autophagosome accumulation through size-dependent nanoparticle uptake and lysosome impairment. *ACS Nano* **2011,** *5*, 8629-8639.

(130) Li, W.; Chen, C.; Ye, C.; Wei, T.; Zhao, Y.; Lao, F.; Chen, Z.; Meng, H.; Gao, Y.; Yuan, H.; Xing, G.; Zhao, F.; Chai, Z.; Zhang, X.; Yang, F.; Han, D.; Tang, X.; Zhang, Y., The translocation of fullerenic nanoparticles into lysosome via the pathway of clathrin-mediated endocytosis. *Nanotechnology* **2008,** *19*, 145102.

(131) Qian, M.; Cai, D.; Verhey, K.; Tsai, B., A lipid receptor sorts polyomavirus from the endolysosome to the endoplasmic reticulum to cause infection. *PLoS Pathogens* **2009,** *5*, e1000465.

(132) Buzea, C.; Pacheco, I. I.; Robbie, K., Nanomaterials and nanoparticles: sources and toxicity. *Biointerphases* **2007,** *2*, MR17-MR71.

(133) Siddiqui, I. A.; Adhami, V. M.; Bharali, D. J.; Hafeez, B. B.; Asim, M.; Khwaja, S. I.; Ahmad, N.; Cui, H.; Mousa, S. A.; Mukhtar, H., Introducing nanochemopreention as a novel approach for cancer control: proof of principle with green tea polyphenol epigallocatechin-3-gallate. *Cancer Research* **2009,** *69*, 1712-1716.

(134) Parveen, S.; Mitra, M.; Krishnakumar, S.; Sahoo, S. K., Enhanced antiproliferative activity of carboplatin-loaded chitosan-alginate nanoparticles in a retinoblastoma cell line. *Acta Biomaterialia In Press, Corrected Proof*.

(135) Tseng, C.-L.; Su, W.-Y.; Yen, K.-C.; Yang, K.-C.; Lin, F.-H., The use of biotinylated-EGF-modified gelatin nanoparticle carrier to enhance cisplatin accumulation in cancerous lungs via inhalation. *Biomaterials* **2009,** *30*, 3476-3485.

(136) Cerdá, B.; Llorach, R.; Cerón, J. J.; Espín, J. C.; Tomás-Barberán, F. A., Evaluation of the bioavailability and metabolism in the rat of punicalagin, an antioxidant polyphenol from pomegranate juice. *European Journal of Nutrition* **2003,** *42*, 18-28.

(137) Seeram, N.; Lee, R.; Hardy, M.; Heber, D., Rapid large scale purification of ellagitannins from pomegranate husk, a by-product of the commercial juice industry. *Separation and Purification Technology* **2005,** *41*, 49-55.

(138) Kaplan, M.; Hayek, T.; Raz, A.; Coleman, R.; Dornfield, L.; Vaya, J.; Aviram, M., Pomegranate juice supplementation to atherosclerotic mice reduces macrophage lipid peroxidation, cellular cholesterol accumulation and development of atherosclerosis. *Journal of Nutrition* **2001,** *131*, 2082-2089.

(139) Adams, L. S.; Seeram, N. P.; Aggarwal, B. B.; Takada, Y.; Sand, D.; Heber, D., Pomegranate juice, total pomegranate ellagitannins, and punicalagin suppress inflammatory cell signaling in colon cancer cells. *Journal of Agricultural and Food Chemistry* **2006,** *54*, 980-985.

(140) Heber, D.; Seeram, N. P.; Wyatt, H.; Henning, S. M.; Zhang, Y.; Ogden, L. G.; Dreher, M.; Hill, J. O., Safety and antioxidant activity of a pomegranate ellagitannin-enriched polyphenol dietary supplement in overweight individuals with increased waist size. *Journal of Agricultural and Food Chemistry* **2007,** *55*, 10050-10054.

(141) Seeram, N. P.; Aronson, W. J.; Zhang, Y.; Henning, S. M.; Moro, A.; Lee, R.-p.; Sartippour, M.; Harris, D. M.; Rettig, M.; Suchard, M. A.; Pantuck, A. J.; Belldegrun, A.; Heber, D., Pomegranate ellagitannin-derived metabolites inhibit prostate cancer growth and localize to the mouse prostate gland. *Journal of Agricultural and Food Chemistry* **2007,** *55*, 7732-7737.

(142) Simon, C.; Barathieu, K.; Laguerre, M.; Schmitter, J.-M.; Fouquet, E.; Pianet, I.; Dufourc, E. J., Three-dimensional structure and dynamics of wine tannin−saliva protein complexes. A multitechnique approach. *Biochemistry* **2003,** *42*, 10385-10395.

(143) Gawel, R., Red wine astringency: a review. *Australian Journal of Grape and Wine Research* **1998,** *4*, 74-95.

(144) Mousia, Z.; Farhat, I. A.; Pearson, M.; Chesters, M. A.; Mitchell, J. R., FTIR microspectroscopy study of composition fluctuations in extruded amylopectin-gelatin blends. *Biopolymers* **2001,** *62*, 208-218.

(145) Chang, M. C.; Ko, C.-C.; Douglas, W. H., Preparation of hydroxyapatite-gelatin nanocomposite. *Biomaterials* **2003,** *24*, 2853-2862.

(146) Kulkarni, A. P.; Aradhya, S. M.; Divakar, S., Isolation and identification of a radical scavenging antioxidant - punicalagin from pith and carpellary membrane of pomegranate fruit. *Food Chemistry* **2004,** *87*, 551-557.

(147) Meghashri, S.; Vijay Kumar, H.; Gopal, S., Antioxidant properties of a novel flavonoid from leaves of Leucas aspera. *Food Chemistry* **2010,** *122*, 105-110.

(148) Payne, K. J.; Veis, A., Fourier transform ir spectroscopy of collagen and gelatin solutions: Deconvolution of the amide I band for conformational studies. *Biopolymers* **1988,** *27*, 1749-1760.

(149) Kuo, S. W.; Chang, F. C., Studies of miscibility behavior and hydrogen bonding in blends of poly(vinylphenol) and poly(vinylpyrrolidone). *Macromolecules* **2001,** *34*, 5224-5228.

(150) Hagerman, A. E.; Butler, L. G., The specificity of proanthocyanidin-protein interactions. *The Journal of Biological Chemistry* **1981,** *256*, 4494-4497.

(151) Deaville, E. R.; Green, R. J.; Mueller-Harvey, I.; Willoughby, I.; Frazier, R. A., Hydrolyzable tannin structures influence relative globular and random coil protein binding strengths. *Journal of Agricultural and Food Chemistry* **2007,** *55*, 4554-4561.

(152) Haslam, E., Natural polyphenols (vegetable tannins) as drugs: possible modes of action. *Journal of Natural Products* **1996,** *59*, 205-215.

(153) Barch, D. H.; Rundhaugen, L. M.; Stoner, G. D.; Pillay, N. S.; Rosche, W. A., Structure-function relationships of the dietary anticarcinogen ellagic acid. *Carcinogenesis* **1996,** *17*, 265-269.

(154) Rehman, I.; Bonfield, W., Characterization of hydroxyapatite and carbonated apatite by photo acoustic FTIR spectroscopy. *Journal of Materials Science: Materials in Medicine* **1997,** *8*, 1-4.

(155) Kawamoto, H.; Nakatsubo, F.; Murakami, K., Stoichiometric studies of tannin-protein co-precipitation. *Phytochemistry* **1996,** *41*, 1427-1431.

(156) Jahanshahi, M.; Babaei, Z., Protein nanoparticle: a unique system as drug delivery vehicles. *African Journal of Biotechnology* **2008,** *7*, 4926-4934.

(157) Mohanraj, V. J.; Chen, Y., Nanoparticles- a review. *Tropical Journal of Pharmaceutical Research* **2006,** *5*, 561-573.

(158) Desai, M. P.; Labhasetwar, V.; Amidon, G. L.; Levy, R. J., Gastrointestinal uptake of biodegradable microparticles: effect of particle size. *Pharmaceutical Research* **1996,** *13*, 1838-1845.

(159) Jani, P.; Halbert, G. W.; Langridge, J.; Florence, A. T., Nanoparticle uptake by the rat gastrointestinal mucosa: quantitation and particle size dependency. *Journal of Pharmacy and Pharmacology* **1990,** *42*, 821-826.

(160) Opanasopit, P.; Apirakaramwong, A.; Ngawhirunpat, T.; Rojanarata, T.; Ruktanonchai, U., Development and characterization of pectinate micro/nanoparticles for gene delivery. *AAPS PharmSciTech* **2008,** *9*, 67-74.

(161) Takeuchi, H.; Yamamoto, H.; Kawashima, Y., Mucoadhesive nanoparticulate systems for peptide drug delivery. *Advanced Drug Delivery Reviews* **2001,** *47*, 39-54.

(162) Cerda, B.; Ceron, J. J.; Tomas-Barberan, F. A.; Espin, J. C., Repeated oral administration of high doses of the pomegranate ellagitannin punicalagin to rats for 37 days is not toxic. *Journal of Agricultural and Food Chemistry* **2003,** *51*, 3493-3501.

(163) Chen, L.-G.; Huang, W.-T.; Lee, L.-T.; Wang, C.-C., Ellagitannins from Terminalia calamansanai induced apoptosis in HL-60 cells. *Toxicology in Vitro* **2009,** *23*, 603-609.

(164) Surh, Y.-J., Molecular mechanisms of chemopreventive effects of selected dietary and medicinal phenolic substances. *Mutation Research/Fundamental and Molecular Mechanisms of Mutagenesis* **1999,** *428*, 305-327.

(165) Chen, H.; Weiss, J.; Shahidi, F., Nanotechnology in nutraceuticals and functional foods. *Food Technology* **2006,** *60*, 30-36.

(166) Müller, R. H.; Jacobs, C.; Kayser, O., Nanosuspensions as particulate drug formulations in therapy: Rationale for development and what we can expect for the future. *Advanced Drug Delivery Reviews* **2001,** *47*, 3-19.

(167) Hu, B.; Pan, C.; Sun, Y.; Hou, Z.; Ye, H.; Zeng, X., Optimization of fabrication parameters to produce chitosan−tripolyphosphate nanoparticles for delivery of tea catechins. *Journal of Agricultural and Food Chemistry* **2008,** *56*, 7451-7458.

(168) Opanasopit, P.; Apirakaramwong, A.; Ngawhirunpat, T.; Rojanarata, T.; Ruktanonchai, U., Development and characterization of pectinate micro/nanoparticles for gene delivery. *AAPS PharmSciTech* **2008,** *9*, 67-74.

(169) Sanguansri, P.; Augustin, M. A., Nanoscale materials development – a food industry perspective. *Trends in Food Science & Technology* **2006,** *17*, 547-556.

(170) Li, Z.; Percival, S. S.; Bonard, S.; Gu, L., Fabrication of nanoparticles using partially purified pomegranate ellagitannins and gelatin and their apoptotic effects. *Molecular Nutrition & Food Research* **2011,** *55*, 1096-1103.

(171) Hagerman Ann, E., Tannin—protein interactions. In *Phenolic Compounds in Food and Their Effects on Health I*, American Chemical Society: Washington, DC, 1992; pp 236-247.

(172) Pasch, H.; Pizzi, A., Considerations on the macromolecular structure of chestnut ellagitannins by matrix-assisted laser desorption/ionization-time-of-flight mass spectrometry. *Journal of Applied Polymer Science* **2002,** *85*, 429-437.

(173) Naczk, M.; Amarowicz, R.; Zadernowski, R.; Shahidi, F., Protein precipitating capacity of condensed tannins of beach pea, canola hulls, evening primrose and faba bean. *Food Chemistry* **2001,** *73*, 467-471.

(174) Xu, L.; Diosady, L. L., Interactions between canola proteins and phenolic compounds in aqueous media. *Food Research International* **2000,** *33*, 725-731.

(175) Daniel, E. M.; Ratnayake, S.; Kinstle, T.; Stoner, G. D., The effects of pH and rat intestinal contents on the liberation of ellagic acid from purified and crude ellagitannins. *Journal of Natural Products* **1991,** *54*, 946-952.

(176) Bialonska, D.; Kasimsetty, S. G.; Khan, S. I.; Ferreira, D., Urolithins, intestinal microbial metabolites of pomegranate ellagitannins, exhibit potent antioxidant activity in a cell-based assay. *Journal of Agricultural and Food Chemistry* **2009,** *57*, 10181-10186.

(177) Harrington, W. F.; Von Hippel, P. H., The structure of collagen and gelatin. *In Advances in Protein Chemistry*. C.B. Anfinsen, J. M. L. A. K. B.; John, T. E., Eds. Academic Press:: 1962; Vol. 16, p 95-108.

(178) Zhang, Y.; Wang, D.; Lee, R.-p.; Henning, S. M.; Heber, D., Absence of pomegranate ellagitannins in the majority of commercial pomegranate extracts: Implications for standardization and quality control. *Journal of Agricultural and Food Chemistry* **2009,** *57*, 7395-7400.

(179) Balentine, D. A.; Wiseman, S. A.; Bouwens, L. C. M., The chemistry of tea flavonoids. *Critical Reviews in Food Science and Nutrition* **1997,** *37*, 693-704.

(180) Jung, Y. D.; Kim, M. S.; Chay, K. O.; Ahn, B. W.; Liu, W.; Bucana, C. D.; Gallick, G. E.; Ellis, L. M., EGCG, a major component of gree tea, inhibits tumour growth by inhibiting VEGF induction in human colon carcinoma cells. *British Journal of Cancer* **2001,** *84*, 844-850.

(181) Annabi, B.; Bouzeghrane, M.; Moumdjian, R.; Moghrabi, A.; Béliveau, R., Probing the infiltrating character of brain tumors: inhibition of RhoA/ROK-mediated CD44 cell surface shedding from glioma cells by the green tea catechin EGCg. *Journal of Neurochemistry* **2005,** *94*, 906-916.

(182) Chung, L. Y.; Cheung, T. C.; Kong, S. K.; Fung, K. P.; Choy, Y. M.; Chan, Z. Y.; Kwok, T. T., Induction of apoptosis by green tea catechins in human prostate cancer DU145 cells. *Life Sciences* **2001,** *68*, 1207-1214.

(183) Ahn, W. S.; Huh, S. W.; Bae, S.-M.; Lee, I. P.; Lee, J. M.; Namkoong, S. E.; Kim, C. K.; Sin, J.-I., A major constituent of green tea, EGCG, inhibits the growth of a human cervical cancer cell line, CaSki cells, through apoptosis, G1 arrest, and regulation of gene expression. *DNA and Cell Biology* **2003,** *22*, 217-224.

(184) Kemberling, J. K.; Hampton, J. A.; Keck, R. W.; Gomez, M. A.; Selman, S. H., Inhibition of bladder tumor growth by the green tea derivative epigallocatechin-3-gallate. *The Journal of Urology* **2003,** *170*, 773-776.

(185) Nagle, D. G.; Ferreira, D.; Zhou, Y.-D., Epigallocatechin-3-gallate (EGCG): Chemical and biomedical perspectives. *Phytochemistry* **2006,** *67*, 1849-1855.

(186) Zhu, M.; Chen, Y.; Li, R. C., Oral absorption and bioavailability of tea catechins. *Planta Medica* **2000,** *66*, 444-447.

(187) Nakagawa, K.; Miyazawa, T., Absorption and distribution of tea catechin, (-)-epigallocatechin-3-gallate, in the rat. *Journal of Nutritional Science and Vitaminology* **1997,** *43*, 679-684.

(188) Yang, C. S.; Chen, L.; Lee, M. J.; Balentine, D.; Kuo, M. C.; Schantz, S. P., Blood and urine levels of tea catechins after ingestion of different amounts of green tea by human volunteers. *Cancer Epidemiology Biomarkers & Prevention* **1998,** *7*, 351-354.

(189) Tian, X.; Yang, X.; Wang, K.; Yang, X., The efflux of flavonoids morin, isorhamnetin-3-O-rutinoside and diosmetin-7-O-beta-D-xylopyranosyl-(1-6)-beta-D-glucopyranoside in the human intestinal cell line Caco-2. *Pharmaceutical Research* **2006,** *23*, 1721-1728.

(190) Bowman, K.; Leong, K. W., Chitosan nanoparticles for oral drug and gene delivery. *Int J Nanomedicine* **2006,** *1*, 117-128.

(191) Dube, A.; Ng, K.; Nicolazzo, J. A.; Larson, I., Effective use of reducing agents and nanoparticle encapsulation in stabilizing catechins in alkaline solution. *Food Chemistry* **2010,** *122*, 662-667.

(192) Loftsson, T.; Jarho, P.; Másson, M.; Järvinen, T., Cyclodextrins in drug delivery. *Expert Opinion on Drug Delivery* **2005,** *2*, 335-351.

(193) Smith, J. M.; Dornish, M.; Wood, E. J., Involvement of protein kinase C in chitosan glutamate-mediated tight junction disruption. *Biomaterials* **2005,** *26*, 3269-3276.

(194) Mei, D.; Mao, S.; Sun, W.; Wang, Y.; Kissel, T., Effect of chitosan structure properties and molecular weight on the intranasal absorption of tetramethylpyrazine phosphate in rats. *European Journal of Pharmaceutics and Biopharmaceutics* **2008,** *70*, 874-881.

(195) Hu, B.; Ting, Y.; Yang, X.; Tang, W.; Zeng, X.; Huang, Q., Nanochemoprevention by encapsulation of (-)-epigallocatechin-3-gallate with bioactive peptides/chitosan nanoparticles for enhancement of its bioavailability. *Chem. Commun.* **2012,** *48*, 2421-2423.

(196) Herce, H. D.; Garcia, A. E., Cell penetrating peptides: how do they do it? *J biol Phys* **2007,** *33*, 345-356.

(197) Lundberg, M.; Wikstrom, S.; Johansson, M., Cell surface adherence and endocytosis of protein transduction domains. *Mol Ther* **2003,** *8*, 143-150.

(198) Rustenbeck, I.; Löptien, D.; Fricke, K.; Lenzen, S.; Reiter, H., Polyamine modulation of mitochondrial calcium transport: II. inhibition of mitochondrial permeability transition by aliphatic polyamines but not by aminoglucosides. *Biochemical Pharmacology* **1998,** *56*, 987-995.

(199) Deshayes, S.; Gerbal-Chaloin, S.; Morris, M. C.; Aldrian-Herrada, G.; Charnet, P.; Divita, G.; Heitz, F., On the mechanism of non-endosomial peptide-mediated cellular delivery of nucleic acids. *Biochimica et Biophysica Acta (BBA) - Biomembranes* **2004,** *1667*, 141-147.

(200) Murugeshu, A.; Astete, C.; Leonardi, C.; Morgan, T.; Sabliov, C. M., Chitosan/PLGA particles for controlled release of α-tocopherol in the GI tract via oral administration. *Nanomedicine* **2011,** *6*, 1513-1528.

(201) Luo, Y.; Zhang, B.; Whent, M.; Yu, L.; Wang, Q., Preparation and characterization of zein/chitosan complex for encapsulation of α-tocopherol, and its in vitro controlled release study. *Colloids and Surfaces B: Biointerfaces* **2011,** *85*, 145-152.

(202) Zhao, D.; Zhao, X.; Zu, Y.; Li, J.; Zhang, Y.; Jiang, R.; Zhang, Z., Preparation, characterization, and *in vitro* targeted delivery of folate-decorated paclitaxel-loaded bovine serum albumin nanoparticles. *International Journal of Nanomedicine* **2010,** *5*, 669-677.

(203) Arnedo, A.; Irache, J. M.; Merodio, M.; Espuelas Millán, M. S., Albumin nanoparticles improved the stability, nuclear accumulation and anticytomegaloviral activity of a phosphodiester oligonucleotide. *Journal of Controlled Release* **2004,** *94*, 217-227.

(204) Zhang, L.; Hou, S.; Mao, S.; Wei, D.; Song, X.; Lu, Y., Uptake of folate-conjugated albumin nanoparticles to the SKOV3 cells. *International Journal of Pharmaceutics* **2004,** *287*, 155-162.

(205) Gaumet, M.; Gurny, R.; Delie, F., Interaction of biodegradable nanoparticles with intestinal cells: the effect of surface hydrophilicity. *International Journal of Pharmaceutics* **2010,** *390*, 45-52.

(206) Riggio, C.; Calatayud, M. P.; Hoskins, C.; Pinkernelle, J.; Sanz, B.; Torres, T. E.; Ibarra, M. R.; Wang, L.; Keilhoff, G.; Goya, G. F.; Raffa, V.; Cuschieri, A., Poly-l-lysine-coated magnetic nanoparticles as intracellular actuators for neural guidance. *International Journal of Nanomedicine* **2012,** *7*, 3155-3166.

(207) Kim, S. H.; Jeong, J. H.; Chun, K. W.; Park, T. G., Target-specific cellular uptake of PLGA nanoparticles coated with poly(l-lysine)−poly(ethylene glycol)−folate conjugate. *Langmuir* **2005,** *21*, 8852-8857.

(208) Papadopoulou, A.; Green, R. J.; Frazier, R. A., Interaction of flavonoids with bovine serum albumin: A fluorescence quenching study. *Journal of Agricultural and Food Chemistry* **2004,** *53*, 158-163.

(209) Singh, H. D.; Wang, G.; Uludag, H.; Unsworth, L. D., Poly-l-lysine-coated albumin nanoparticles: Stability, mechanism for increasing in vitro enzymatic resilience, and siRNA release characteristics. *Acta Biomaterialia* **2010,** *6*, 4277-4284.

(210) Shutava, T. G.; Balkundi, S. S.; Vangala, P.; Steffan, J. J.; Bigelow, R. L.; Cardelli, J. A.; O'Neal, D. P.; Lvov, Y. M., Layer-by-layer-coated gelatin nanoparticles as a vehicle for delivery of natural polyphenols. *ACS Nano* **2009,** *3*, 1877-1885.

(211) Peng, Z. G.; Hidajat, K.; Uddin, M. S., Adsorption of bovine serum albumin on nanosized magnetic particles. *Journal of Colloid and Interface Science* **2004,** *271*, 277-283.

(212) Ensign, L. M.; Cone, R.; Hanes, J., Oral drug delivery with polymeric nanoparticles: The gastrointestinal mucus barriers. *Advanced Drug Delivery Reviews* **2012,** *64*, 557-570.

(213) Dube, A.; Nicolazzo, J. A.; Larson, I., Chitosan nanoparticles enhance the intestinal absorption of the green tea catechins (+)-catechin and (−)-epigallocatechin gallate. *European Journal of Pharmaceutical Sciences* **2010,** *41*, 219-225.

(214) Bae, M.-J.; Ishii, T.; Minoda, K.; Kawada, Y.; Ichikawa, T.; Mori, T.; Kamihira, M.; Nakayama, T., Albumin stabilizes (–)-epigallocatechin gallate in human serum: Binding capacity and antioxidant property. *Molecular Nutrition & Food Research* **2009,** *53*, 709-715.

(215) Gao, S.; Hu, M., Bioavailability challenges associated with development of anti-cancer phenolics. *Mini Rev Med Chem.* **2010,** *10*, 550-567.

(216) Walgren, R. A.; Walle, U. K.; Walle, T., Transport of quercetin and its glucosides across human intestinal epithelial Caco-2 cells. *Biochemical Pharmacology* **1998,** *55*, 1721-1727.

(217) Hillaireau, H.; Couvreur, P., Nanocarriers' entry into the cell: relevance to drug delivery. *Cellular and Molecular Life Sciences* **2009,** *66*, 2873-2896.

(218) Smith, J.; Wood, E.; Dornish, M., Effect of Chitosan on Epithelial Cell Tight Junctions. *Pharmaceutical Research* **2004,** *21*, 43-49.

(219) Capanni, C.; Taddei, N.; Gabrielli, S.; Messori, L.; Orioli, P.; Chiti, F.; Stefani, M.; Ramponi, G., Investigation of the effects of copper ions on protein aggregation using a model system. *Cellular and Molecular Life Sciences* **2004,** *61*, 982-991.

(220) Cuccioloni, M.; Sparapani, L.; Amici, M.; Lupidi, G.; Eleuteri, A. M.; Angeletti, M., Kinetic and equilibrium characterization of the interaction between bovine trypsin and I-ovalbumin. *Biochimica et Biophysica Acta (BBA) - Proteins and Proteomics* **2004,** *1702*, 199-207.

(221) Martos, G.; Contreras, P.; Molina, E.; López-FandiÑo, R., Egg White Ovalbumin Digestion Mimicking Physiological Conditions. *Journal of Agricultural and Food Chemistry* **2010,** *58*, 5640-5648.

(222) Moncrief, J. A.; Darin, J. C.; Canizaro, P. C.; Sawyer, R. B., Use of dextran to prevent arterial and venous thrombosis. *Annals of Surgery* **1963,** *158*, 553-559.

(223) de Raucourt, E.; Mauray, S.; Chaubet, F.; Maiga-Revel, O.; Jozefowicz, M.; Fischer, A. M., Anticoagulant activity of dextran derivatives. *Journal of Biomedical Materials Research* **1998,** *41*, 49-57.

(224) Varga, R.; Török, L.; Szabó, A.; Kovács, F.; Keresztes, M.; Varga, G.; Kaszaki, J.; Boros, M., Effects of colloid solutions on ischemia-reperfusion-induced periosteal microcirculatory and inflammatory reactions: comparison of dextran, gelatin, and hydroxyethyl starch. *Critical Care Medicine* **2008,** *36*, 2828-2837.

(225) Sery, T. W.; Hehre, E. J., Degradation of dextrans by enzymes of intestinal bacteria. *Journal of Bacteriology* **1956,** *71*.

(226) Jaeger, H.; Janositz, A.; Knorr, D., The Maillard reaction and its control during food processing. The potential of emerging technologies. *Pathologie Biologie* **2010,** *58*, 207-213.

(227) Kato, A.; Sasaki, Y.; Furuta, R.; Kobayashi, K., Functional Protein-Polysaccharide Conjugate Prepared by Controlled Dry-heating of Ovalbumin-Dextran Mixtures. *Agricultural and Biological Chemistry* **1990,** *54*, 107-112.

(228) Choi, S. J.; Kim, H. J.; Park, K. H.; Moon, T. W., Molecular characteristics of ovalbumin–dextran conjugates formed through the Maillard reaction. *Food Chemistry* **2005,** *92*, 93-99.

(229) Zhou, H.; Sun, X.; Zhang, L.; Zhang, P.; Li, J.; Liu, Y.-N., Fabrication of Biopolymeric Complex Coacervation Core Micelles for Efficient Tea Polyphenol Delivery via a Green Process. *Langmuir* **2012,** *28*, 14553-14561.

(230) Deng, W.; Li, J.; Yao, P.; He, F.; Huang, C., Green Preparation Process, Characterization and Antitumor Effects of Doxorubicin–BSA–Dextran Nanoparticles. *Macromolecular Bioscience* **2010,** *10*, 1224-1234.

(231) Sun, G.; Shen, Y.-I.; Ho, C. C.; Kusuma, S.; Gerecht, S., Functional groups affect physical and biological properties of dextran-based hydrogels. *Journal of Biomedical Materials Research Part A* **2010,** *93A*, 1080-1090.

(232) Jang, H.; Ryoo, S.-R.; Kostarelos, K.; Han, S. W.; Min, D.-H., The effective nuclear delivery of doxorubicin from dextran-coated gold nanoparticles larger than nuclear pores. *Biomaterials* **2013,** *34*, 3503-3510.

(233) Mellet, P.; Michels, B.; Bieth, J. G., Heat-induced conversion of ovalbumin into a proteinase inhibitor. *The Journal of Biological Chemistry* **1996,** *271*, 30311-30314.

(234) Shah, P.; Jogani, V.; Bagchi, T.; Misra, A., Role of Caco-2 Cell Monolayers in Prediction of Intestinal Drug Absorption. *Biotechnology Progress* **2006,** *22*, 186-198.

BIOGRAPHICAL SKETCH

Zheng Li was born in Beijing, China. He received his B.S. degree in food bioengineering at China Agricultural University in 2007, and enrolled into master's program in food biotechnology at the same university. He had three publications as the first author from his master's project. After his graduation with M.S. degree from China Agricultural University in 2009, he entered the food science doctoral program at the University of Florida under the supervision of Dr. Liwei Gu. During his doctoral period, Zheng published three papers as the first author. Upon his completion of the Ph. D. degree in August 2013, Zheng plans to continue his research as a post-doc at other university and looks forward to any challenge that life will bring.